

AN ABSTRACT OF THE THESIS OF

Jessica Young for the degree of Master of Science in Civil Engineering presented on May 4, 2012.

Title: Uplift Capacity and Displacement of Helical Anchors in Cohesive Soil

Abstract approved:

Armin W. Stuedlein

Helical anchors are a type of deep foundation element that can be installed quickly in almost any location and can accept the immediate application of operational loads. The use of helical anchors has expanded in recent decades from its established application in the power transmission industry to more traditional civil engineering applications such as residential construction, communication tower installations, and static and seismic structural retrofitting and reconstruction. Despite the wide range of helical anchor applications, few advances have been made in improving the understanding of their behavior. For example, existing helical anchor design methods, for cases where the anchors are loaded in uplift in cohesive soils, are based on the assumption that the soil above the helical plate is mobilized in a manner analogous to

that beneath a deep foundation in bearing. An appropriate design method would acknowledge the effect of load directionality on the assumed failure mechanism.

This thesis evaluates the existing cylindrical shear and individual plate bearing design methods for helical anchor capacity in uplift. Additionally, new capacity models are proposed to improve prediction accuracy and reduce prediction variability. A load test database of helical anchors loaded in tension is established from tests reported in the literature. The existing and proposed capacity models are compared to the capacities observed during loading tests using the statistical bias and its distribution. Load and Resistance Factor Design (LRFD) resistance factors are derived from closed-form solutions using First Order Second Moment (FOSM) reliability procedures.

Finally, load-displacement models are developed through the evaluation of observed individual anchor plate breakout behavior and back-calculation of side shear capacity from load tests on multi-plate anchors. The new displacement models are compared to the load-displacement tests in the database. In general the comparisons indicate that the displacement-based models developed in this thesis provide a reasonable estimate of load-displacement behavior of helical anchors for service-level displacements. These findings provide engineers with new tools for design of helical anchor foundations.

©Copyright by Jessica Young
May 4, 2012
All Rights Reserved

Uplift Capacity and Displacement of Helical Anchors in Cohesive Soil

by
Jessica Young

A THESIS

submitted to

Oregon State University

in partial fulfillment of
the requirements for the
degree of

Master of Science

Presented May 4, 2012
Commencement June 2012

Master of Science thesis of Jessica Young presented on May 4, 2012.

APPROVED:

Major Professor, representing Civil Engineering

Head of the School of Civil and Construction Engineering

Dean of the Graduate School

I understand that my thesis will become part of the permanent collection of Oregon State University libraries. My signature below authorizes release of my thesis to any reader upon request.

Jessica Young, Author

ACKNOWLEDGEMENTS

First and foremost I would like to thank all of the faculty and staff of the Oregon State University School of Civil and Construction Engineering, the dedication and support did not go unnoticed. I would like to express my genuine gratitude to my major advisor, Dr. Armin Stuedlein for his guidance throughout this project. You believed in me from the very beginning and pushed me to realize my potential. I am grateful for the comments and support provided by my graduate committee: Dr. Karl Haapala, Dr. Ben Mason, and Dr. Mike Olsen. Thank you all for your dedication, and for pushing me to be a better engineer.

Finally I would like to thank those closest to me, I am extremely grateful to my family and friends. All of them have been a constant source of support in my life, and this thesis would certainly not have existed without them.

It is thanks to my father that I first became interested in construction and engineering when I was young. He always impressed upon me my ability to be and do anything my heart desired, and it is to him that this thesis is dedicated.

TABLE OF CONTENTS

	<u>Page</u>
1 Introduction.....	1
1.1 Problem Statement.....	1
1.2 Outline of Research.....	2
2 Literature Review	4
2.1 Helical Anchors.....	4
2.1.1 History.....	7
2.1.2 Modern Usage.....	9
2.2 Behavior of Helical Anchors.....	11
2.3 Bearing Capacity of Helical Anchors.....	18
2.3.1 Individual Plate Bearing.....	19
2.3.2 Cylindrical Shear.....	22
2.4 Pullout Capacity Analysis	23
2.4.1 Individual Plate Uplift.....	23
2.4.2 Cylindrical Shear Uplift.....	24
2.5 Torque Based Analysis.....	26
2.6 Design Considerations.....	27
2.7 Summary of Literature Review	29
3 Research Objectives.....	31
3.1 Objectives of this Study.....	31
3.2 Research Program.....	31

TABLE OF CONTENTS, CONTINUED.

	<u>Page</u>
4 Load Test Database.....	33
4.1 Single Plate Pull out Tests in Clay	33
4.1.1 Laboratory Model Test Description	33
4.1.2 Results of the Single Plate Pull out Tests	35
4.2 Multi-Plate Pull out Tests in Clay	38
4.2.1 Marine Clay Site, Massena, NY.....	38
4.2.2 Oregon State University Soil Test Site, Corvallis, OR	43
4.2.3 Beaumont Clay Site, Baytown, TX.....	48
4.2.4 Varved Clay Site, Amherst, MA	55
4.2.5 Laboratory Testing in Clay	60
4.3 Summary	66
5 Development of an Uplift Capacity Model.....	71
5.1 Statistical Approach for Characterization of New and Existing Models	71
5.2 Determination of the Uplift Capacity Factor.....	74
5.3 Accounting for Uncertainty in the Uplift Behavior of Helical Anchors	80
5.3.1 Uncertainty in the Uplift Capacity Factor	83
5.3.2 Uncertainty in Capacity Models.....	90
5.4 Summary	103
6 Development of a Load-Displacement Model.....	105
6.1 Development of Normalized Load Test Curves	105
6.2 Breakout Load-Displacement Model for Single Plate Anchors	106
6.3 Side Shear Load-Displacement Model for Multi-Helix Anchors.....	109

TABLE OF CONTENTS, CONTINUED.

	<u>Page</u>
6.4 Displacement Prediction Models.....	112
6.4.1 Individual Displacement Prediction Model	112
6.4.2 Combined Displacement Prediction Model	113
6.5 Evaluation of Displacement Model Accuracy.....	114
6.6 Summary	124
7 Summary and Conclusions	125
7.1 Summary of Findings	125
7.2 Conclusions	126
7.2.1 Development of an Uplift Capacity Model.....	126
7.2.2 Development of a Load-Displacement Model	128
7.3 Statement of Limitations	130
7.4 Suggestions for Future Research.....	130
References	132
Appendices.....	137
Appendix A: Displacement Predictions	138

LIST OF FIGURES

<u>Figure</u>	<u>Page</u>
Figure 2.1 Helical plate being torqued into the soil (Magnum Piering, 2012).	4
Figure 2.2 Typical helical foundation element, after Perko (2009).	5
Figure 2.3 Mitchel screw pile (Perko, 2009).	8
Figure 2.4 Boardwalk built on helical piles through a marshland. The previous foundation had failed due to settlement; helical piles were used for reconstruction (Hubbel, 2012).	10
Figure 2.5 Hydraulic hand pack installation of helical anchors (Francis & Lewis International, 2012).	10
Figure 2.6 Backhoe with torque head installing a helical element (Francis & Lewis International, 2012).	11
Figure 2.7 Conceptual load curve for a plate anchor in plastic and brittle clay, breakout is indicated by the round marker.	13
Figure 2.8 Tensile shear pattern of a plate anchor with an depth vs diameter ratio of 1.5 (Ali, 1969).	14
Figure 2.9 Idealized deep failure mode for a helical anchor (Mooney, et al., 1985).	16
Figure 2.10 Conceptual sketches showing the assumed shearing mechanisms for (a) individual plate bearing and (b) cylindrical shear.....	19
Figure 2.11 Uplift capacity factor, N_{cu} (data from Mooney et al., 1985).....	21
Figure 2.12 Conceptual sketch of assumed mechanism for individual plate breakout in uplift (Lutenegger, 2009).	24
Figure 2.13 Conceptual sketch of assumed mechanism for cylindrical shear in uplift (Lutenegger, 2009).	25

LIST OF FIGURES, CONTINUED.

<u>Figure</u>	<u>Page</u>
Figure 2.14 Square bar installation cross section depicting void space between bar and soil due to installation rotation; adapted from (Pack, 2006).	28
Figure 4.1 Experimental model setup used for load tests of round plate anchors in remolded bentonite clay after Ali (1969).....	35
Figure 4.2 Load-displacement curves after Ali (1969), plate anchor laboratory tests in bentonite clay.....	37
Figure 4.3 Massena, NY site map depicting the anchor and boring locations for the marine clay anchor site; after Clemence (1983).....	39
Figure 4.4 Model anchors one quarter scale of field anchors. Scaled anchors were used in laboratory testing; after Mooney (1985).	40
Figure 4.5 Load-displacement curves from Clemence (1983), multi-helix field tests in marine clay.....	42
Figure 4.6 Soil boring log at the OSU Geotechnical Field Research Site, as published by Handojo (1997).....	44
Figure 4.7 Anchor layout on the OSU Field test site; after Handojo (1997). Note: Anchor 17 is H1.	45
Figure 4.8 Experimental load frame configuration for axial tensile load testing after Handojo (1997).	46
Figure 4.9 Load-displacement curve from Handojo (1997), multi-helix field test in clayey silt.....	47
Figure 4.10 Load test setup for a large footing after Stuedlein (2008), using helical anchors as reaction.	48
Figure 4.11 Site and exploration layout for load tests; after Stuedlein (2008).	50
Figure 4.12 Subsurface cross section through section A-A' illustrated in Figure 4.11; after Stuedlein (2008).	51

LIST OF FIGURES, CONTINUED.

<u>Figure</u>	<u>Page</u>
Figure 4.13 Slack Correction on the load test for Anchor S2 (F2A1), (a) Initial slope, or anchor engagement, for the raw load test data (b) Corrected load test data showing initial and secondary anchor engagement.....	53
Figure 4.14 Three helical anchors, not tested to failure, used for tensile reaction and monitored during the testing of spread footings on aggregate pier reinforced clay.....	54
Figure 4.15 Four helical anchors, tested to failure, used for tensile reaction and monitored during the testing of spread footings on aggregate pier reinforced clay.....	55
Figure 4.16 Soil Profile and typical variation in soil properties for the national geotechnical experimentation site at the University of Massachusetts; after Lutenegeger (2000).	56
Figure 4.17 Load-displacement curves from Lutenegeger (2009), multi-helix field tests in varved clay.....	59
Figure 4.18 Experimental test setup for uplift capacity tests; after Rao et al. (1991).....	62
Figure 4.19 Photograph of piles pulled out during the uplift testing. The pictured anchors had S/D ratios, from left to right, of 1.5, 2.3, and 4.6; after Rao et al. (1991).	63
Figure 5.1 Conceptual visualization of the defined bias assuming a normal distribution; adapted from Strahler (2012).....	73
Figure 5.2 Back-calculated uplift capacity factor, N_{cu}	75
Figure 5.3 Graphical representations of the dependence of the Mooney et al. (1985) uplift capacity factor, N_{cu} , on (a) the embedment (H/D), and (b) the observed values of N_{cu} used in model development.....	76
Figure 5.4 Uplift capacity factors, N_{cu} , fit with a piecewise hyperbolic model, given by Equation 5.4, to approximate N_{cu}	77

LIST OF FIGURES, CONTINUED.

<u>Figure</u>	<u>Page</u>
Figure 5.5 Graphical representations of the dependence of the proposed uplift capacity factor, N_{cu} , on (a) the embedment (H/D), and (b) the observed values of N_{cu} used in model development.	79
Figure 5.6 Conceptual illustration of potential probability distribution functions (PDF) for a normally distributed load and resistance, Q and R respectively; from (Stuedlein, 2008).	81
Figure 5.7 Conceptual illustration of the combined probability function representative of the margin of safety, β is the reliability index, adapted from (Stuedlein, 2008).	82
Figure 5.8 Cumulative distribution function (CDF) plot of the bias for the proposed uplift capacity factor model with fitted distributions.	86
Figure 5.9 Cumulative distribution function (CDF) plot of the bias for the Mooney et al. (1985) uplift capacity factor model with fitted distributions.	88
Figure 5.10 Fitted distribution for capacity, based solely on the available field data. The data seems to be normally distributed, however without more data, a clear distribution cannot be defined.	92
Figure 5.11 Fitted distribution for uplift capacity of helical anchors using the proposed individual plate breakout model.	93
Figure 5.12 Fitted distribution for uplift capacity of helical anchors using the proposed cylindrical shear model.	94
Figure 5.13 Fitted distribution for uplift capacity of helical anchors using the individual plate breakout equation.	95
Figure 5.14 Fitted distribution for uplift capacity of helical anchors using the cylindrical shear equation.	96
Figure 5.15 Resistance factors for calculating helical anchor capacity with the proposed cylindrical shear model.	101

LIST OF FIGURES, CONTINUED.

<u>Figure</u>	<u>Page</u>
Figure 5.16 Resistance factors for calculating helical anchor capacity with the proposed individual plate breakout model.	102
Figure 6.1 Observed load test data and normalized load test data for plate anchor A4, (a) observed load-displacement curve (b) normalized load-displacement curve.....	106
Figure 6.2 Proposed normalized breakout curve for plate anchors in cohesive soil compared to the normalized load-displacement curves, original data after Ali (1969).	108
Figure 6.3 Graphical representation of a side shear calculation.	110
Figure 6.4 Final normalized side shear displacement model for multi-plate helical anchors in cohesive soil.....	111
Figure 6.5 Calculated versus measured load-displacement curve for Anchor C1, the displacement models are calculated with an N_{cu} of 11.2.	115
Figure 6.6 Predicted and measured load displacement curves for Anchor L1, $S/D = 0.75$	118
Figure 6.7 Predicted and measured load displacement curves for Anchor L2, $S/D = 3.0$	119
Figure 6.8 Predicted and measured load displacement curves for Anchor S4, $S/D = 3.0$	120
Figure 6.9 Bias CDF for the cylindrical shear displacement prediction model. The model shows a narrow range of variability, and a lognormally distributed tail.	122
Figure 6.10 Bias CDF for the individual plate breakout displacement prediction model. The model shows a lognormal distribution well characterized by the fit-to-tail.	123

LIST OF TABLES

<u>Table</u>	<u>Page</u>
Table 4.1 Short term laboratory test results for plate anchors in bentonite clay, where δ_{MAX} is the displacement and Q_{MAX} is the ultimate load; after Ali (1969).....	36
Table 4.2 Short term field load test results for multi-helix anchors in marine clay, where δ_{MAX} is the displacement and Q_{MAX} is the ultimate load; after Clemence (1985).....	41
Table 4.3 Short term field test results for multi-helix anchors in Beaumont clay, where δ_{MAX} is the displacement and Q_{MAX} is the ultimate load. after Stuedlein (2008).....	52
Table 4.4 Short term field test results for multi-helix anchors in varved clay, where δ_{MAX} is the displacement and Q_{MAX} is the ultimate load. after Lutenegger (2009).....	58
Table 4.5 Estimated Soil properties for the uplift capacity tests performed by Rao et al. (1991).....	61
Table 4.6 laboratory test results for multi-helix anchors in clay, where Q_{MAX} is the ultimate load. after Rao et al. (1991).....	64
Table 4.7 laboratory test results for multi-helix anchors in clay, where Q_{MAX} is the ultimate load. after Rao and Prasad (1993).....	65
Table 4.8 Helical anchor load test database summary.	67
Table 5.1 Statistical summary of fitted distributions for the biases of both the Mooney et al. (1985) N_{cu} model and the proposed N_{cu} model.	89
Table 5.2 Statistical summary of the distribution approximations for the capacity bias calculations.....	97
Table 5.3 The AASHTO load statistics used in resistance factor calibration.....	99
Table 5.4 Combined statistics for dead load and live load based on the AASHTO load statistics.....	100

LIST OF TABLES, CONTINUED.

<u>Table</u>	<u>Page</u>
Table 5.5 Calculated load resistance factors for $\beta = 1.0\%$ and 0.1% accounting only for dead load.....	100
Table 5.6 Calculated load resistance factors for $\beta = 1.0\%$ and 0.1% accounting only for live load.	101
Table 5.7 Generated resistance factor equations for varying ratios of dead and live load.....	103
Table 6.1 Statistical summary of the performance of the two proposed displacement prediction models.....	116

LIST OF APPENDIX FIGURES

<u>Figure</u>	<u>Page</u>
Figure A.1 Load-displacement curve for anchor C1, compared to the predicted curves using the proposed cylindrical shear and individual plate breakout models, calculated with the typical, theoretical, and proposed N_{cu} values of 9.0, 9.4, and 11.2 respectively.....	139
Figure A.2 Load-displacement curve for anchor C2, compared to the predicted curves using the proposed cylindrical shear and individual plate breakout models, calculated with the typical, theoretical, and proposed N_{cu} values of 9.0, 9.4, and 11.2 respectively.....	140
Figure A.3 Load-displacement curve for anchor C3, compared to the predicted curves using the proposed cylindrical shear and individual plate breakout models, calculated with the typical, theoretical, and proposed N_{cu} values of 9.0, 9.4, and 11.2 respectively.....	141
Figure A.4 Load-displacement curve for anchor C4, compared to the predicted curves using the proposed cylindrical shear and individual plate breakout models, calculated with the typical, theoretical, and proposed N_{cu} values of 9.0, 9.4, and 11.2 respectively.....	142
Figure A.5 Load-displacement curve for anchor C5, compared to the predicted curves using the proposed cylindrical shear and individual plate breakout models, calculated with the typical, theoretical, and proposed N_{cu} values of 9.0, 9.4, and 11.2 respectively.....	143
Figure A.6 Load-displacement curve for anchor C6, compared to the predicted curves using the proposed cylindrical shear and individual plate breakout models, calculated with the typical, theoretical, and proposed N_{cu} values of 9.0, 9.4, and 11.2 respectively.....	144
Figure A.7 Load-displacement curve for anchor C7, compared to the predicted curves using the proposed cylindrical shear and individual plate breakout models, calculated with the typical, theoretical, and proposed N_{cu} values of 9.0, 9.4, and 11.2 respectively.....	145

LIST OF APPENDIX FIGURES, CONTINUED.

<u>Figure</u>	<u>Page</u>
Figure A.8 Load-displacement curve for anchor C8, compared to the predicted curves using the proposed cylindrical shear and individual plate breakout models, calculated with the typical, theoretical, and proposed N_{cu} values of 9.0, 9.4, and 11.2 respectively.	146
Figure A.9 Load-displacement curve for anchor H1, compared to the predicted curves using the proposed cylindrical shear and individual plate breakout models, calculated with the typical, theoretical, and proposed N_{cu} values of 9.0, 9.4, and 11.2 respectively.	147
Figure A.10 Load-displacement curve for anchor L1, compared to the predicted curves using the proposed cylindrical shear and individual plate breakout models, calculated with the typical, theoretical, and proposed N_{cu} values of 9.0, 9.4, and 11.2 respectively.	148
Figure A.11 Load-displacement curve for anchor L2, compared to the predicted curves using the proposed cylindrical shear and individual plate breakout models, calculated with the typical, theoretical, and proposed N_{cu} values of 9.0, 9.4, and 11.2 respectively.	149
Figure A.12 Load-displacement curve for anchor S1, compared to the predicted curves using the proposed cylindrical shear and individual plate breakout models, calculated with the typical, theoretical, and proposed N_{cu} values of 9.0, 9.4, and 11.2 respectively.	150
Figure A.13 Load-displacement curve for anchor S2, compared to the predicted curves using the proposed cylindrical shear and individual plate breakout models, calculated with the typical, theoretical, and proposed N_{cu} values of 9.0, 9.4, and 11.2 respectively.	151
Figure A.14 Load-displacement curve for anchor S3, compared to the predicted curves using the proposed cylindrical shear and individual plate breakout models, calculated with the typical, theoretical, and proposed N_{cu} values of 9.0, 9.4, and 11.2 respectively.	152

LIST OF APPENDIX FIGURES, CONTINUED.

<u>Figure</u>	<u>Page</u>
Figure A.15 Load-displacement curve for anchor S4, compared to the predicted curves using the proposed cylindrical shear and individual plate breakout models, calculated with the typical, theoretical, and proposed N_{cu} values of 9.0, 9.4, and 11.2 respectively.	153
Figure A.16 Load-displacement curve for anchor S5, compared to the predicted curves using the proposed cylindrical shear and individual plate breakout models, calculated with the typical, theoretical, and proposed N_{cu} values of 9.0, 9.4, and 11.2 respectively.	154
Figure A.17 Load-displacement curve for anchor S6, compared to the predicted curves using the proposed cylindrical shear and individual plate breakout models, calculated with the typical, theoretical, and proposed N_{cu} values of 9.0, 9.4, and 11.2 respectively.	155
Figure A.18 Load-displacement curve for anchor S7, compared to the predicted curves using the proposed cylindrical shear and individual plate breakout models, calculated with the typical, theoretical, and proposed N_{cu} values of 9.0, 9.4, and 11.2 respectively.	156

LIST OF SYMBOLS

s_u	Undrained Shear Strength
N_{cu}	Uplift Capacity Factor
D	Diameter
H	Embedment Depth of Top Helical Plate
H_f	Embedment Depth of the Lead Helical Plate
H_i	Embedment Depth of Bottom Helical Plate
S	Plate Spacing
H/D	Embedment Ratio
S/D	Spacing Ratio
A	Area
P_{shaft}	Shaft Perimeter
H_{eff}	Shaft Length
C_α	Adhesion
K_t	Torque Factor
T	Torque
Q	Load
Q_n	Nominal Load
\bar{Q}	Average Load
R	Resistance
R_n	Nominal Resistance
\bar{R}	Average Resistance
λ	Bias
$\bar{\lambda}$	Mean Bias
σ	Standard Deviation
COV	Coefficient of Variation

LIST OF SYMBOLS, CONTINUED.

P_i	Probability of Occurrence
Z_i	Standard Normal Variate
Φ	Probability Density Function
i	Rank
n	Number of Values
PDF	Probability Density Function
CDF	Cumulative Density Function
FS	Factor of Safety
\bar{g}	Average Margin of Safety
β	Reliability Index
γ_Q	Load Factor
φ_R	Resistance Factor
DL	Dead Load
LL	Live Load
ξ	Load Ratio

1 INTRODUCTION

Helical anchors were traditionally used in the power transmission industry to resist the tension loads on transmission towers and guy wires. Presently, helical anchors are used in more conventional civil engineering applications such as tie-down of structures for uplift, communication tower installations, static and seismic retrofit and reconstruction, as well as underpinning of settling structures.

1.1 PROBLEM STATEMENT

Despite the increase in the use of helical anchors, the understanding of behavior is somewhat unsatisfactory and has essentially gone unchanged over the past 20 years (Merifield, 2011). With rising construction and material costs, and shortened design and construction phases, it is likely that the popularity of helical anchors will continue to grow. Consequently, it is important that new methods be developed to improve design, and increase the understanding of helical anchor behavior.

In this study, the uplift capacity of individual and variably spaced multi-helix plates is assessed using a load test database. Both existing and proposed methods of predicting anchor capacity, as well as proposed and existing uplift capacity factors, were evaluated to estimate the uncertainty and variability in helical anchor capacity estimations, limited to application in cohesive soils.

1.2 OUTLINE OF RESEARCH

The work herein concentrates on the behavior of helical anchors installed in cohesive soil deposits, intending to increase understanding of helical anchor behavior in clays. Chapter 2 presents a detailed literature review of helical anchors. This addresses the history, modern use, current design methods, and considerations.

Chapter 3 presents the objectives of this study and research program outline.

Chapter 4 addresses the need for and generation of a load test database, established using helical anchor load-displacement tests published by various authors. An overview of the site location, soil conditions, and tests conditions for each site is given.

Chapter 5 presents the development and evaluation of an uplift capacity model. This chapter discusses the statistical approaches used in the research, the determination of the uplift capacity factor, and the process through which uncertainty was accounted in the current and proposed models. Additionally, LRFD resistance factors for uplift capacity of helical anchors were developed.

Chapter 6 addresses the development of a load-displacement prediction model, evaluating both breakout of helical plates and the side shear behavior of cylindrical shear failure. Anchor capacities were evaluated with respect to failure mode:

cylindrical shear or individual plate breakout. The uncertainty in the displacement models was characterized to evaluate the models.

Finally, Chapter 7 provides a summary and the findings developed in this study, and the conclusions therein. Chapter 7 is followed by a complete list of references and the Appendix. Appendix A provides the complete load-displacement anchor database, and a comparison of measured and predicted load-displacement curves of helical anchors in cohesive soils.

2 LITERATURE REVIEW

This chapter provides an overview of the development of helical anchors for the support of structures and discusses previous research of the behavior of helical foundations.

2.1 HELICAL ANCHORS

Helical anchors consist of a solid square or hollow pipe shaft made of steel, with a minimum of one helical plate fixed to the shaft, as shown in Figure 2.1. These deep foundation elements are screwed into the ground using hydraulic torque motors. Due to the pitch of the helical plate, these elements produce no spoils and create minimal disturbance in the area surrounding the anchor installation.



Figure 2.1 Helical plate being torqued into the soil (Magnum Piering, 2012).

Helical anchors are installed in sections ranging from three to seven feet long, as shown in Figure 2.2. The typical helical anchor has one lead segment to which the helical plates are attached, followed by extensions that are coupled and bolted together. In some instances, where the lead segment is not long enough to mount more plates, it is necessary to have helical plates attached to additional segments as needed to generate the required design resistance.

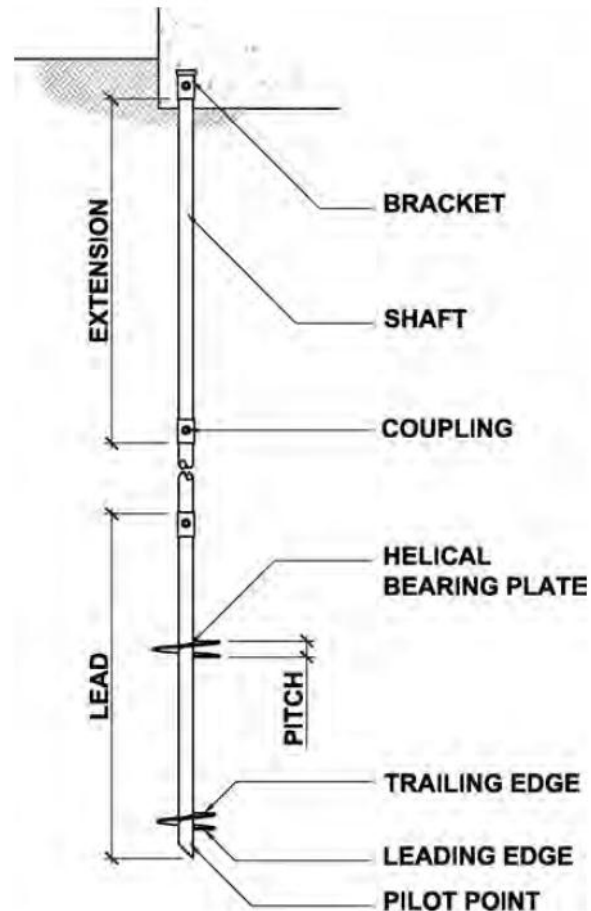


Figure 2.2 Typical helical foundation element, after Perko (2009).

Helical foundation installations are typically less expensive than other deep foundations, due to low steel requirements and ease of installation, owing to the segmented design. They can also be used to repair existing foundations with marginal disruption to the surrounding soil or installed to serve as a new foundation. Helical foundations are often used on ecologically delicate or limited-access sites due to negligible disturbance to the natural environment.

Helical foundations are used commonly in areas that have highly expansive soils that affect foundations built within the active zone. The active zone of soil is significantly affected by seasonal fluctuations in moisture content. Expansive clay will shrink and swell with increasing and decreasing moisture contents, respectively, and often causes serious damage to foundations that are not designed and constructed to mitigate these effects. By embedding the helical plate below the depth of active seasonal movements, helical anchors can act as a bearing medium unaffected by the fluctuations in seasonal moisture (Pack, 2006).

As with any engineering tool there are some disadvantages to helical anchors. One disadvantage is that helical plates are sensitive to damage by rocks and cobbles during installation in rocky soils; the capacity of the anchor is dependent on the plate area so damage can cause significant reductions in resistance. Contact with rocks and cobbles can also affect the directionality of the anchor, this generates difficulty in keeping the anchor plumb during installation. Another disadvantage to helical anchors

is the potential for installation damage due to high torque on the steel shaft. The reduced section of the shaft and the bolted connections of each anchor segment limit the torque capacity of the anchor. The bolted connections are also a potential location of failure along the anchor during uplift loading; therefore installers must stay within manufacture recommended limits during torque installation and engineers must account for the bolted connects in design.

2.1.1 History

While helical anchors are becoming more popular, helical pile foundations have been implemented since the early 1800s. In 1833 the screw pile was officially patented in London, credited to Alexander Mitchell; an example is shown in Figure 2.3. These screw piles were successfully used to support lighthouses in sandy soils. The Maplin Sands lighthouse was constructed on the River Thames in England in 1838. The foundations consisted of eight wrought-iron screw piles in an octagonal arrangement surrounding one center pile. Each helical anchor consisted of a four foot helical plate on a five inch shaft. These piles were installed to 22 feet depth over nine days by laborers using a capstan keyed into the soil (Lutenegger, 2003).



Figure 2.3 Mitchel screw pile (Perko, 2009).

By the mid-19th century the screw pile was being used throughout England. British expansion then led to the globalization of the screw pile. In the mid 1800's Alexander Mitchell visited the United States to consult on the first helical foundations in the states. Over the next 40 years at least 100 lighthouses were built on helical foundations along the eastern seaboard of North America. From 1900 to 1950 helical use declined dramatically due to major advances in mechanical pile driving and drilling (Perko, 2009).

2.1.2 Modern Usage

Helical anchors have many applications ranging from utility installations, such as transmission tower foundations and guy wire anchors, to residential construction. The cost and time savings from helical anchor usage can be considerable, especially in remote locations, due to the reduction of concrete and labor needs.

Residential construction applications for helical foundations include new construction, support of additions, and repair to damaged existing foundations. Since 1987, approximately 130,000 square shaft helical piles have been installed for both repair and new construction in Colorado alone (Pack, 2006).

Structures in environmentally sensitive areas can be constructed using helical anchors due to the unique design and minimal equipment required for installation. In sensitive areas, helical elements are sometimes used to create a stable foundation for elevated pathways; an example is provided in Figure 2.4. The elements are lightweight due to the small shaft size accompanied by the helical bearing plates, which allows installation by many different types of equipment and ease of transportation.

During installation a torqueing head rotates the anchor into the soil column. The hydraulic equipment necessary to engage the torqueing head ranges from hand-pack size (Figure 2.5), to small excavators, as shown in Figure 2.6. Small material and installation footprints create much less environmental impact and more economical equipment mobilization and construction.



Figure 2.4 Boardwalk built on helical piles through a marshland. The previous foundation had failed due to settlement; helical piles were used for reconstruction (Hubbel, 2012).



Figure 2.5 Hydraulic hand pack installation of helical anchors (Francis & Lewis International, 2012).



Figure 2.6 Backhoe with torque head installing a helical element (Francis & Lewis International, 2012).

2.2 BEHAVIOR OF HELICAL ANCHORS

Helical foundation systems are referred to by many names (e.g., screw piles, helical anchors, helical piles, helical piers, etc.); however, these terms apply roughly to the same system. Differences in these systems point to the relative manner with which they are designed. Typically, the terminology *helical piers* refer to shallow foundations; whereas *helical piling* refers to deep foundation systems. The Deep Foundation Institute (2005) adopted the term *helical pile* due to the depth of installation of a typical helical foundation element versus the diameter of the helix.

Helical anchor is the term adopted for a helical pile in which the primary or governing mode of loading is in tension.

Research into different kinds of anchors, including helical and plate anchors, has been ongoing over the past several decades. The studies discussed in this chapter have shown that uplift capacity of a plate anchor is a function of the shape of the anchor, the depth of embedment, the overburden stress, and the soil properties surrounding the installation. Merrifield (2011) proposed that round plate anchors loaded in tension breakout in the same manner as typical single helical anchors. The breakout load of an anchor is defined as the load at which the full resistance is mobilized. This breakout load is the maximum load an anchor can resist. Figure 2.7 shows a conceptualized load curve for an anchor in plastic and brittle clay where the breakout value of each is indicated. The geometry of a plate does not significantly affect the capacity; instead, the capacity is governed by the undrained soil strength, s_u . The soil strength affects the capacity available to anchors in both the individual plate breakout failure, where each plate is expected to behave independently, as well as for the breakout of the top plate in a cylindrical shear failure.

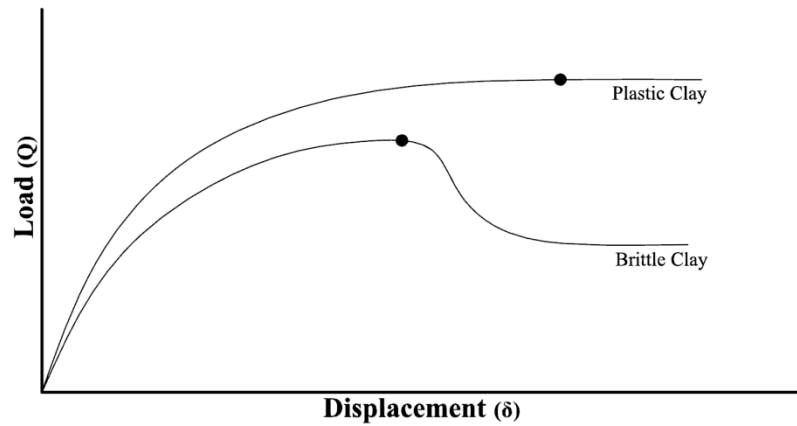


Figure 2.7 Conceptual load curve for a plate anchor in plastic and brittle clay, breakout is indicated by the round marker.

Ali (1969) tested small scale plate anchors in reconstituted bentonite soil to investigate their behavior in cohesive soil. The results showed a progression from a cylindrical to a conical failure above the anchors. Figure 2.8 presents a cutaway of a plate anchor in uplift loading, taken at Duke University during testing of plate anchors in cohesive soil by Ali (1969), displaying the pattern of shear failure. An important finding during the loading test was that after a certain depth, the failure phenomenon, or breakout, was the same whether the anchor is loaded in tension or compression (Ali, 1969).

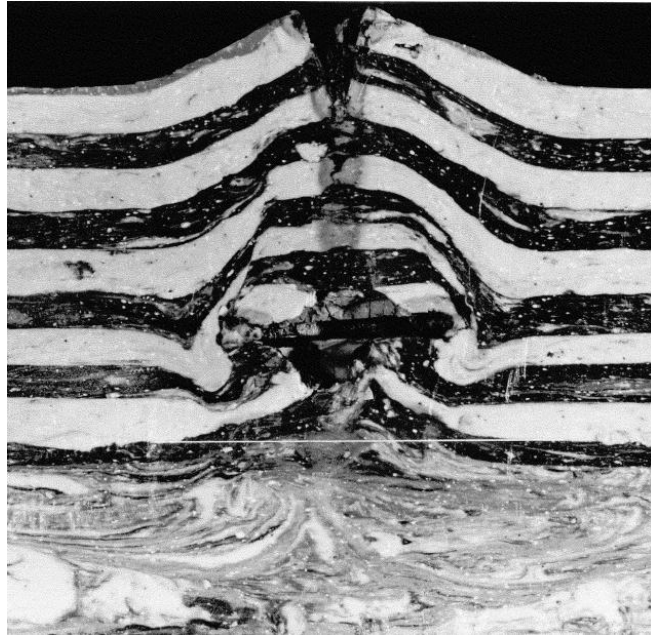


Figure 2.8 Tensile shear pattern of a plate anchor with an depth vs diameter ratio of 1.5 (Ali, 1969).

Anchor breakout is the behavior with which a soil-anchor system exhibits when exposed to uplift forces, and can be divided into two categories: immediate breakaway and no-breakaway, as defined by Rowe and Davis (1982). Immediate breakaway assumes the soil anchor interface beneath the anchor cannot sustain the tension force acting on the anchor. Upon tensile loading, the vertical stress goes to zero under the helical plate; therefore, no adhesion develops between the soil and the bottom of the anchor plate. This manifests as the base of the anchor plate anchor lifting up off of the soil directly beneath it, and losing contact; this results in a pullout or uplift condition. The no-breakaway behavior assumes that the interface between the soil and anchor can sustain the tension and the anchor remains in contact with the

surrounding soil, this is due to adhesion, and possibly suction, forces between the soil and anchor.

Multi plate helical anchor behavior depends on the spacing between the helical plates. If the spacing between the plates is greater than three times the preceding plate diameter then the plates will all act individually, and there is no interaction between the failure surfaces associated with each plate. On the other hand, if the spacing is less than three diameters, the soil between the helical plates will typically act as a relatively rigid, cylindrical shaft between the top and bottom plate.

Furthermore, anchors behavior can be categorized by the occurrence of a deep or shallow failure mode. The deep anchor failure mode is characterized by localized shear surrounding the anchor plates and is unaffected by the soil surface, as illustrated in Figure 2.9. Deep failure is reached only if the anchor is embedded at depths equal to or deeper than the critical embedment depth of that anchor. Critical embedment depth is defined as the depth at which the weight of the soil cone above the shallowest helical plate offsets uplift forces acting on the anchor. If deep failure occurs the capacity achieved will represent the maximum limiting value of the anchor.

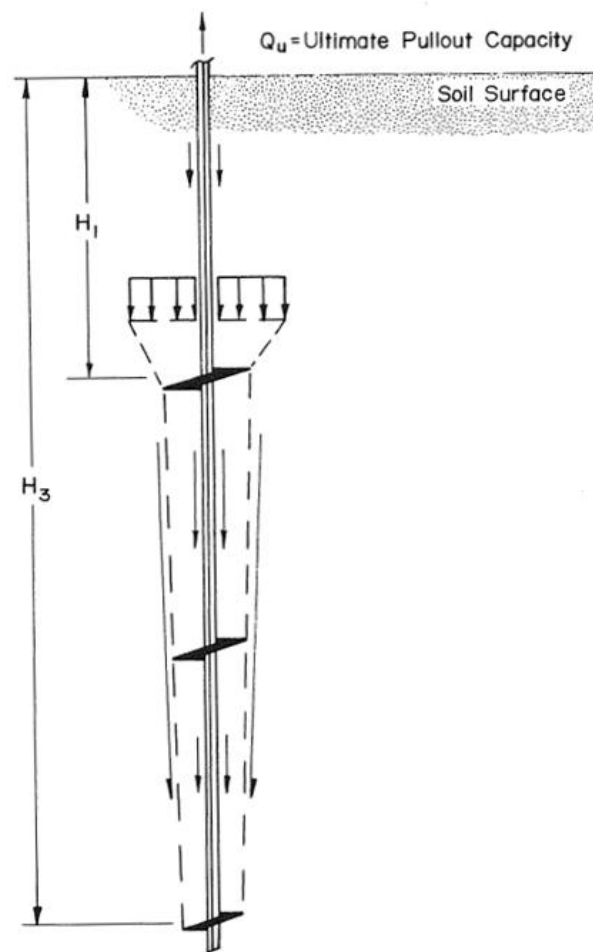


Figure 2.9 Idealized deep failure mode for a helical anchor (Mooney, et al., 1985).

Shallow failure occurs when uplift forces acting on an anchor overcome the mobilized strength. If the shallow failure mode occurs, the failure surface will reach and breach the soil surface. The capacity will no longer increase for embedment beyond the critical depth, but the embedment must be greater than the minimum to prevent shallow failure. Therefore, embedment is an important factor in design of helical anchors.

Prasad et al. (1993), Mitsch and Clemence (1995), Perko (1999), and Lutenecker (2009; 2011) investigated deep and shallow failure modes. Prasad et al. (1993) performed experiments on model anchors in remolded, soft marine clays with different embedment depths and they determined that the shallow failure mode governed when ratio of depth, H , to diameter, D , or H/D , was less than two. The H/D ratio references the depth of embedment of the top helical plate. Prasad et al. (1993) found that the failure mode transitioned gradually to the deep as H/D increases from two to four; correspondingly, Prasad et al. (1993) defined the deep failure modes as governing when H/D exceeds four. Mitsch and Clemence (1995) suggested that helical piles follow the behavior described by Meyerhof and Adam (1968) who called for a shallow failure mechanism for H/D less than five and deep thereafter. Furthermore, Perko (1999) suggested the transition zone in fine grained soils occurs at a shallower embedment than those in coarse grained soils.

Mooney et al. (1985) studied anchors in remolded and normally consolidated silts and clays. The study concluded that the major contributions to the uplift resistance of helical anchors in clay results from a cylindrical failure surface and the uplift bearing (i.e., “breakout”) of the top helix. The undrained shear strength, s_u , of the clay will provide the resistance to movement along the shaft. Additionally, Mooney et al. (1985) concluded that the undrained shear strength should be decreased to account for installation disturbance in sensitive clays.

2.3 BEARING CAPACITY OF HELICAL ANCHORS

This section introduces expressions for the determination of compressive capacity of helical piles; following this section is a discussion on the pullout capacity of helical anchors. There are two methods for the determination of the bearing capacity of helical piles: individual plate, and cylindrical shear. There are significant differences between the assumed behavior for individual plate bearing and cylindrical shear models, as shown in Figure 2.10.

Over the last few decades, research has been conducted in the field and laboratory to determine the behavior of helical piles (Lutenegger 2009; 2011, Prasad and Rao 1996, Rao et al. 1991; 1993, Rao and Prasad 1993, Mooney et al. 1985). However, much of the research was conducted in remolded materials rather than natural soil deposits; this limits the application in natural soil deposits, which exhibit the soil structure relevant to field behavior. Lutenegger (2009) evaluated the differences between laboratory and field behavior. Based on the field investigation, in which helical anchors were tested with plate spacing ranging from 0.75 to three diameters, Lutenegger (2009) determined that there was no distinctive transition from individual plate bearing to cylindrical shear behavior. This contrasted the suggestions of previous research, that a transition from cylindrical to individual should occur at a S/D equal to 2.25. Lutenegger (2009) concluded that the difference may be related to installation disturbance and reduction in mobilized shear strength.

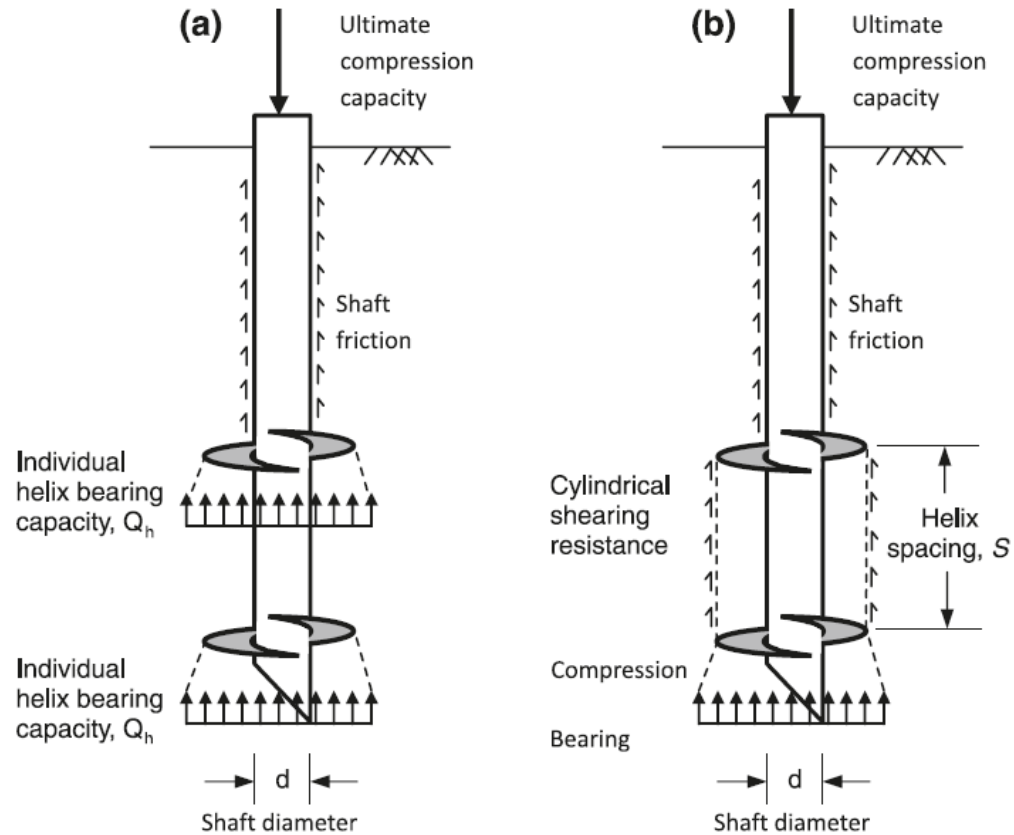


Figure 2.10 Conceptual sketches showing the assumed shearing mechanisms for (a) individual plate bearing and (b) cylindrical shear.

2.3.1 Individual Plate Bearing

The individual plate bearing capacity analysis for compressive loading treats each helical plate as an individual member that bears on the soil at the corresponding plate elevation. This assumes that each helical bearing plate displaces the soil in a deep failure mode. Each plate is anticipated to produce a uniform pressure distribution at the base of the plate, and the anchor is assumed to generate shaft resistance along the length of the shaft. The bearing capacity is equal to the sum of the individual

bearing capacities of all of the individual plates and resistance along the shaft, as shown in Figure 2.9. Mooney et al. (1985) proposed the following equation for individual bearing in fine-grained cohesive soils:

$$R_u = \sum_{i=1}^n A_i s_{ui} N_{cu} + P_{shaft} H_{eff} C_\alpha \quad 2.1$$

where A_i equals the area of the i^{th} bearing plate, s_{ui} equals the undrained shear strength at the i^{th} bearing plate, N_{cu} equals the uplift capacity factor, P_{shaft} is the perimeter of the shaft, H_{eff} equals the shaft length above top helix, and C_α equals the unit shaft resistance. Suction below the bottom helix is neglected due to minimal contribution to overall capacity. Note: the uplift capacity factor is used for both the bearing and uplift.

The N_{cu} value is a function of the ratio between the depth of embedment and the diameter (H/D) of the helical plate, and has been back-calculated using various field and laboratory tests. As indicated in Figure 2.11, the uplift capacity factor, N_{cu} , levels off as the H/D reaches a value of five. This indicates that deep anchors approach a condition with N_{cu} approaching the common theoretical bearing capacity N_c used with traditional deep foundations (Mooney, 1985). The uplift capacity factor is commonly estimated to be equal to the theoretical value of $N_c = 9$, however Mooney et al. (1985) recommends an average N_{cu} of 9.4, shown in Figure 2.11.

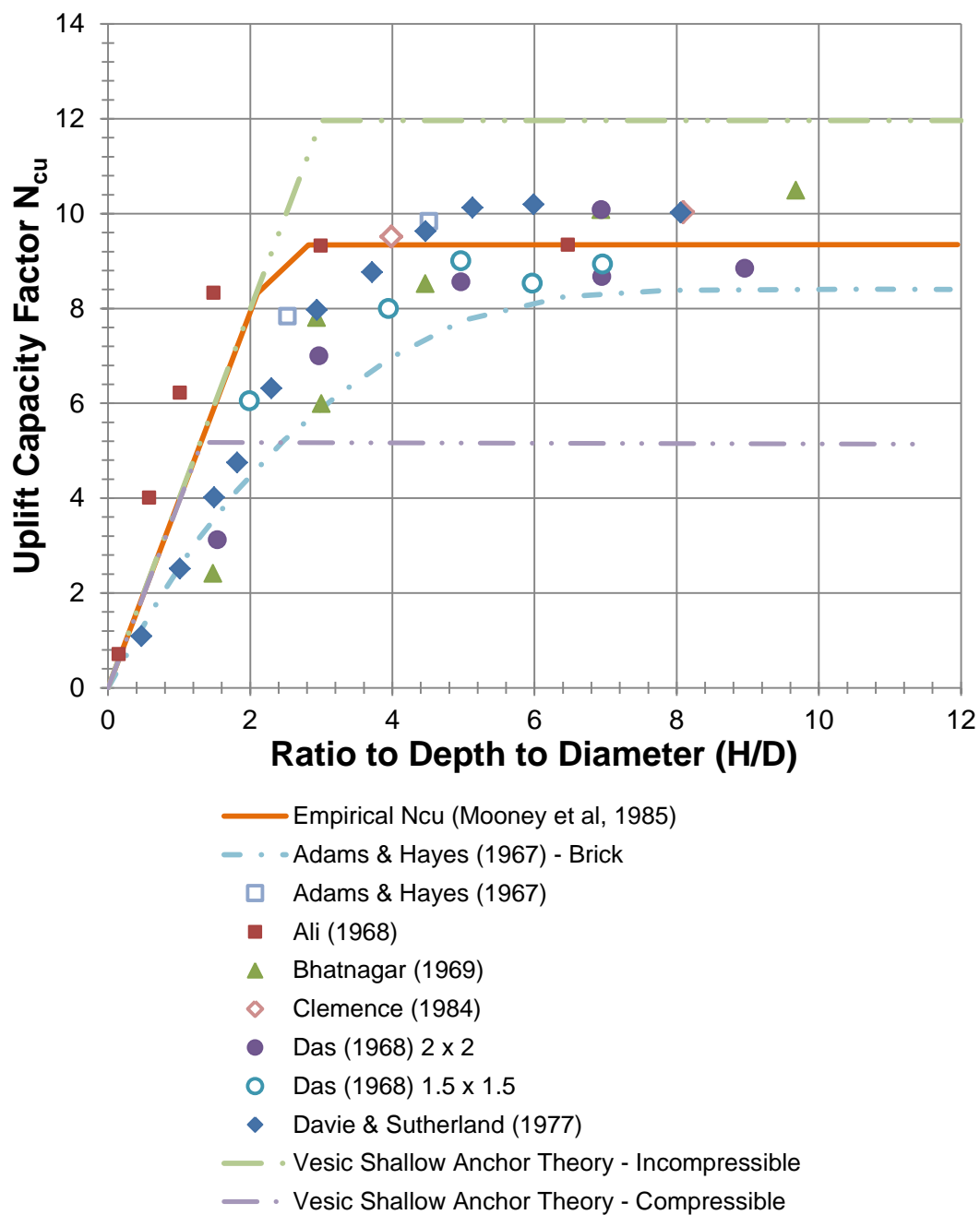


Figure 2.11 Uplift capacity factor, N_{cu} (data from Mooney et al., 1985).

2.3.2 Cylindrical Shear

Mooney et al. (1985) found that individual plate bearing was not always the governing limit state and recommended that a cylindrical shear model should be used to predict axial capacity for compression elements. In the cylindrical shear failure mode, the shear strength of the soil along the surface of the presumed cylinder between helical bearing plates is assumed to mobilize. It is assumed that a uniform pressure distribution develops under the lead helical plate and the rest of the plates are encased in the assumed cylindrical envelope. In this method, it is assumed that adhesion acts along the shaft of the piling above the top plate. The ultimate resistance for this failure mechanism is given by Mooney et al. (1985):

$$R_u = A_t s_u N_{cu} + \pi D_{avg} s_u (H_f - H_i) + P_{shaft} H_{eff} C_\alpha \quad 2.2$$

where A_t is the area of the lead helical bearing plate, D_{avg} is the average helix diameter, H_f is the depth to the lead (in bearing the lead is the bottom helical plate) and H_i equals the depth to the top helical plate. The difference between H_f and H_i is defined as the length of the cylinder over which the undrained shear strength is mobilized. All of the other variables are previously defined for the individual bearing capacity, Equation 2.1, in Section 2.3.1.

2.4 PULLOUT CAPACITY ANALYSIS

The theories developed for pullout or uplift capacity are similar to those for bearing capacity. The analysis of resistance has been adapted to account for the plate resisting the upward motion of the anchor. The following section addresses the estimation of helical anchor capacity in uplift for individual plate uplift and cylindrical shear.

2.4.1 Individual Plate Uplift

The individual plate uplift capacity estimation method assumes that failures occur concurrently above all of the bearing plates on an anchor. Therefore, it is anticipated that the uplift capacity of the anchor is equal to the sum of the resistances of the helical plates. Additionally, the resistance along a round pipe shaft may be included, as shown in Figure 2.12.

$$R_u = \sum_{i=1}^n A_i S_{ui} N_{cu} + P_{shaft} H_{eff} C_\alpha$$

2.3

where all variables have been defined previously. Uplift capacity developed along square shafts is not incorporated, as will be described in more detail below.

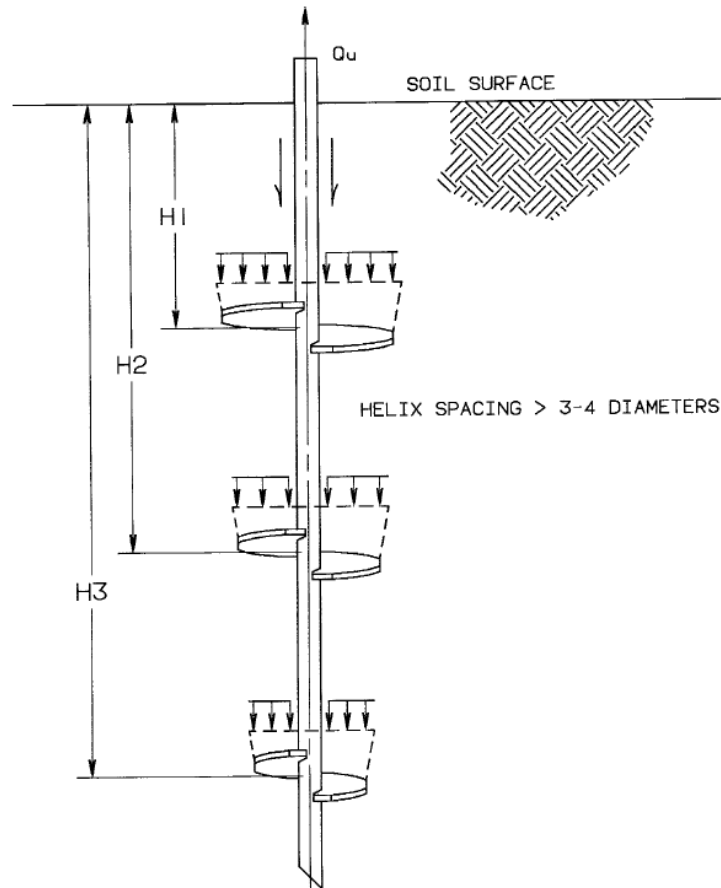


Figure 2.12 Conceptual sketch of assumed mechanism for individual plate breakout in uplift (Lutenegger, 2009).

2.4.2 Cylindrical Shear Uplift

The cylindrical shear method for determining uplift resistance assumes that the plates and the soil between the plates will act as a cylinder as previously described in Section 2.3.2 for bearing capacity analyses. The uplift resistance is assumed to take on the same characteristics of failure as bearing capacity. However, in uplift, the uppermost plate is referred to as the lead plate, rather than the bottom plate. The

cylindrical shear mechanism is depicted in Figure 2.13 and the capacity computed using:

$$R_u = A_t s_u N_{cu} + \pi D_{avg} s_u (H_f - H_i) + P_{shaft} H_{eff} C_\alpha$$

2.4

where all variables have been defined in previous sections.

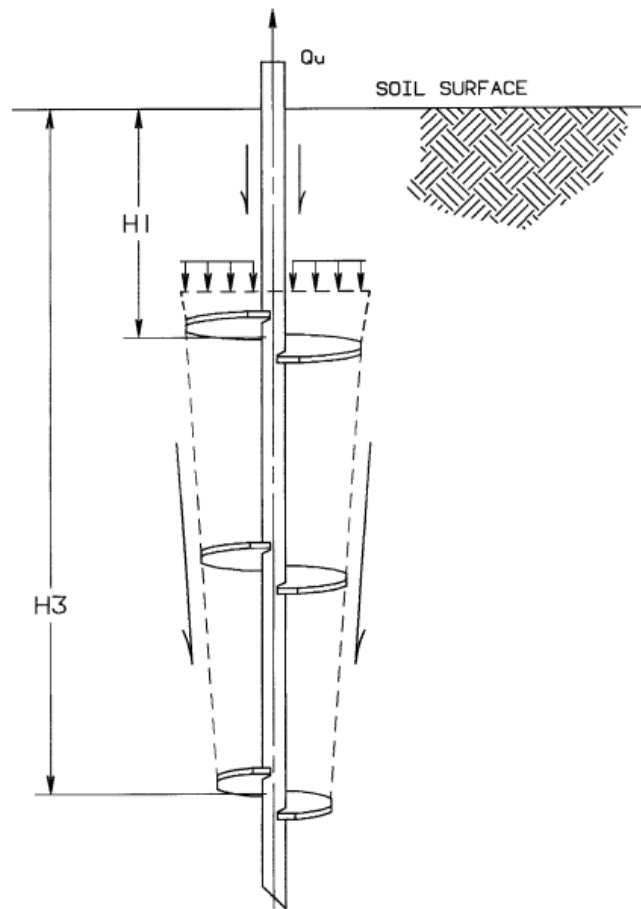


Figure 2.13 Conceptual sketch of assumed mechanism for cylindrical shear in uplift (Lutenegger, 2009).

2.5 TORQUE BASED ANALYSIS

The installation torque of a helical pile or anchor has been used to evaluate the anchor capacity. The process of the helical bearing plate cutting through soil is similar to a plate penetrometer; therefore the capacity of an anchor can be determined by analyzing the torque required for the installation. Installation torque-based capacity estimation methods have aided in increasing popularity of helical foundation systems. These methods allow for a simple way to verify that a helical pile or anchor has been installed to an appropriate depth.

In the torque-based method, the uplift capacity is a function of the torque during installation and an empirical factor, given by Hoyt and Clemence (1989), and shown in Equation 2.5. In this equation T is simply the torque applied, and K_t is the empirical factor. For all square shafts, and round shafts less than 3.5 inches in diameter, K_t is equal to 10 ft^{-1} . For round shafts 3.5 inches in diameter K_t is equal to 7 ft^{-1} , and for 8.63 inches in diameter round shafts the factor is 3 ft^{-1} .

$$Q_u = K_t * T \quad 2.5$$

The relationship between torque and capacity has been used as a rule of thumb for decades, however, data was kept proprietary and absent from reports until the late 1970's (Perko, 2009). Hoyt and Clemence (1989) compared actual and calculated capacities to determine the accuracy of the torque method. The individual plate bearing, cylindrical shear, and torque correlation methods were statistically analyzed

by Hoyt and Clemence (1989) and exhibited wide capacity variability. Hoyt and Clemence (1989) determined that torque correlation yielded the most consistent results; therefore, the torque method may be used as an independent check of capacity in the field.

2.6 DESIGN CONSIDERATIONS

It is often suggested that analyses of capacity should include both the individual plate bearing and the cylindrical shear methods. The lowest capacity between the two should then be used as the estimated capacity. Prasad et al. (1993) concluded that the spacing of helical plates control load carrying capacities in clays. The study consisted of testing four model anchors in remolded clays in the laboratory. Prasad et al. (1993) found that piles with anchor spacing ratios greater than 1.5 the failure surfaces acted individually, not cylindrically.

Lutenegger (2009) researched the transition from individual plate bearing to cylindrical shear and found that multi-helix anchors with plate spacing ranging from 0.75 to three helical plate diameters displayed no transition from cylindrical shear to individual plate bearing. Furthermore, Rao et al. (1993) suggested that the individual plate bearing method should be corrected for spacing ratios greater than 2 to take the spacing of the helical bearing plates into account. According to their research, done on experimental model piles in soft clays, the current individual bearing method gives a nominal underestimate of capacity (Rao, et al., 1993).

Another consideration is the effect of square shafts. Due to the rotation during installation, the adhesion is neglected in anchors with square shafts as shown in Figure 2.14. The rotation of the shaft produces a void surrounding the square bar, such that only the corners of the shaft are in contact with the surrounding soil immediately following installation. However, it should be noted that adhesion is often neglected for all shafts to add a small amount of conservatism to the overall design.

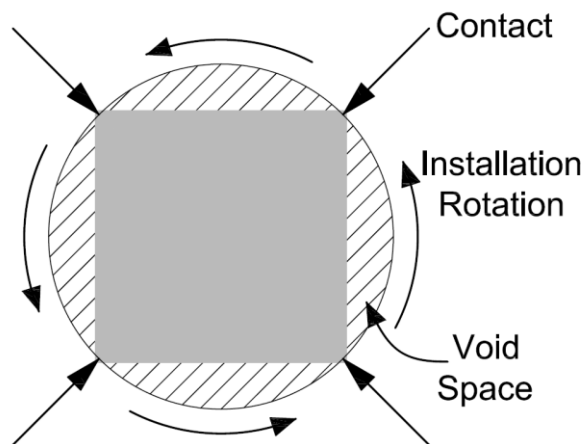


Figure 2.14 Square bar installation cross section depicting void space between bar and soil due to installation rotation; adapted from (Pack, 2006).

Displacement is an important issue to address in the design of all foundation elements. Helical piles designed with a factor of safety of at least 2.0 generally exhibit acceptable displacements when installed in a competent soil site; however, a competent soil is difficult to define, therefore requiring good engineering judgment. Still, some structures are extremely sensitive to displacement and require limitations to the total allowable movement. For sensitive systems, the allowable load of the helical

piles must be reduced to prevent the extent of deflection from exceeding the allowable deflection. The allowable deflection may affect not only the capacity requirements of the helical anchors, but also the number of anchors that are installed.

Current design methods do not account for allowable deflection or displacement; instead anchors are tested to determine the amount of displacement that occurs over a given load. With current designs hinging on the allowable deflection of the structure, engineers may overlook helical foundations, due to time constraints and limited funding during early design work which limits the ability to complete full scale testing.

2.7 SUMMARY OF LITERATURE REVIEW

The three methods that are currently used for design and analysis of helical anchors, individual plate bearing, cylindrical shear, and the torque based method, have been in use for years. These methods could benefit from new research and analysis to increase the statistical accuracy of the approaches. With enough load test data a new Load Resistance Factor Design, or LRFD, style design method could be established to incorporate the variability that is inherent in geotechnical projects. Design requirements for all types of structures are becoming increasingly more stringent and critical, therefore it is inevitable that design methods need to be updated as the technology and knowledge evolves.

Furthermore, there is a complete lack of displacement-based helical anchor design, and therefore there is a need for research in the displacement behavior of helical anchors, particularly in cohesive soils. The current helical industry is largely narrowed to a group of proprietary companies that have private databases of load tests, and experiences, which are used to increase the accuracy of helical designs. However, most installations in areas where helical foundations have not commonly been used involve testing a majority of the anchors installed to ensure required capacities are met. With improved design procedures, testing requirements could be decreased, resulting in decreased design and system costs overall.

3 RESEARCH OBJECTIVES

3.1 OBJECTIVES OF THIS STUDY

The objective of this study is to improve the ability to predict the capacity and displacement behavior of helical anchors in cohesive soils. Specifically, the objectives include:

1. Evaluation of the breakout (i.e., uplift) capacity and displacement behavior of plate anchors in cohesive soils;
2. Estimation of the side shear capacity and displacement behavior associated with multi-helix anchors;
3. Generation of a combined side shear and plate breakout model for the prediction of helical anchor capacity with respect to displacement;
4. Comparison of capacity predicted using the combined model to that predicted using the standard cylindrical shear and individual plate bearing capacity models; and,
5. Characterization of the uncertainty associated with the new methods of prediction for helical anchor capacity.

3.2 RESEARCH PROGRAM

The research program performed for this study, to achieve the objectives outlined above, includes:

1. Development of a load test database comprised of well documented tests of helical anchors in cohesive soils (Chapter 4);
2. Evaluation and statistical characterization of the uplift capacity factor, N_{cu} , back-calculated from load test data (Chapter 5);
3. Development of an uplift capacity model (Chapter 5);
4. Evaluation of the accuracy and uncertainty associated with the proposed and existing uplift capacity models (Chapter 5);
5. Development of a displacement prediction model using normalized single and multi-plate load curves (Chapter 6);
6. Comparison of the proposed displacement models with load tests from the load test database (Chapter 6);

4 LOAD TEST DATABASE

This Chapter discusses the data used in the analysis of helical anchor performance. These load tests were conducted and documented by other parties. Therefore, further information on the load testing can be found in the referenced documents. To develop and evaluate a displacement based analysis, including side shear for helical anchors, load test data from single plate and multi-plate uplift tests were analyzed.

4.1 SINGLE PLATE PULL OUT TESTS IN CLAY

Through previous research on helical anchors, it has been noted that the individual helical plates behave in the same manner as a straight-plate anchor when the spacing of the helical anchors is larger than three times the diameter of the preceding plate. Similarly, in cylindrical shear, the top helical plate also behaves like a plate anchor. Therefore, plate breakout behavior for anchors in uplift loading developed in this research was based on plate anchor load tests performed in clay.

4.1.1 Laboratory Model Test Description

Ali (1969) performed vertical uplift testing on five plate anchors in soft bentonite clay. The testing was performed in remolded clay samples in the laboratory at Duke University. Each anchor consisted of a flat circular steel plate 6 mm ($\frac{1}{4}$ inch) thick and 75 mm (3 inches) in diameter. The clay was placed in 13 mm ($\frac{1}{2}$ inch) thick

layers in a 762 mm by 762 mm (30 inches by 30 inches) aluminum box, during which time anchors were set in place and balanced. The clay layers were placed with alternating light and dark hues to allow for the observation of failure patterns, as shown previously in Figure 2.7. The dark layers were created by adding lampblack to the bentonite soil.

Once each test setup was completed the model was allowed to rest for 24 hours before testing to allow for thixotropic regain of soil strength. This procedure was followed for each of the single plate load tests. The bentonite clay was classified as highly plastic, having a plastic limit of 59 and a liquid limit of 542 with water content during testing ranging from 285 to 305 percent. Standard axisymmetric triaxial tests were used to determine the average undrained shear strength of approximately 5.2 kPa (0.75 psi) (Ali, 1969).

Uplift testing of the plate anchors commenced following the 24 hour rest period. Loads were applied at five minute intervals in increments of approximately one tenth the expected ultimate load (Ali, 1969). Figure 4.1 presents an image of the experimental setup. The loading apparatus consisted of a steel cable running through a two-pulley system. Lead weights were added to provide incremental loads. Anchor movement was recorded using dial gauges; three were placed to monitor anchor displacement and eight were spaced across the clay surface to detect movement on the soil surface.

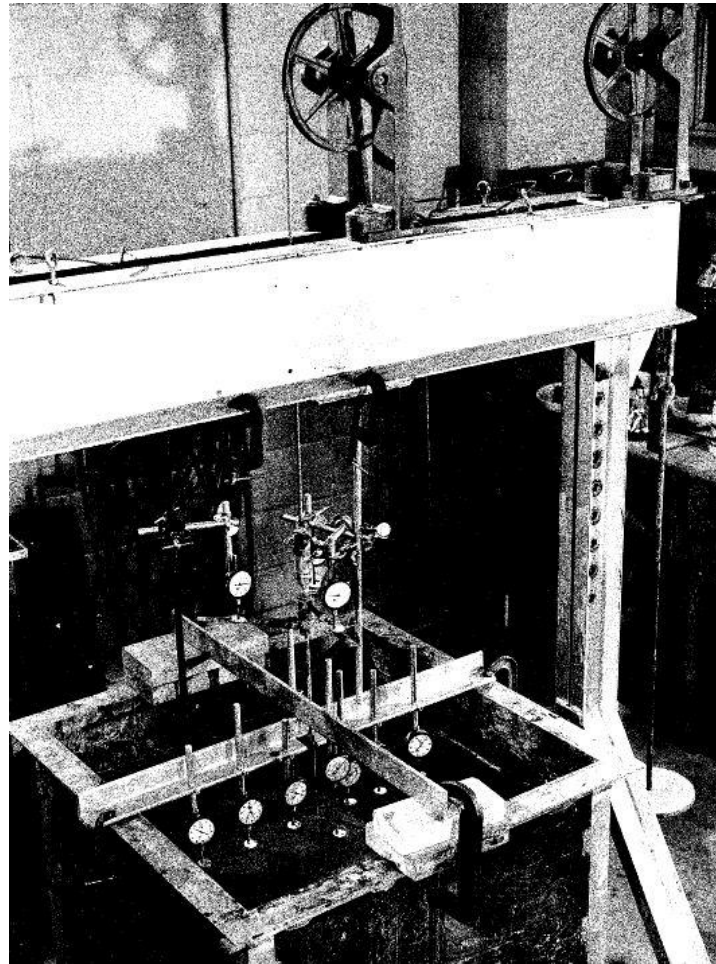


Figure 4.1 Experimental model setup used for load tests of round plate anchors in remolded bentonite clay after Ali (1969).

4.1.2 Results of the Single Plate Pull out Tests

Ali (1969) examined the failure surfaces following testing, and determined that the plates exhibited a cylindrical-type failure up to a depth of one diameter. Thereafter a wedge type failure was observed. This failure mechanism greatly reduced the rate of increase of pull-out capacity with increasing depth. Beyond a depth of embedment of

three plate diameters, and upon reaching the limit state, the anchor moved upward in a constant manner and produced a conical failure wedge immediately above the anchor. The failure pattern observed above the plate was similar to that below model deep foundations loaded in the same bentonite clay (Ali, 1969).

Table 4.1 presents the results of the plate load tests and Figure 4.2 presents the load-displacement curves for each of the five anchors. Anchor A1 was removed from model development due to the lack of data points along the curve and the very small H/D ratio.

Table 4.1 Short term laboratory test results for plate anchors in bentonite clay, where δ_{MAX} is the displacement and Q_{MAX} is the ultimate load; after Ali (1969).

Load Test	H/D	δ_{MAX} (mm)	Q_{MAX} (kN)
A1	0.12	35.6	0.09
A2	0.33	35.6	0.15
A3	1.09	35.7	0.22
A4	3.00	35.6	0.29
A5	3.00	35.6	0.29

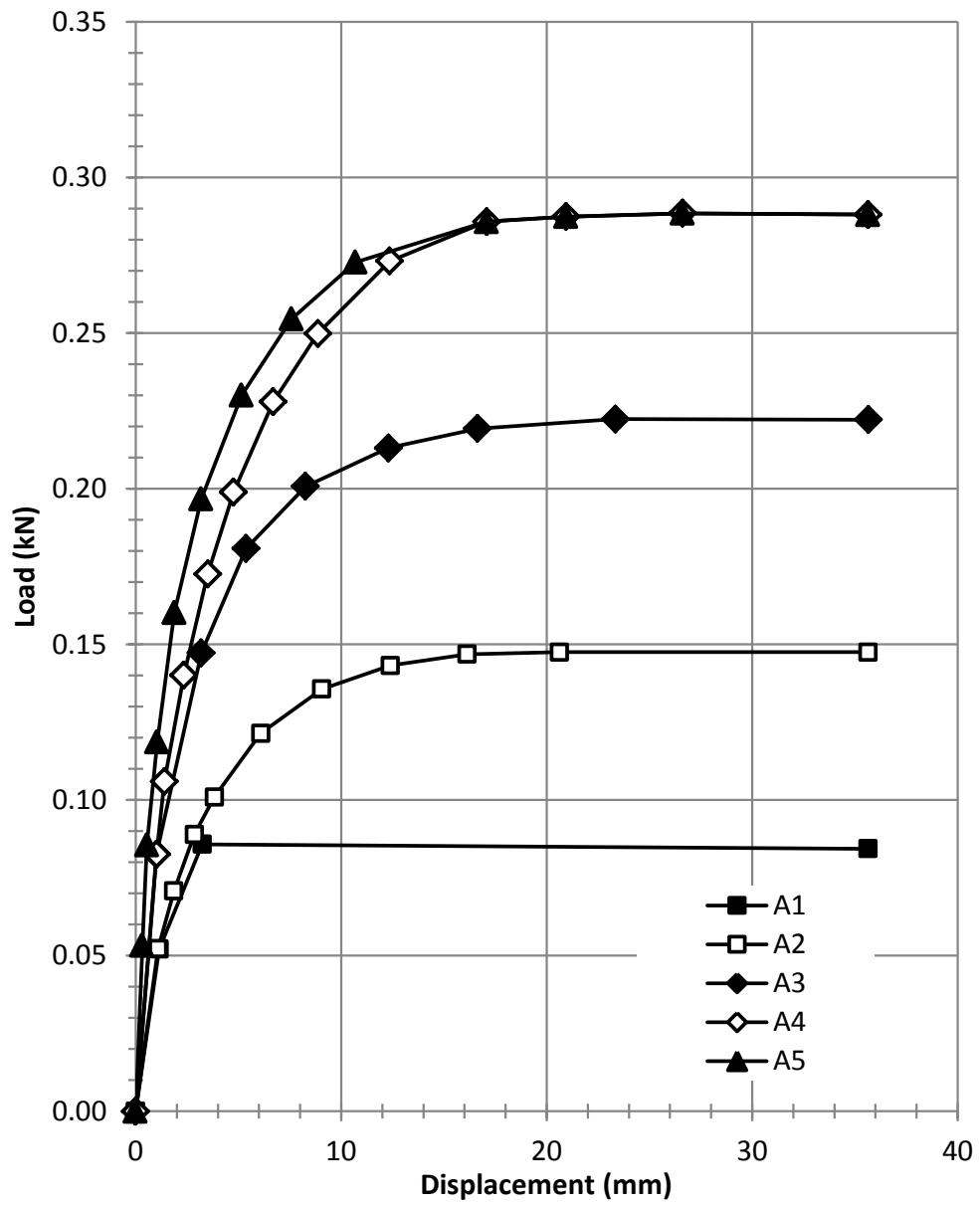


Figure 4.2 Load-displacement curves after Ali (1969), plate anchor laboratory tests in bentonite clay.

4.2 MULTI-PLATE PULL OUT TESTS IN CLAY

Load tests conducted by Clemence (1983) in marine clay were used to establish the multi-helix displacement model. After the model was developed it was used to evaluate and compare with anchor behavior for three other sites.

4.2.1 Marine Clay Site, Massena, NY

The Niagara Mohawk Power Corporation contracted research on the performance of helical anchors in cohesive soil. The research was conducted and documented by Clemence (1983).

4.2.1.1 Site Description

The marine clay site was located near Massena, New York adjacent to Snell Locks. Three Standard Penetration Test (SPT) borings were performed through the center of the test site, along with five Vane Shear Tests (VSTs) at varying depths along the river side of the site. Figure 4.3 presents the site layout published by Clemence (1983). The soil at the site consisted of medium-stiff marine clay deposits, with average undrained soil strength of 24 kPa (3.5 psi). The natural water content was reported as 50.3 percent with a plastic limit of 22 and liquid limit of 62 (Mooney, et al., 1985).

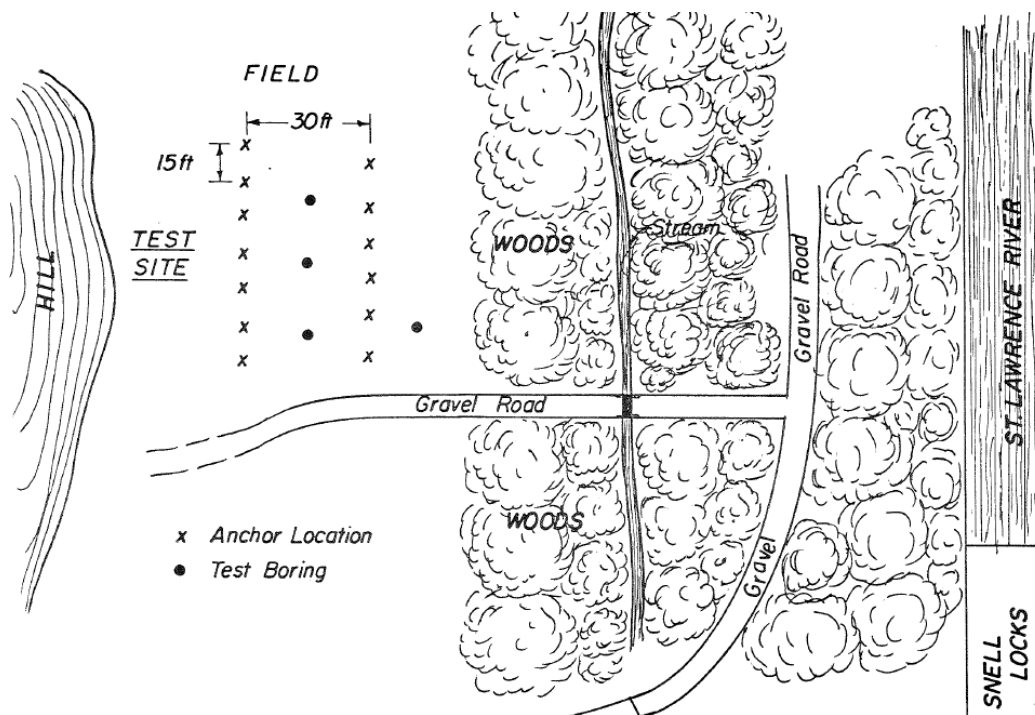


Figure 4.3 Massena, NY site map depicting the anchor and boring locations for the marine clay anchor site; after Clemence (1983).

4.2.1.2 Testing Program

Eight full-scale multi-helix anchors were loaded over a short time interval. The anchor configuration consisted of three plates with diameters of 287 mm (11.3 inches), 254 mm (10.0 inches), and 203 mm (8.0 inches) spaced 914 mm (36 inches) apart along the shaft. Figure 4.4 displays the anchor configuration used in the field at one quarter scale.

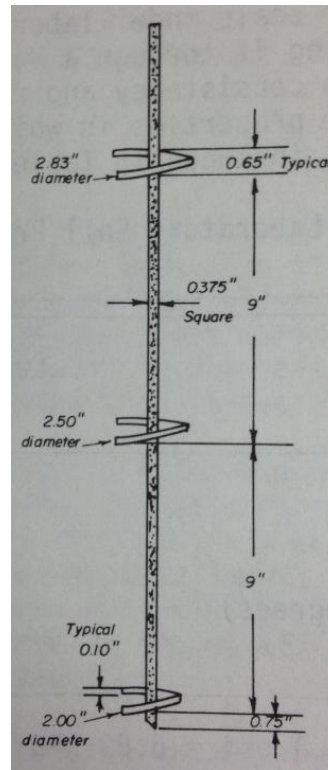


Figure 4.4 Model anchors one quarter scale of field anchors. Scaled anchors were used in laboratory testing; after Mooney (1985).

The anchors were installed using a truck mounted auger system. The installation torque was continuously monitored during the installation. Each anchor was embedded at depth to diameter (H/D) ratio ranging from four to twelve. The final installation torque averaged approximately 0.7 kN-m (500 ft-lbs) (Mooney, et al., 1985). The load tests were performed to failure using a hydraulic jack that reacted against the ground. The rate of loading for the short term anchors was constant and rapidly increased, to induce failure quickly. This was intended to prevent the dissipation of generated pore pressure. Failure was defined by large continuous

deformations under constant load. Table 4.2 presents a summary of the load test results by anchor.

Table 4.2 Short term field load test results for multi-helix anchors in marine clay, where δ_{MAX} is the displacement and Q_{MAX} is the ultimate load; after Clemence (1985).

Load Test	H/D	Torque (kN-m)	δ_{MAX} (mm)	Q_{MAX} (kN)
C1	4	0.68	63.5	53.2
C2	4	0.68	76.2	53.2
C3	8	0.68	76.6	49.4
C4	8	0.54	76.5	51.7
C5	10	0.68	77.2	49.5
C6	10	0.00	76.6	47.2
C7	12	0.68	76.0	49.6
C8	12	0.34	76.0	46.9

4.2.1.3 Results

The load tests exhibited a well-defined failure at displacements ranging from 25 to 50 mm (1 to 2 inches). Table 4.2 is a summary of the load test values for each anchor; the test curves for each anchor are also presented in Figure 4.5. The initial stiffness of the anchors is consistent, with increasing difference in behavior as the strength mobilizes around the plates and failure is reached. This change in behavior appears to be a function of the embedment depth of the anchors, as the embedment (H/D) increased the resistance decreased. Suggesting that the sum of capacities for individual plate bearing is greater (for the anchor geometry investigated) than the capacity from a cylindrical shear mechanism.

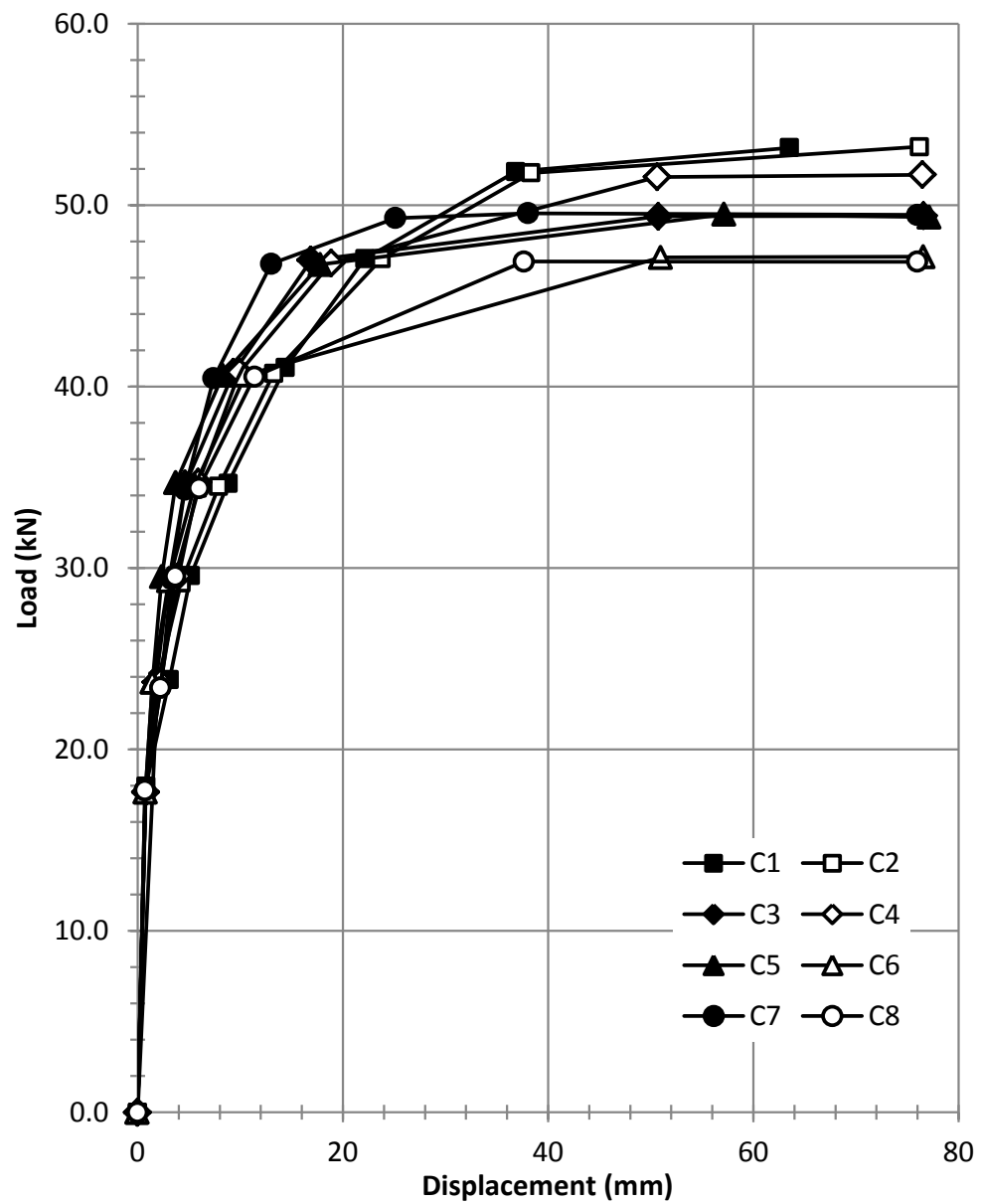


Figure 4.5 Load-displacement curves from Clemence (1983), multi-helix field tests in marine clay.

4.2.2 Oregon State University Soil Test Site, Corvallis, OR

Shipton (1997) and Handojo (1997) reported full scale multi-helix field testing at the OSU field test site in Corvallis, Oregon. Axial tensile and/or axial cyclic loading was conducted on 22 helical anchors spaced across the site. Of the 22 anchors tested only one, Anchor 17, was embedded in clayey silt, as a result of the natural soil stratigraphy. Anchor 17 will be referred to as H1 for the remainder of this work.

4.2.2.1 Site Description

The OSU field research site has been used for many geotechnical studies, and as a result the site stratigraphy has been well documented. The exploration completed by Handojo (1997) and Shipton (1997) characterized the soil in the embedded plate zone for anchor H1 as a very stiff brown clayey silt, underlying the Upper Willamette Silt formation. Figures 4.6 and 4.7 present the boring log that was used in the determination of the soil stratigraphy and properties and the site layout. The average undrained shear strength where Anchor H1 was embedded was approximately 79 kPa (11.5 psi). The water content was reported as 39 percent, with a plastic limit of 34 and a liquid limit of 53 (Shipton, 1997).

Boring Log
 project Helical pier investigation location Hinsdale Wave lab inspector Brett Shipton
 job no 1 date 8/23/96 elevation (top) 240 ft drill rig mud rotary
 hole no 1 time started 10:30 AM drillers Geo-Tech model CME 55
 time finished 2:40 PM drillers name Date water table N.A.

depth (ft)		soil description	sample depth(top)	blowcounts*	% recovery	type & No.	unified symbol	remarks
from	to							
0	5	very stiff, highly plastic, brown clayey SILT						
5	10	very stiff, highly plastic, brown clayey silt	5	1-3-4	100	SPT #1	MH	
10	13	stiff to very stiff, brown clayey silt with occasional gravel	10		100	shelby #1	MH	
15	18	stiff to very stiff, brown clayey silt with occasional gravel	15		100	shelby #2	MH	
18	22	silty sand and gravel						ground and drill rig vibration
22	25	very stiff gray silt						
25	30	very stiff gray silt	25		20	shelby #3	MH	shelby tube buckled @ 600 lb force.
			25.5	7-11-16	100	SPT #2	MH	
30	32	gray silt and silty sand	30		100	D&M #1	MH	140 lb hammer dropped through 2.5 ft. sample shows soil layer interface
32	35	very stiff gray silt						ground and drill rig vibration
35	41.5	very stiff gray silt	35	7-10-14	100	SPT #3	MH	
			40	5-7-13	100	SPT #4	MH	

* split spoon sampler driven 18" w/ 140 lb hammer falling 2.5' except in the case of the D&M sampler

depth (ft)	Atterberg limits		moisture content (%)	dry density (pcf)	sample no	type of sampler	comments
	LL (%)	PI					
5	75	49.7	32.6		SPT#1	split spoon	
10					shelby #1	shelby	
15					shelby #2	shelby	
25					shelby #3	shelby	refusal @ 6"
25.5	97.5	40.7	61		SPT#2	split spoon	
30	86.5	42.9	46.3		D&M#1a	D&M	soil layer interface
30			42.96		D&M#1b	D&M	interface
35			40.35		SPT#3	split spoon	
40	84.5	38.8	46.25		SPT#4	split spoon	

Figure 4.6 Soil boring log at the OSU Geotechnical Field Research Site, as published by Handojo (1997).

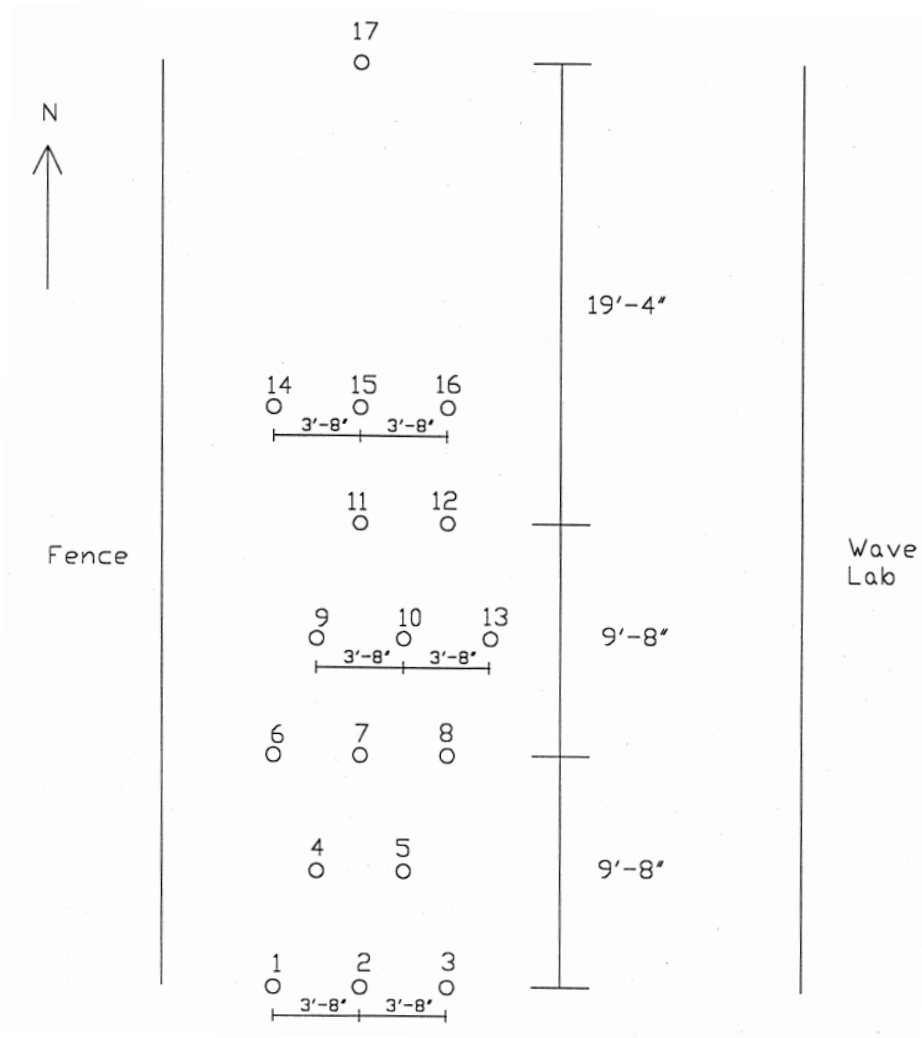


Figure 4.7 Anchor layout on the OSU Field test site; after Handojo (1997). Note: Anchor 17 is H1.

4.2.2.2 Testing Program

H1 was loaded in axial tension using a hydraulic jack and load frame configuration shown in Figure 4.8. Load increments were added when the movement of the anchor slowed to a rate between 0.0254 and 0.0762 mm (0.001 and 0.003

inches) in four to six minutes. The failure criterion was defined as continuous, large deformation under constant load (Handojo, 1997).

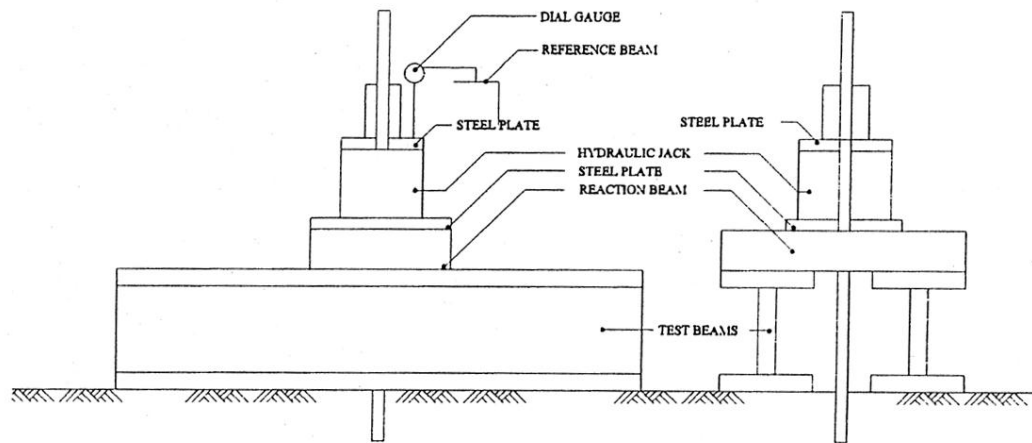


Figure 4.8 Experimental load frame configuration for axial tensile load testing after Handojo (1997).

4.2.2.3 Results

During the study by Handojo (1997) and Shipton (1997), H1 was the only anchor determined to be embedded clay soils. The behavior of this anchor differed from those known to be embedded in cohesionless layers, and provided a smaller uplift capacity. The load-displacement curve from the single anchor tested in cohesive soil is presented in Figure 4.9. The research concluded that the type and strength of the soil where the helical anchor was embedded governed the uplift capacity, and recommended that field tests be performed to validate designs calculated by means of the cylindrical shear method and torque capacity.

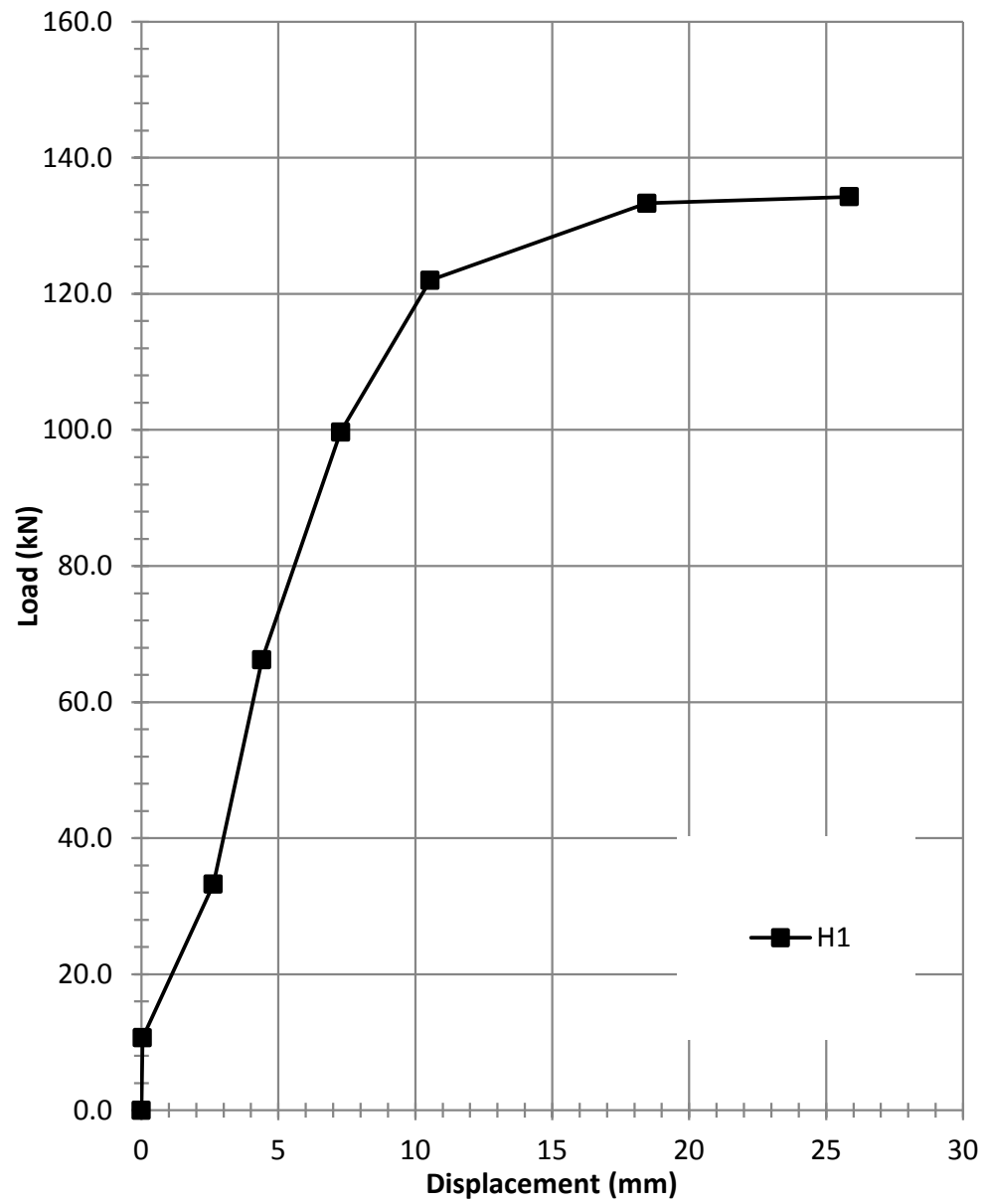


Figure 4.9 Load-displacement curve from Handojo (1997), multi-helix field test in clayey silt.

4.2.3 Beaumont Clay Site, Baytown, TX

Stuedlein (2008) reported the use of helical anchors to provide the reaction for research on test footings near Baytown, Texas. Figure 4.10 presents one of the test footings and experimental setup. The helical anchors were used as reaction anchors for load testing of spread footings on aggregate pier reinforced clay. During the testing it was observed that some of the helical anchors were exhibiting large displacements. The anchors reported here were monitored during the investigation, which allowed for the load-displacement curves to be reported. Seven helical anchors were tested and load-displacement performance documented. Four of the seven anchor tests exhibited clear ultimate resistances.



Figure 4.10 Load test setup for a large footing after Stuedlein (2008), using helical anchors as reaction.

4.2.3.1 Site Description

The test site was located in the Beaumont Clay formation, consisting mainly of desiccated tan and brownish-red clay (Stuedlein, 2008). An extensive exploration program was conducted using both Standard Penetration Testing (SPT) with Shelby tube sampling and Cone Penetration Testing (CPT) throughout the site. The in-situ data was used to create a subsurface model at the testing locations by means of kriging, a geostatistical technique used to interpolate values from the test location to adjacent locations (Stuedlein et al., In Press). Figure 4.11 presents the site layout and Figure 4.12 shows a subsurface cross section, for section A-A' at the test site.

Although the undrained shear strength varied significantly at shallow depths, the kriged Cone Penetration Test results indicated an average undrained shear strength of 93 kPa (13.5 psi) over the depth of interest, where the plates on the helical anchors were embedded. The average natural water content in the lower clay layer was reported as 27.4 percent, along with a plasticity index of 42 and liquidity index of 0.07 (Stuedlein, 2008).

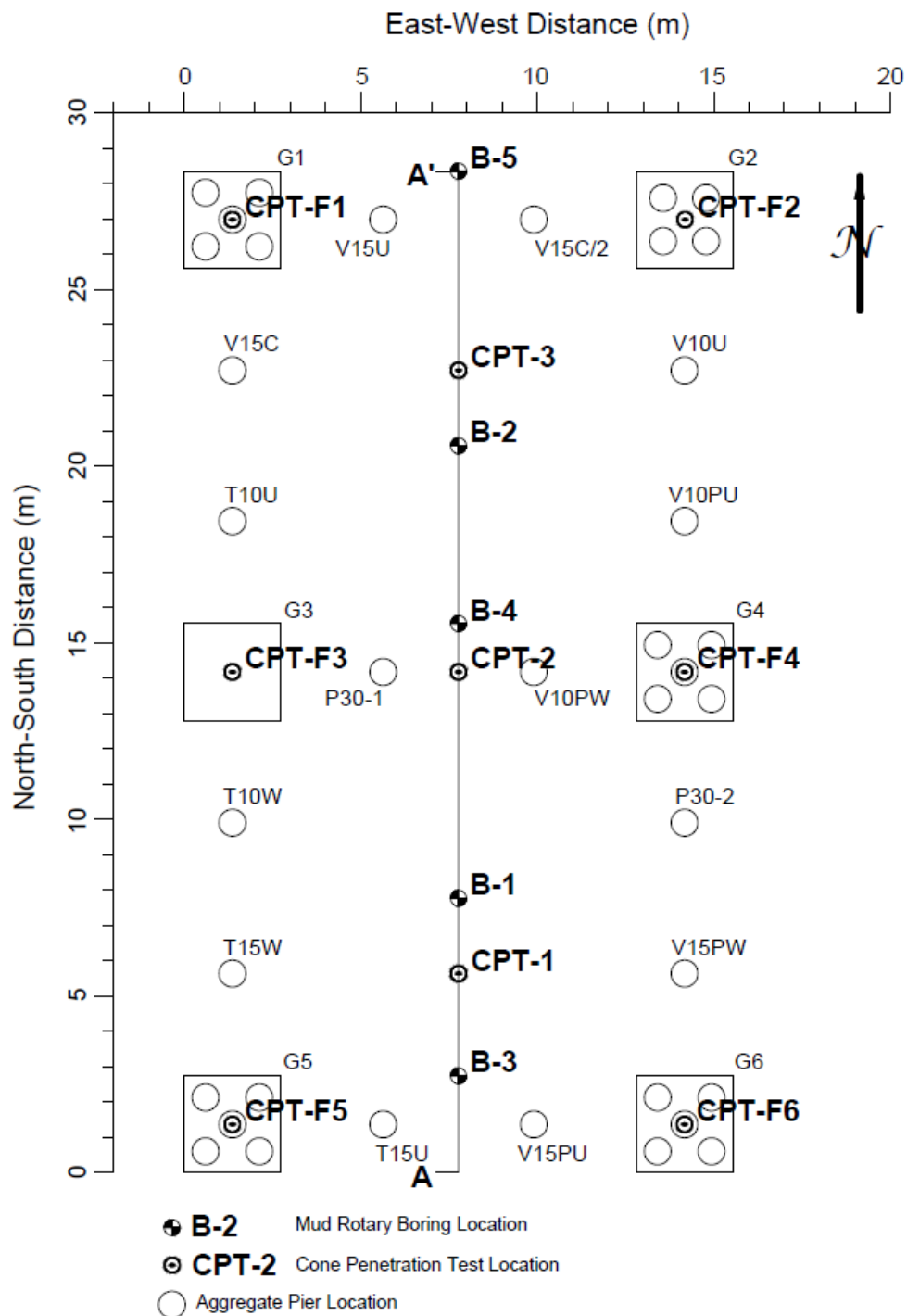


Figure 4.11 Site and exploration layout for load tests; after Stuedlein (2008).

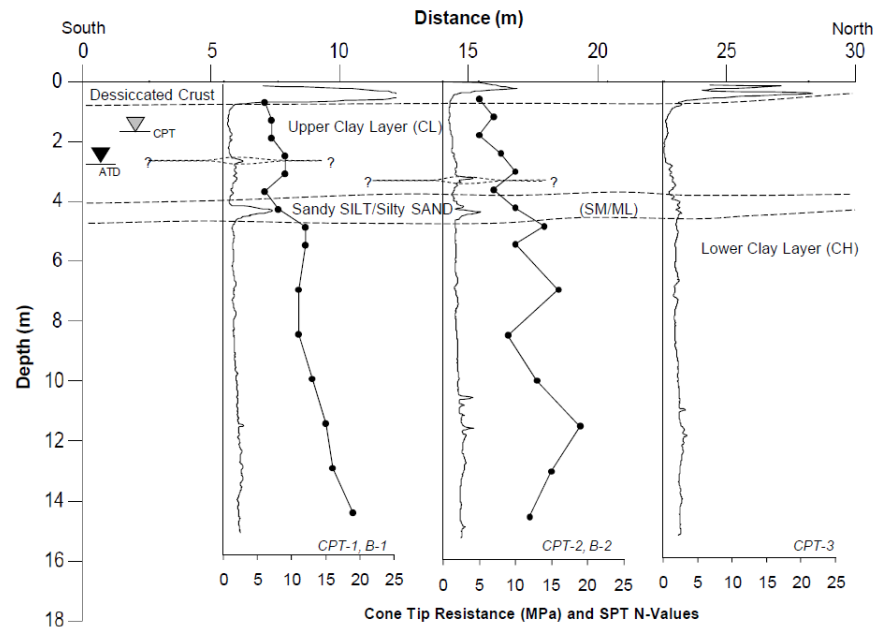


Figure 4.12 Subsurface cross section through section A-A' illustrated in Figure 4.11; after Stuedlein (2008).

Although the soil on the site was found to vary significantly in strength, the kriged data provided estimates for the undrained shear strength at the anchor locations with respect to depth. This allowed the strength parameters used in further calculations to be much more precise than those at the other sites discussed in this chapter, focusing on only the soil profile within the embedded plate zone of the anchors.

4.2.3.2 Results

Seven helical anchors were monitored and reported. Of the seven, two helical anchors were deliberately failed, two helical anchors reached failure accidentally, and three helical anchors were not loaded to failure. The anchors taken to failure reached

an ultimate resistance with less than 60 mm (2.4 inches) of displacement. Table 4.3 presents the load test data; the maximum recorded value is reported for the anchors that did not reach failure.

Table 4.3 Short term field test results for multi-helix anchors in Beaumont clay, where δ_{MAX} is the displacement and Q_{MAX} is the ultimate load. after Stuedlein (2008).

Load Test	H/D	δ_{MAX} (mm)	Q_{MAX} (kN)
S1	18.9	28.1 *	342.1 *
S2	18.9	28.7 *	355.4 *
S3	18.9	131.1	363.9
S4	18.9	27.9 *	358.3 *
S5	18.9	55.6	395.4
S6	18.9	81.3	309.6
S7	18.9	65.9	516.0

* no observed failure, maximum reported value

The bolted connection between different stem sections can produce slack for some anchors, depending on the anchor specific installation procedure. Therefore, there is some movement within the connection that occurs during tensile loading. In order to understand the anchor behavior the slack must be removed from the load curve.

To remove the slack, a line is fit to the initial slope of the load displacement curve as presented in Figure 4.13. The y-intercept of the line is divided by the slope of the line to determine the necessary slack correction, in inches. The corrected

displacement is equal to the measured displacement minus the slack correction. Figure 4.13 shows an example of a load curve before and after a slack correction has been completed. Figure 4.14 and 4.15 present the seven load-displacement curves corrected for anchor slack as required.

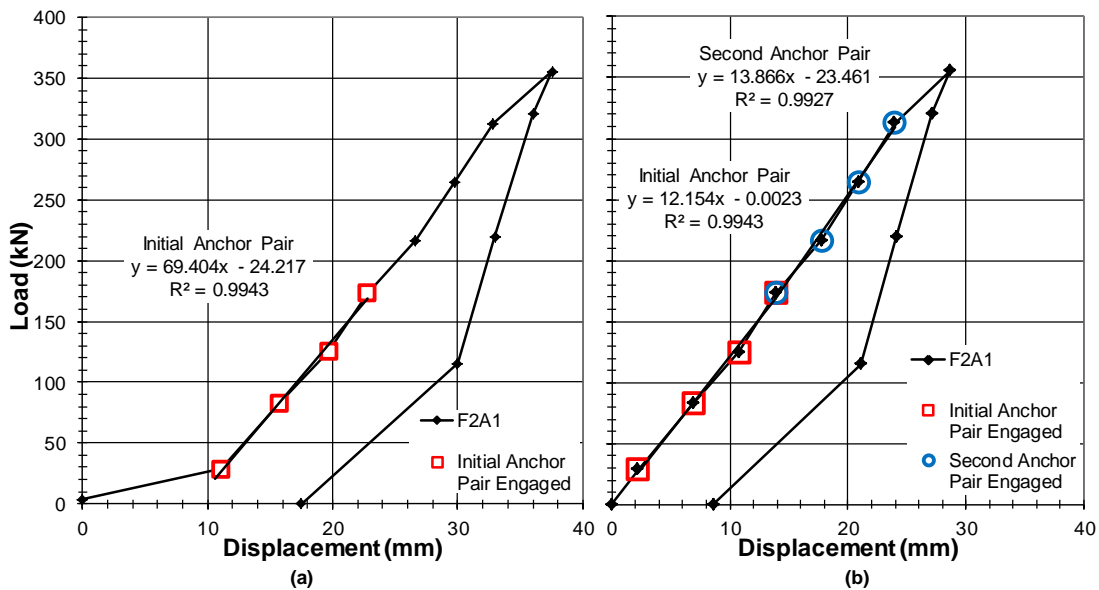


Figure 4.13 Slack Correction on the load test for Anchor S2 (F2A1), (a) Initial slope, or anchor engagement, for the raw load test data (b) Corrected load test data showing initial and secondary anchor engagement.

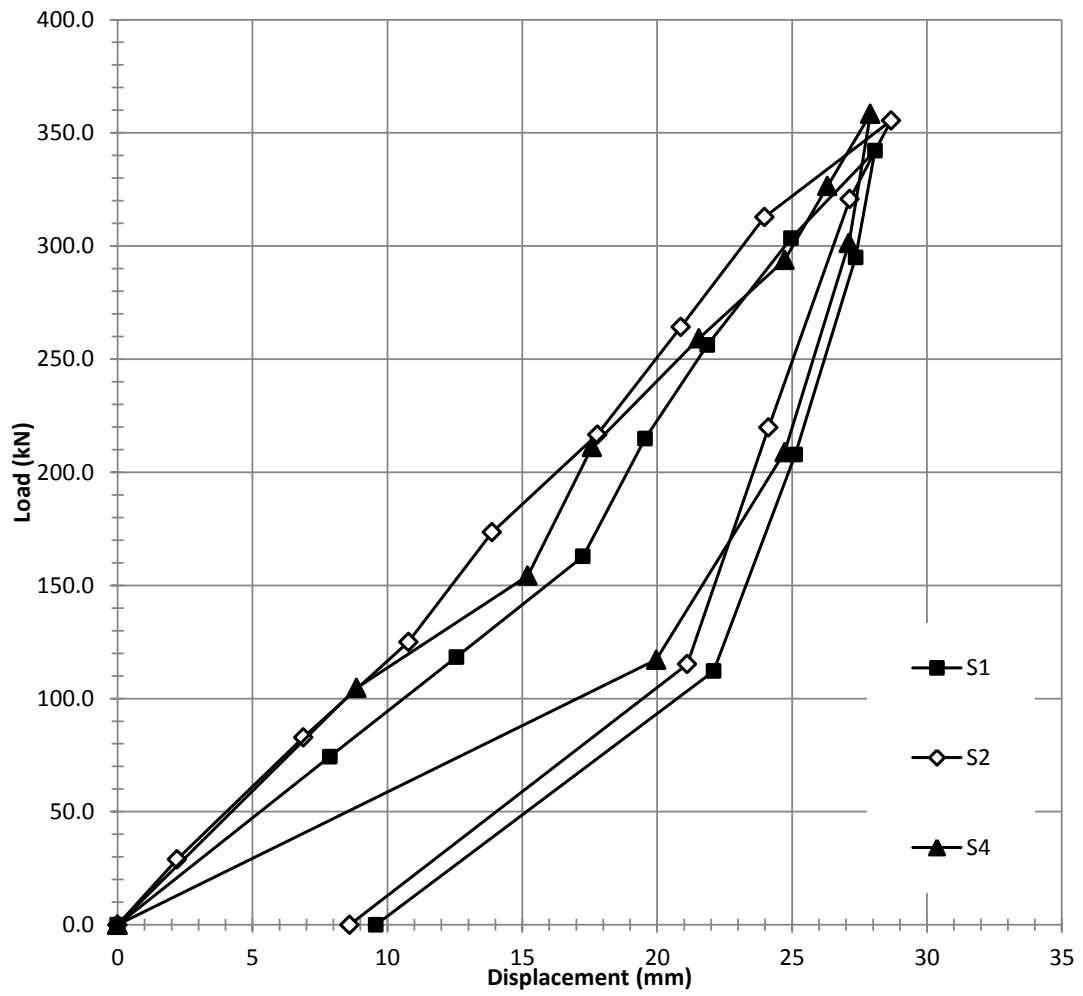


Figure 4.14 Three helical anchors, not tested to failure, used for tensile reaction and monitored during the testing of spread footings on aggregate pier reinforced clay.

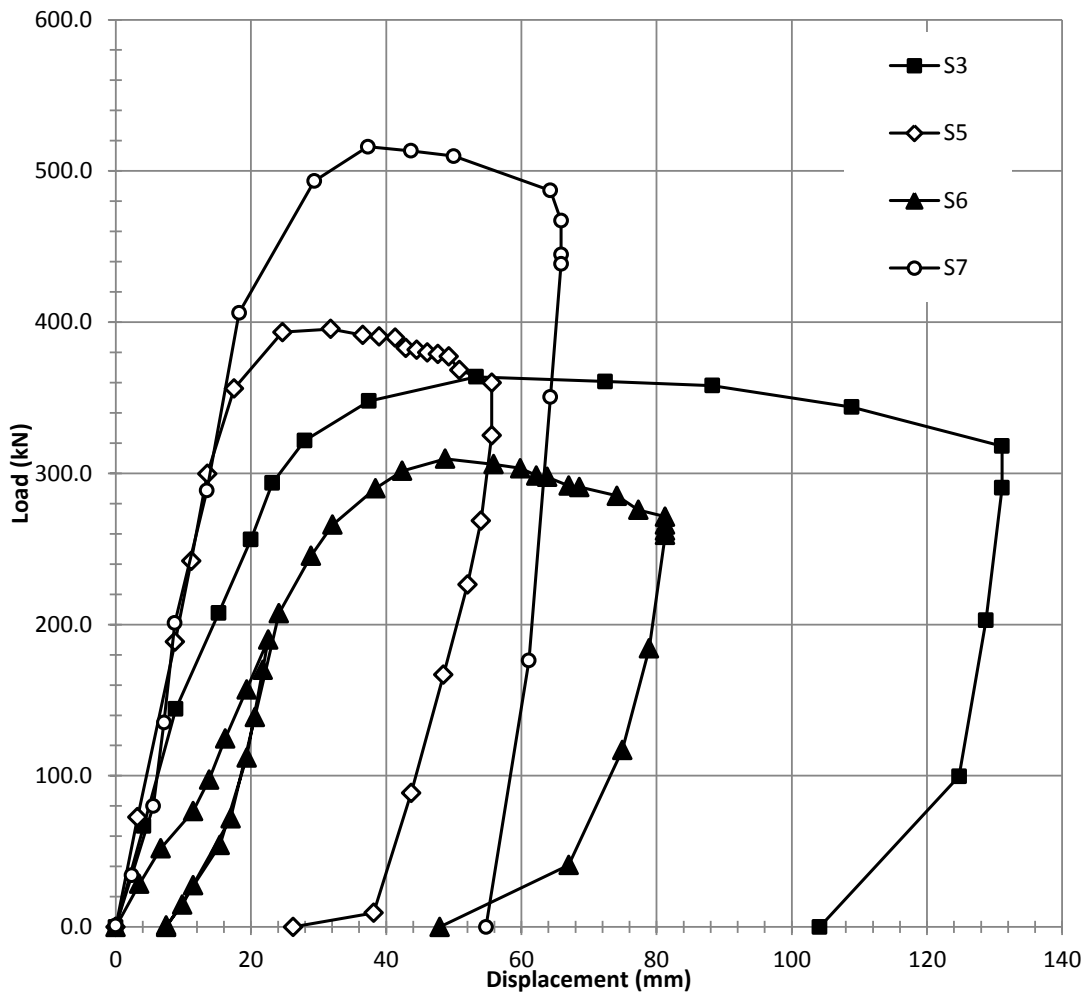


Figure 4.15 Four helical anchors, tested to failure, used for tensile reaction and monitored during the testing of spread footings on aggregate pier reinforced clay.

4.2.4 Varved Clay Site, Amherst, MA

Lutenegger (2009) presented uplift test results on helical anchors in clay. Ten load tests were performed, five at a depth of 3.05 m (10 feet) and five at a depth of 6.10 m (20 feet), with anchor plate spacing, S/D , varied from 0.75 to 3.0. The results of the field testing were then compared to those resulting from laboratory testing

presented in the research of Rao et al. (1991), as well as values calculated using the standard cylindrical shear and individual plate bearing equations.

4.2.4.1 Site Description

The site stratigraphy can be represented by two distinct layers, as presented in Figure 4.16. The layers consist of two meters (six feet) of stiff silty-clay fill over a large deposit of lacustrine varved clay. Field vane tests were conducted at depths of 3.05 meters (10 feet) and 6.10 meters (20 feet), and indicated undrained shear strengths of 191 kPa (29 psi) and 31 kPa (4.4 psi), respectively (Lutenegger, 2009). The characterization also indicated that the deeper clay was sensitive.

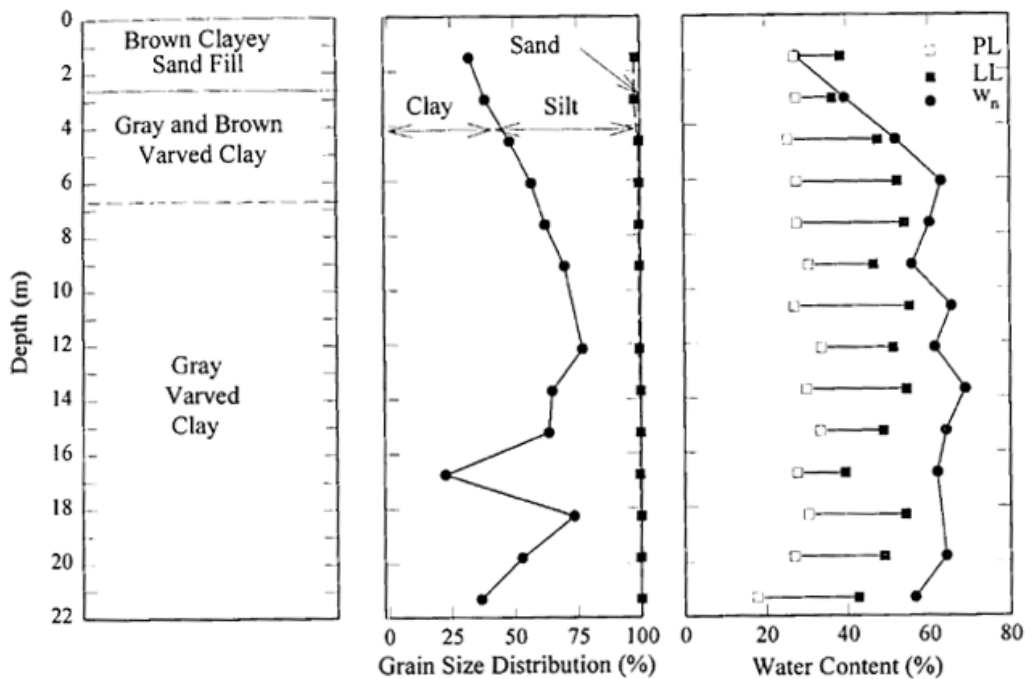


Figure 4.16 Soil Profile and typical variation in soil properties for the national geotechnical experimentation site at the University of Massachusetts; after Lutenegger (2000).

4.2.4.2 Testing Program

Load was applied to the helical anchors using a hydraulic jack placed on top of two reaction beams over wood cribbing, and transferred through a threaded rod. Increments were set to be roughly 10 percent of the estimated capacity and maintained for 15 minutes. This loading scheme allowed a relative displacement of the anchor to reach roughly 20 percent of the helix diameter (40.6 mm or 1.6 inches) in four hours.

4.2.4.3 Results

Only two of the load test curves were published, a summary of the load tests for these two anchors is presented Table 4.4. The load tests were only performed to a relative displacement of 20% of the helix diameter, therefore the two anchors did not reach an ultimate resistance; the maximum observed values are reported. To estimate the likely ultimate resistance, a hyperbolic curve was fit to the data (Kondner, 1963). The extrapolated ultimate is also presented in Table 4.4. The load-displacement curves are reproduced in Figure 4.10, where anchor L1 had spacing between the anchor plates of 304 mm (12 inches), and L2 had spacing between the anchor plates of 1220 mm (48 inches).

Table 4.4 Short term field test results for multi-helix anchors in varved clay, where δ_{MAX} is the displacement and Q_{MAX} is the ultimate load. after Lutenegeger (2009).

Load Test	H/D	S/D	δ_{MAX} [*] (mm)	Q_{MAX} [*] (kN)	Extrapolated Q_{MAX} (kN)
L1	28.50	0.75	57.1	20.0	24.9
L2	24.00	3.00	53.0	29.0	36.7
L3 ^x	27.00	1.13	N/A	27.9	N/A
L4 ^x	26.27	1.50	N/A	18.6	N/A
L5 ^x	24.76	2.25	N/A	22.4	N/A
L6 ^x	12.75	0.75	N/A	37.9	N/A
L7 ^x	12.01	1.13	N/A	38.9	N/A
L8 ^x	11.26	1.50	N/A	51.1	N/A
L9 ^x	9.76	2.25	N/A	55.7	N/A
L10 ^x	8.26	3.00	N/A	73.5	N/A

^x load test not reported

^{*} maximum reported value

Lutenegeger compared the field testing with the behavior found in laboratory model testing previously reported by Rao et al. (1991). The field test results suggested that at least up to a plate spacing of three diameters the anchor will behave in a cylindrical shear manner, with no distinct transition to individual plate bearing. Furthermore, the Rao et al (1991) laboratory results were completed in remolded clay, which is likely to have a low sensitivity not indicative of natural soils (Lutenegeger, 2009).

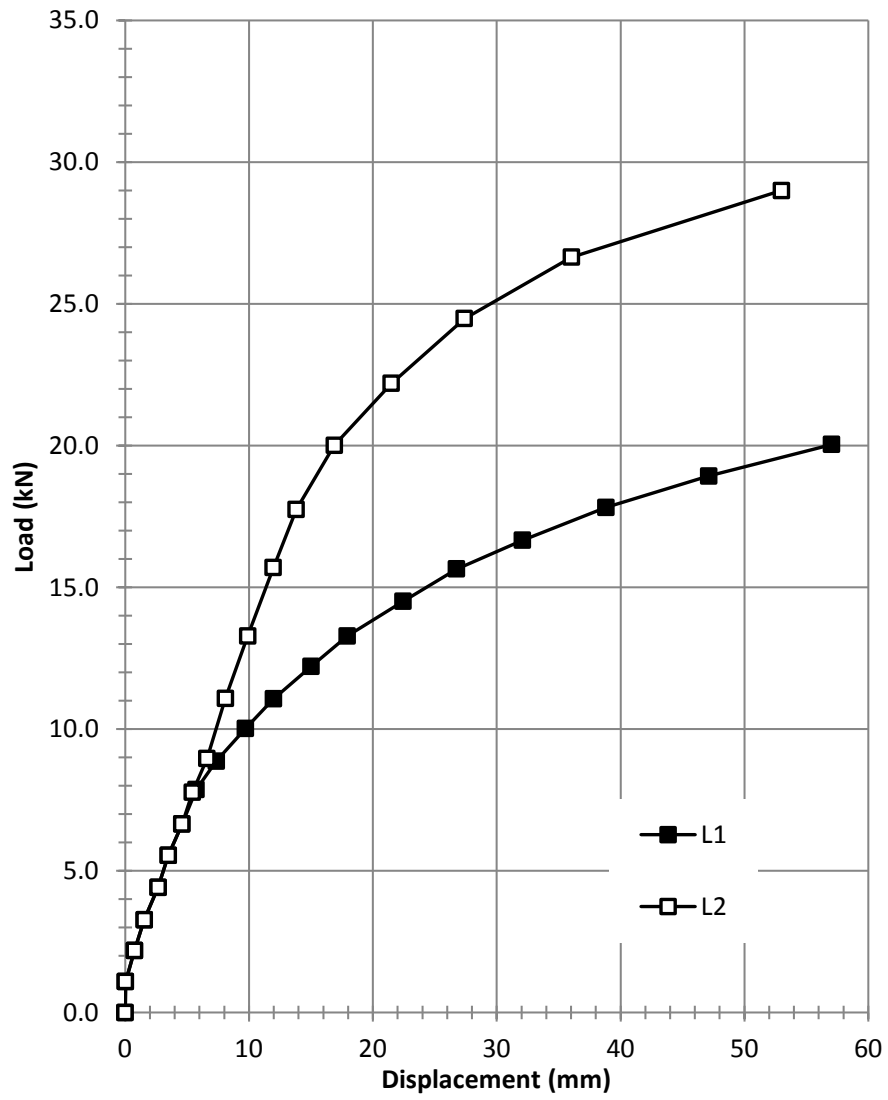


Figure 4.17 Load-displacement curves from Lutenegeger (2009), multi-helix field tests in varved clay.

4.2.5 Laboratory Testing in Clay

Laboratory pullout testing on model helical screw piles was conducted by Rao et al. (1991) and Rao and Prasad (1993). The investigations were intended to develop helical anchors suitable for use in soft to medium stiff clays. A total of 86 uplift tests were performed using 15 different anchors.

4.2.5.1 Laboratory Model Test Description

For Rao et al. (1991), two sets of helical anchors were made of galvanized iron pipes with welded helical plates. The first set of anchors, used in tests P1 through P12, was made up of six anchors; three anchors had a shaft with a diameter of 44 mm (1.7 inches) and plate diameter of 100mm (3.9 inches), and three had a shaft and plate diameter of 60mm (2.4 inches) and 150mm (5.9 inches) respectively. The second set consisted of five anchors, used in tests P13 through P22. These anchors were made with the same plate and shaft diameters. The plate spacing for all of the anchors was varied from an S/D of 4.6 to 0.8.

Similarly, the tests were performed in three different clay soils, with consistency ranging from soft to medium stiff. The average undrained shear strength was measured using a Vane Shear apparatus at 16 different locations within the tank for each test, the average of which was reported as the in-situ undrained shear strength. Table 5.4 presents the estimated properties and the tests that were performed in each soil.

Table 4.5 Estimated Soil properties for the uplift capacity tests performed by Rao et al. (1991).

Soil	Liquid Limit	Plastic Limit	average S_u (kPa)	Test Range
Soil 1	75	25	7.1	R1 - R12
Soil 2	38	16	6.2	R13 - R17
Soil 3	65	23	13.5	R18 - R22

The clay was placed in 50mm (2 inch) thick lifts in an 800mm by 800mm (31.5 inch by 31.5 inch) test tank. The moisture content was varied from 26% to 50.4% depending on the test. Once the tank had been filled a helical anchor was screwed into the soil and left to rest for two days to allow the pore pressures that built up during installation to dissipate before testing commenced. This procedure was repeated for each anchor test.

For tension testing the upward movement was monitored using two dial gauges. The test load was created by a system of two pulley system loaded with cast iron weights; Figure 4.18 presents the experimental setup. The loads were continuously placed until the anchor pulled out of the top of the soil bed; this final load was considered the ultimate pullout capacity.

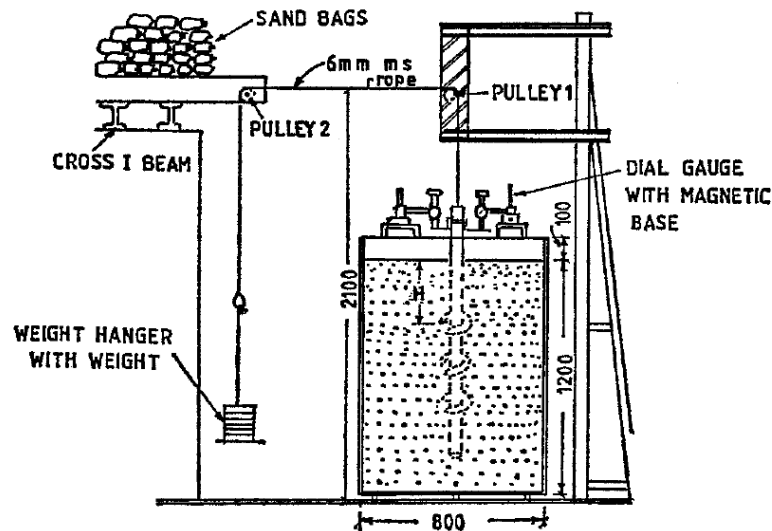


Figure 4.18 Experimental test setup for uplift capacity tests; after Rao et al. (1991).

Rao and Prasad (1993) performed 64 tensile load tests on 4 anchors. A total of 16 tests were performed on each anchor, labeled P1 through P64. The model anchors were made of 13.8 mm mild steel shafts with 33 mm diameter plates. Anchor A1 consisted of two plates spaced at an S/D of 4.5, and A2 had 3 plates spaced at an S/D of 2.3. Anchors A3 and A4 consisted of 4 plates spaced at an S/D of 1.5 and 5 plates spaced at an S/D of 1.1 respectively.

The clay used in the study was marine clay from the west coast of India, with a plastic limit of 32 and a liquid limit of 82. The average undrained shear strength of the soil ranged from 3.0 kPa to 4.4 kPa, measured using an in-situ vane shear test. Placed in a 350 mm diameter cylindrical test tanks in 50 mm lifts, each layer was hand

packed and pressed with a template. Loading was then completed in a similar manner to the tests completed by Rao et al. (1991).

4.2.5.2 Results

Rao et al. (1991) and Rao and Prasad (1993) concluded that helical piles were very useful for resisting uplift forces, showing promise for future helical anchor use. The research indicated that piles with a spacing ratio, S/D , of 1.0 to 1.5 produce a nearly cylindrical failure surface. However, with increasing S/D the resisting area decreased, eventually transitioning from cylindrical shear to individual plate. This difference in the resisting area is presented in Figure 4.19. The reported ultimate resistances are presented in Table 4.6 and 4.7.

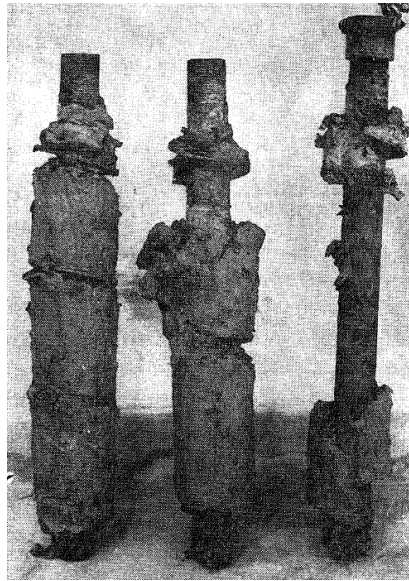


Figure 4.19 Photograph of piles pulled out during the uplift testing. The pictured anchors had S/D ratios, from left to right, of 1.5, 2.3, and 4.6; after Rao et al. (1991).

Table 4.6 laboratory test results for multi-helix anchors in clay, where Q_{MAX} is the ultimate load. after Rao et al. (1991).

Test	No. of Plates	H/D	S/D	Q_{MAX} (kN)
R1	2	4.58	4.58	0.84
R2	3	2.29	2.29	0.97
R3	4	1.53	1.53	1.34
R4	2	4.58	4.58	0.67
R5	3	2.29	2.29	0.91
R6	4	1.53	1.53	0.97
R7	2	4.58	4.58	0.55
R8	3	2.29	2.29	0.63
R9	4	1.53	1.53	0.73
R10	4	3.05	3.05	1.48
R11	5	1.53	1.53	1.67
R12	6	1.02	1.02	1.72
R13	2	6.13	4.00	0.69
R14	3	6.13	2.00	0.83
R15	4	6.13	1.33	0.90
R16	2	6.13	1.67	0.65
R17	3	6.13	0.83	0.71
R18	2	6.13	4.00	1.52
R19	3	6.13	2.00	1.86
R20	4	6.13	1.33	2.13
R21	2	6.13	1.67	1.19
R22	3	6.13	0.83	1.48

Table 4.7 laboratory test results for multi-helix anchors in clay, where Q_{MAX} is the ultimate load. after Rao and Prasad (1993).

Test	No. of Plates	H/D	S/D	Q_{MAX} (kN)	Test	No. of Plates	H/D	S/D	Q_{MAX} (kN)
P1	1	4.5	4.5	0.032	P33	3	1.5	1.5	0.046
P2	2	1	4.5	0.045	P34	4	1	1.5	0.058
P3	2	2	4.5	0.052	P35	4	2	1.5	0.066
P4	2	3	4.5	0.055	P36	4	3	1.5	0.069
P5	2	4	4.5	0.060	P37	4	4	1.5	0.074
P6	2	6	4.5	0.067	P38	4	6	1.5	0.080
P7	2	8	4.5	0.073	P39	4	8	1.5	0.087
P8	2	10	4.5	0.080	P40	4	10	1.5	0.094
P9	1	4.5	4.5	0.052	P41	3	1.5	1.5	0.068
P10	2	1	4.5	0.068	P42	4	1	1.5	0.083
P11	2	2	4.5	0.078	P43	4	2	1.5	0.094
P12	2	3	4.5	0.084	P44	4	3	1.5	0.100
P13	2	4	4.5	0.089	P45	4	4	1.5	0.104
P14	2	6	4.5	0.098	P46	4	6	1.5	0.113
P15	2	8	4.5	0.103	P47	4	8	1.5	0.119
P16	2	10	4.5	0.112	P48	4	10	1.5	0.127
P17	2	2.3	2.3	0.043	P49	4	1.1	1.1	0.046
P18	3	1	2.3	0.055	P50	5	1	1.1	0.059
P19	3	2	2.3	0.062	P51	5	2	1.1	0.066
P20	3	3	2.3	0.065	P52	5	3	1.1	0.069
P21	3	4	2.3	0.071	P53	5	4	1.1	0.074
P22	3	6	2.3	0.077	P54	5	6	1.1	0.081
P23	3	8	2.3	0.083	P55	5	8	1.1	0.087
P24	3	10	2.3	0.090	P56	5	10	1.1	0.093
P25	2	2.3	2.3	0.065	P57	4	1.1	1.1	0.068
P26	3	1	2.3	0.082	P58	5	1	1.1	0.084
P27	3	2	2.3	0.091	P59	5	2	1.1	0.094
P28	3	3	2.3	0.096	P60	5	3	1.1	0.099
P29	3	4	2.3	0.102	P61	5	4	1.1	0.104
P30	3	6	2.3	0.110	P62	5	6	1.1	0.113
P31	3	8	2.3	0.116	P63	5	8	1.1	0.118
P32	3	10	2.3	0.124	P64	5	10	1.1	0.127

4.3 SUMMARY

The load test locations and data included in the helical anchor database were discussed in this Chapter. This includes a description of the soil properties and location of each test site, the procedures established for tensile load testing and how they differ between the locations, and the final documented load tests on helical anchors. For the purpose of this research, only load tests for anchors embedded in well characterized cohesive soils were included. Six sources were accepted, establishing a database of five plate anchors and 18 multi-plate anchor load-displacement curves and 94 capacity results. A summary of the anchor information is presented in Table 4.7.

Table 4.8 Helical anchor load test database summary.

Test	H/D	Depth (m)	B (plate diameter) (mm)					S/D	average S _u (kPa)	δ _{MAX} (mm)	Q _{MAX} (kN)	Reference
			P1	P2	P3	P4	P5					
C1	4.00	2.82	288	254	203			0.92	24.0	63.5	53.2	Clemence (1983)
C2	4.00	2.82	288	254	203			0.92	24.0	76.2	53.2	Clemence (1983)
C3	8.00	3.81	288	254	203			0.92	24.0	76.6	49.4	Clemence (1983)
C4	8.00	3.81	288	254	203			0.92	24.0	76.5	51.7	Clemence (1983)
C5	10.00	4.31	288	254	203			0.92	24.0	77.2	49.5	Clemence (1983)
C6	10.00	4.31	288	254	203			0.92	24.0	76.6	47.2	Clemence (1983)
C7	12.00	4.81	288	254	203			0.92	24.0	76.0	49.6	Clemence (1983)
C8	12.00	4.81	288	254	203			0.92	24.0	76.0	46.9	Clemence (1983)
H1	10.50	5.18	305	254	203			3.60	79.0	25.9	134.3	Handojo (1997)
L1*	27.75	6.10	200	200	200			0.75	31.0	57.1	20.0	Lutenegger (2009)
L2*	23.26	6.10	200	200	200			3.00	31.0	53.0	29.0	Lutenegger (2009)
L3*	27.00	6.10	200	200	200			1.13	31.0	40.0	27.9	Lutenegger (2009)
L4*	26.27	6.10	200	200	200			1.50	31.0	40.0	18.6	Lutenegger (2009)
L5*	24.76	6.10	200	200	200			2.25	31.0	40.0	22.4	Lutenegger (2009)
L6*	12.75	3.05	200	200	200			0.75	191.0	40.0	37.9	Lutenegger (2009)
L7*	12.01	3.05	200	200	200			1.13	191.0	40.0	38.9	Lutenegger (2009)
L8*	11.26	3.05	200	200	200			1.50	191.0	40.0	51.1	Lutenegger (2009)
L9*	9.76	3.05	200	200	200			2.25	191.0	40.0	55.7	Lutenegger (2009)
L10*	8.26	3.05	200	200	200			3.00	191.0	40.0	73.5	Lutenegger (2009)
S1*	18.97	10.67	406	406	356	305	254	3.00	93.0	28.1	342.1	Stuedlein (2008)
S2*	18.97	10.67	406	406	356	305	254	3.00	99.0	27.9	358.3	Stuedlein (2008)
S3	18.97	9.14	406	356	305	254		3.00	97.0	131.1	363.9	Stuedlein (2008)
S4*	18.97	10.67	406	406	356	305	254	3.00	98.0	27.9	358.3	Stuedlein (2008)
S5	18.97	10.67	406	406	356	305	254	3.00	97.0	55.6	395.4	Stuedlein (2008)
S6	18.97	10.67	406	406	356	305	254	3.00	86.0	81.3	309.6	Stuedlein (2008)
S7	18.97	9.14	406	356	305	254		3.00	85.0	65.9	516.0	Stuedlein (2008)

* Anchor not taken to failure, maximum observed value reported

x Load reported to have reached a relative displacement of 20% the helix diameter, capacity reported

Table 4.7 Helical anchor load test database summary, continued.

Test	H/D	Depth (m)	B (plate diameter) (mm)					S/D	average S _u (kPa)	δ _{MAX} (mm)	Q _{MAX} (kN)	Reference
			P1	P2	P3	P4	P5					
R1	4.58	0.46	100	100				4.58	7.1	N/A	0.84	Rao (1991)
R2	2.29	0.23	100	100	100			2.29	7.1	N/A	0.97	Rao (1991)
R3	1.53	0.15	100	100	100	100		1.53	7.1	N/A	1.34	Rao (1991)
R4	4.58	0.46	100	100				4.58	7.1	N/A	0.67	Rao (1991)
R5	2.29	0.23	100	100	100			2.29	7.1	N/A	0.91	Rao (1991)
R6	1.53	0.15	100	100	100	100		1.53	7.1	N/A	0.97	Rao (1991)
R7	4.58	0.46	100	100				4.58	7.1	N/A	0.55	Rao (1991)
R8	2.29	0.23	100	100	100			2.29	7.1	N/A	0.63	Rao (1991)
R9	1.53	0.15	100	100	100	100		1.53	7.1	N/A	0.73	Rao (1991)
R10	3.05	0.46	150	150	150	150		3.05	7.1	N/A	1.48	Rao (1991)
R11	1.53	0.23	150	150	150	150	150	1.53	7.1	N/A	1.67	Rao (1991)
R12	1.02	0.15	150	150	150	150	150	1.02	7.1	N/A	1.72	Rao (1991)
R13	6.13	0.46	75	75				4.00	6.2	N/A	0.69	Rao (1991)
R14	6.13	0.46	75	75	75			2.00	6.2	N/A	0.83	Rao (1991)
R15	6.13	0.46	75	75	75	75		1.33	6.2	N/A	0.90	Rao (1991)
R16	6.13	0.46	75	75				1.67	6.2	N/A	0.65	Rao (1991)
R17	6.13	0.46	75	75	75			0.83	6.2	N/A	0.71	Rao (1991)
R18	6.13	0.46	75	75				4.00	13.5	N/A	1.52	Rao (1991)
R19	6.13	0.46	75	75	75			2.00	13.5	N/A	1.86	Rao (1991)
R20	6.13	0.46	75	75	75	75		1.33	13.5	N/A	2.13	Rao (1991)
R21	6.13	0.46	75	75				1.67	13.5	N/A	1.19	Rao (1991)
R22	6.13	0.46	75	75	75			0.83	13.5	N/A	1.48	Rao (1991)

* Anchor not taken to failure, maximum observed value reported

* Load reported to have reached a relative displacement of 20% the helix diameter, capacity reported

Table 4.7 Helical anchor load test database summary, continued.

Test	H/D	Depth (m)	B (plate diameter) (mm)					S/D	average S _u (kPa)	δ _{MAX} (mm)	Q _{MAX} (kN)	Reference
			P1	P2	P3	P4	P5					
P1	4.50	0.15	33	33				4.50	3.0	N/A	0.032	Rao & Prasad (1993)
P2	1.00	0.04	33	33				4.50	3.0	N/A	0.045	Rao & Prasad (1993)
P3	2.00	0.07	33	33				4.50	3.0	N/A	0.052	Rao & Prasad (1993)
P4	3.00	0.10	33	33				4.50	3.0	N/A	0.055	Rao & Prasad (1993)
P5	4.00	0.14	33	33				4.50	3.0	N/A	0.060	Rao & Prasad (1993)
P6	6.00	0.20	33	33				4.50	3.0	N/A	0.067	Rao & Prasad (1993)
P7	8.00	0.27	33	33				4.50	3.0	N/A	0.073	Rao & Prasad (1993)
P8	10.00	0.33	33	33				4.50	3.0	N/A	0.080	Rao & Prasad (1993)
P9	4.50	0.15	33	33				4.50	4.4	N/A	0.052	Rao & Prasad (1993)
P10	1.00	0.04	33	33				4.50	4.4	N/A	0.068	Rao & Prasad (1993)
P11	2.00	0.07	33	33				4.50	4.4	N/A	0.078	Rao & Prasad (1993)
P12	3.00	0.10	33	33				4.50	4.4	N/A	0.084	Rao & Prasad (1993)
P13	4.00	0.14	33	33				4.50	4.4	N/A	0.089	Rao & Prasad (1993)
P14	6.00	0.20	33	33				4.50	4.4	N/A	0.098	Rao & Prasad (1993)
P15	8.00	0.27	33	33				4.50	4.4	N/A	0.103	Rao & Prasad (1993)
P16	10.00	0.33	33	33				4.50	4.4	N/A	0.112	Rao & Prasad (1993)
P17	2.30	0.08	33	33			33	2.30	3.0	N/A	0.043	Rao & Prasad (1993)
P18	1.00	0.04	33	33			33	2.30	3.0	N/A	0.055	Rao & Prasad (1993)
P19	2.00	0.07	33	33			33	2.30	3.0	N/A	0.062	Rao & Prasad (1993)
P20	3.00	0.10	33	33			33	2.30	3.0	N/A	0.065	Rao & Prasad (1993)
P21	4.00	0.14	33	33			33	2.30	3.0	N/A	0.071	Rao & Prasad (1993)
P22	6.00	0.20	33	33			33	2.30	3.0	N/A	0.077	Rao & Prasad (1993)
P23	8.00	0.27	33	33			33	2.30	3.0	N/A	0.083	Rao & Prasad (1993)
P24	10.00	0.33	33	33			33	2.30	3.0	N/A	0.090	Rao & Prasad (1993)
P25	2.30	0.08	33	33			33	2.30	4.4	N/A	0.065	Rao & Prasad (1993)
P26	1.00	0.04	33	33			33	2.30	4.4	N/A	0.082	Rao & Prasad (1993)
P27	2.00	0.07	33	33			33	2.30	4.4	N/A	0.091	Rao & Prasad (1993)
P28	3.00	0.10	33	33			33	2.30	4.4	N/A	0.096	Rao & Prasad (1993)
P29	4.00	0.14	33	33			33	2.30	4.4	N/A	0.102	Rao & Prasad (1993)
P30	6.00	0.20	33	33			33	2.30	4.4	N/A	0.110	Rao & Prasad (1993)
P31	8.00	0.27	33	33			33	2.30	4.4	N/A	0.116	Rao & Prasad (1993)
P32	10.00	0.33	33	33			33	2.30	4.4	N/A	0.124	Rao & Prasad (1993)

* Anchor not taken to failure, maximum observed value reported

* Load reported to have reached a relative displacement of 20% the helix diameter, capacity reported

Table 4.7 Helical anchor load test database summary, continued.

Test	H/D	Depth (m)	B (plate diameter) (mm)					S/D	average S _u (kPa)	δ _{MAX} (mm)	Q _{MAX} (kN)	Reference
			P1	P2	P3	P4	P5					
P33	1.50	0.05	33	33	33	33	33	1.50	3.0	N/A	0.046	Rao & Prasad (1993)
P34	1.00	0.04	33	33	33	33	33	1.50	3.0	N/A	0.058	Rao & Prasad (1993)
P35	2.00	0.07	33	33	33	33	33	1.50	3.0	N/A	0.066	Rao & Prasad (1993)
P36	3.00	0.10	33	33	33	33	33	1.50	3.0	N/A	0.069	Rao & Prasad (1993)
P37	4.00	0.14	33	33	33	33	33	1.50	3.0	N/A	0.074	Rao & Prasad (1993)
P38	6.00	0.20	33	33	33	33	33	1.50	3.0	N/A	0.080	Rao & Prasad (1993)
P39	8.00	0.27	33	33	33	33	33	1.50	3.0	N/A	0.087	Rao & Prasad (1993)
P40	10.00	0.33	33	33	33	33	33	1.50	3.0	N/A	0.094	Rao & Prasad (1993)
P41	1.50	0.05	33	33	33	33	33	1.50	4.4	N/A	0.068	Rao & Prasad (1993)
P42	1.00	0.04	33	33	33	33	33	1.50	4.4	N/A	0.083	Rao & Prasad (1993)
P43	2.00	0.07	33	33	33	33	33	1.50	4.4	N/A	0.094	Rao & Prasad (1993)
P44	3.00	0.10	33	33	33	33	33	1.50	4.4	N/A	0.100	Rao & Prasad (1993)
P45	4.00	0.14	33	33	33	33	33	1.50	4.4	N/A	0.104	Rao & Prasad (1993)
P46	6.00	0.20	33	33	33	33	33	1.50	4.4	N/A	0.113	Rao & Prasad (1993)
P47	8.00	0.27	33	33	33	33	33	1.50	4.4	N/A	0.119	Rao & Prasad (1993)
P48	10.00	0.33	33	33	33	33	33	1.50	4.4	N/A	0.127	Rao & Prasad (1993)
P49	1.10	0.04	33	33	33	33	33	1.10	3.0	N/A	0.046	Rao & Prasad (1993)
P50	1.00	0.04	33	33	33	33	33	1.10	3.0	N/A	0.059	Rao & Prasad (1993)
P51	2.00	0.07	33	33	33	33	33	1.10	3.0	N/A	0.066	Rao & Prasad (1993)
P52	3.00	0.10	33	33	33	33	33	1.10	3.0	N/A	0.069	Rao & Prasad (1993)
P53	4.00	0.14	33	33	33	33	33	1.10	3.0	N/A	0.074	Rao & Prasad (1993)
P54	6.00	0.20	33	33	33	33	33	1.10	3.0	N/A	0.081	Rao & Prasad (1993)
P55	8.00	0.27	33	33	33	33	33	1.10	3.0	N/A	0.087	Rao & Prasad (1993)
P56	10.00	0.33	33	33	33	33	33	1.10	3.0	N/A	0.093	Rao & Prasad (1993)
P57	1.10	0.04	33	33	33	33	33	1.10	4.4	N/A	0.068	Rao & Prasad (1993)
P58	1.00	0.04	33	33	33	33	33	1.10	4.4	N/A	0.084	Rao & Prasad (1993)
P59	2.00	0.07	33	33	33	33	33	1.10	4.4	N/A	0.094	Rao & Prasad (1993)
P60	3.00	0.10	33	33	33	33	33	1.10	4.4	N/A	0.099	Rao & Prasad (1993)
P61	4.00	0.14	33	33	33	33	33	1.10	4.4	N/A	0.104	Rao & Prasad (1993)
P62	6.00	0.20	33	33	33	33	33	1.10	4.4	N/A	0.113	Rao & Prasad (1993)
P63	8.00	0.27	33	33	33	33	33	1.10	4.4	N/A	0.118	Rao & Prasad (1993)
P64	10.00	0.33	33	33	33	33	33	1.10	4.4	N/A	0.127	Rao & Prasad (1993)

* Anchor not taken to failure, maximum observed value reported

x Load reported to have reached a relative displacement of 20% the helix diameter, capacity reported

5 DEVELOPMENT OF AN UPLIFT CAPACITY MODEL

Key contributors to uplift resistance of helical anchors include the breakout capacity of helical plates and cylindrical side shearing resistance. However, existing models do not accurately predict the capacity of helical anchors (Hoyt & Clemence, 1989). For design, it is critical that the prediction accuracy and variability of any model be recognized by engineers. Therefore, it is important to quantify both the accuracy and uncertainty of the models proposed in this thesis. Additionally, design methods are moving towards reliability-based design, accounting for uncertainties. The work herein includes the development of resistance factors for use with reliability-based design.

5.1 STATISTICAL APPROACH FOR CHARACTERIZATION OF NEW AND EXISTING MODELS

A general statistical approach was used in this research to compare datasets. This section introduces the concept of the bias and the coefficient of variation, two statistical quantities that are used to describe the model uncertainty.

In order to compare the measured and predicted values of helical anchor capacity, a general bias formulation was implemented. The bias, λ , is the ratio of the measured and calculated values of a variable of interest, defined by:

$$\lambda = \frac{\textit{Measured Value}}{\textit{Predicted Value}}$$

5.1

The accuracy of a prediction technique can be assessed by calculating the bias of the data and its statistical distribution. An unbiased prediction will produce an average bias of unity. When the mean bias is greater than unity the resistance prediction model is conservative on average; that is, the projected resistance values were less than those measured in field tests. Likewise, the model is unconservative when it produces a mean bias less than unity, or the predicted resistance is found to be more than the resistance measured in the field.

Figure 5.1 presents normal bias distributions of two hypothetical populations, each with a separate standard deviation, σ . The mean bias illustrated in the Figure 5.1 is defined as the arithmetic mean bias of the distribution. If the distributions in Figure 5.1 represent populations of model accuracy, it could be concluded that although both models are equally accurate on average, Model 1 would be preferred due to its relatively smaller variability, σ_1 .

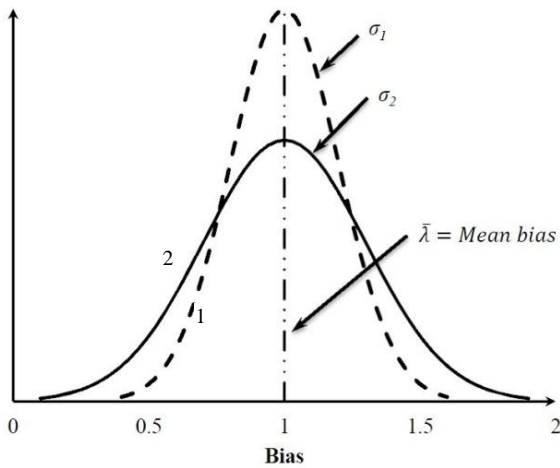


Figure 5.1 Conceptual visualization of the defined bias assuming a normal distribution; adapted from Strahler (2012).

Another indicator of uncertainty is the coefficient of variation (*COV*). The *COV* of a normally distributed dataset is simply the standard deviation normalized by the mean, given as:

$$COV = \frac{\sigma}{\bar{\lambda}} \quad 5.2$$

where $\bar{\lambda}$ is the mean bias. For a lognormal distribution the *COV* is given by:

$$COV = \sqrt{\exp(\sigma^2) - 1} \quad 5.3$$

The *COV* describes the spread in the distribution relative to its average. Generally expressed as a percent, the theoretical and observed bias values for a data set are considered to be in good agreement when the *COV* is less than roughly 20 to 30 percent (Allen, et al., 2005).

5.2 DETERMINATION OF THE UPLIFT CAPACITY FACTOR

For decades, a simplified bearing capacity equation has been used to evaluate helical anchors, in which the soil above the top helix was assumed to behave in a similar manner to a deep foundation element in bearing. The theoretical bearing capacity factor of 9.0 for deep foundations became the standard uplift capacity factor, N_{cu} . Based on a back-calculated N_{cu} values, Mooney et al. (1985) recommended an empirical capacity factor model limited to a maximum value of 9.4.

To update the model established by Mooney et al. (1985), additional N_{cu} values were back-calculated from the load test data discussed in Chapter 4. The N_{cu} values were back-calculated using the individual plate bearing equation, Equation 2.3, and the cylindrical shear equation, Equation 2.4. Figure 5.2 presents the updated plot of back-calculated uplift capacity factors, including the new data set developed in this thesis, and the data Mooney et al. (1985) presented in Figure 2.10.

After careful consideration the Rao and Prasad (1993) load tests on Anchors A3 and A4 were removed from the dataset. These anchors had S/D ratios of 1.5 and 1.1 which is well below the S/D used in the field which is typically equal to 3.0, and were determined to be inappropriate for developing a model to estimate production helical anchor capacity.

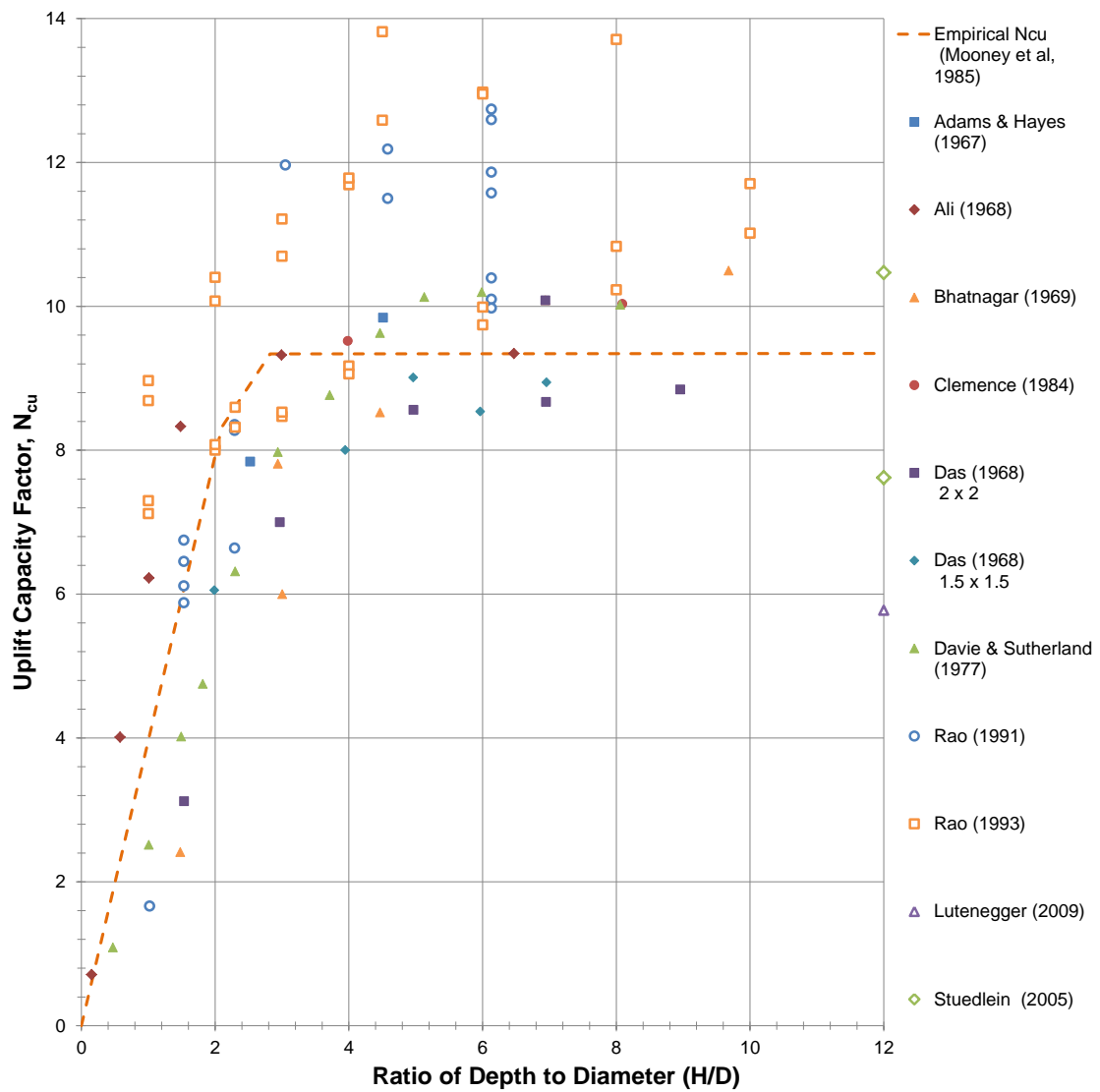


Figure 5.2 Back-calculated uplift capacity factor, N_{cu} .

Upon the addition of new back-calculated uplift capacity factors it became evident that a new uplift capacity factor model should be developed. To evaluate the Mooney et al. (1985) model, values of N_{cu} were calculated and compared to the back-calculated N_{cu} data, by means of the bias. Figure 5.3 presents the bias values for the

uplift capacity factor as a function of embedment (H/D) and as a function of the observed N_{cu} used to develop the model. The slopes of the trend lines indicate the potential dependence of the model accuracy as a function of H/D and magnitude of N_{cu} . Note, a slope of zero is considered to be representative of no model dependence. By evaluating the slope of the trends in bias, it is evident that the N_{cu} model is dependent on the embedment of the anchor, as well as the magnitude of the back-calculated N_{cu} values.

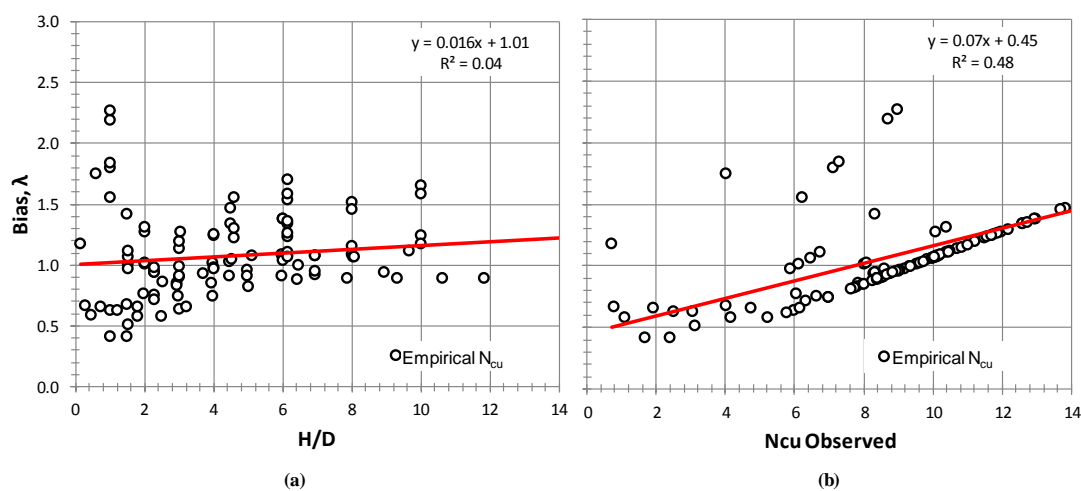


Figure 5.3 Graphical representations of the dependence of the Mooney et al. (1985) uplift capacity factor, N_{cu} , on (a) the embedment (H/D), and (b) the observed values of N_{cu} used in model development.

To produce a new and unbiased model, a piecewise hyperbolic function was found to best fit the updated N_{cu} values using an ordinary least squares approach. Figure 5.4 presents the uplift capacity factor with the best fit curve.

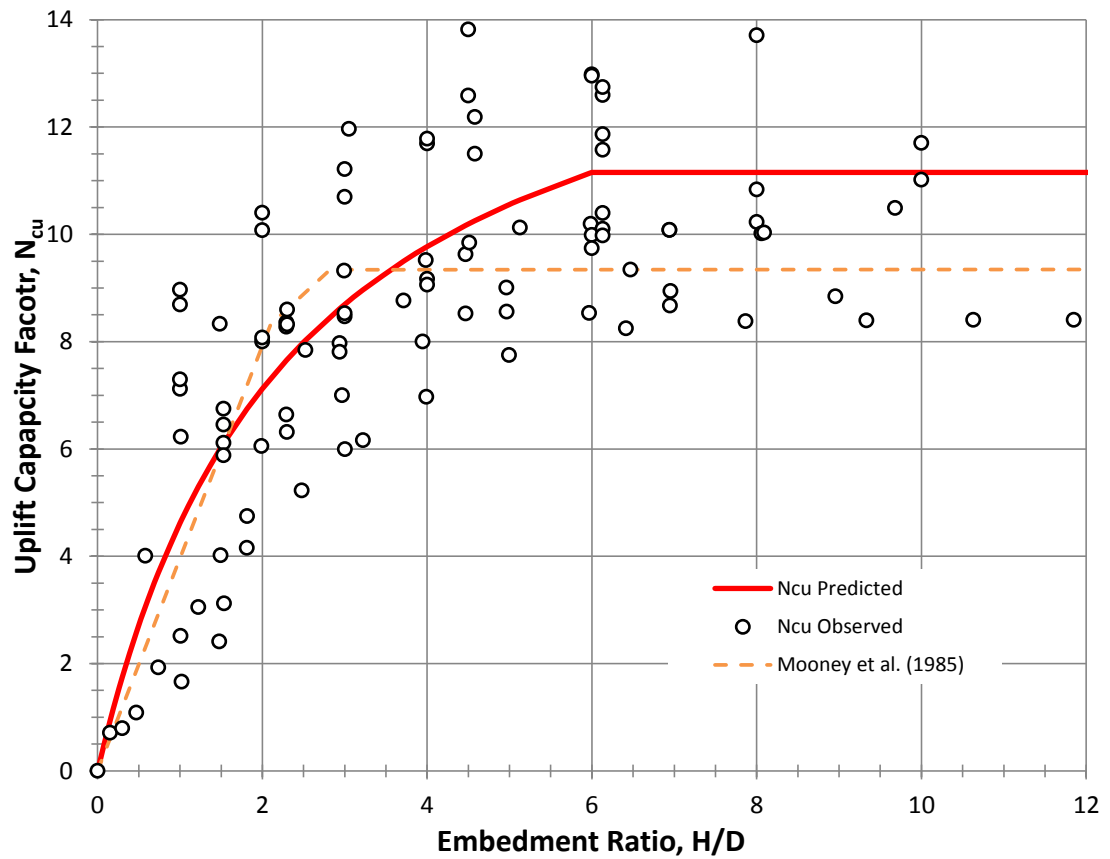


Figure 5.4 Uplift capacity factors, N_{cu} , fit with a piecewise hyperbolic model, given by Equation 5.4, to approximate N_{cu} .

This proposed capacity factor model is given by:

$$N_{cu} = \frac{\frac{H}{D}}{a + (b * \frac{H}{D})} \quad \text{for } \frac{H}{D} < 6.0$$

$$N_{cu} = 11.2 \quad \text{for } \frac{H}{D} \geq 6.0$$

5.4

where a equals 0.152, b equals 0.064, and the uplift capacity factor expresses a plateau at an N_{cu} equal to 11.2.

The proposed uplift capacity factor, which has a maximum N_{cu} value of 11.2, agrees more closely with the Merifield (2011) finite element analysis, which reaches a maximum N_{cu} of 12.6, and the exact limiting factor for a 3D lower bound numerical breakout analysis by Martin and Randolph (2001) for circular, smooth anchors reported as 12.42. However, the finite element analyses and the 3D numerical analysis appear to be idealized.

The Merifield (2011) uplift capacity equation is valid for perfectly smooth, plate anchors, which is an unlikely assumption due to the fabrication process and true soil-plate interface conditions. Further, the finite element analysis was performed for an idealized weightless soil. Allowing for in-situ soil conditions, such as disturbance due to anchor installation and secondary soil structure, and imperfections in the plate geometries, it seems reasonable that the proposed empirical N_{cu} model, developed from field data, would better represent in-situ conditions. Furthermore, the proposed N_{cu} model demonstrates no appreciable dependence on the embedment of the anchor (H/D), as evident in Figure 5.5.

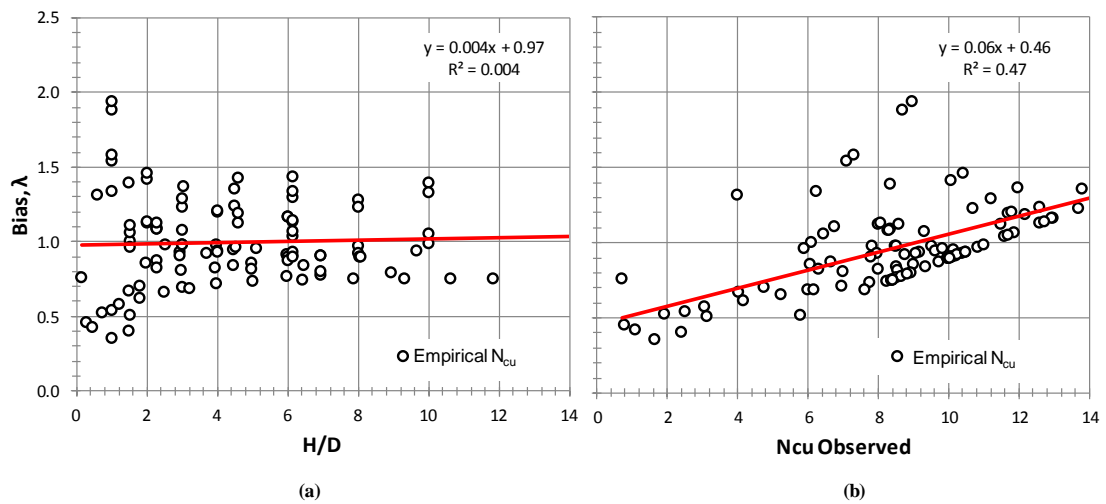


Figure 5.5 Graphical representations of the dependence of the proposed uplift capacity factor, N_{cu} , on (a) the embedment (H/D), and (b) the observed values of N_{cu} used in model development.

In comparison with the bias produced by the Mooney et al. (1985) N_{cu} model, shown in Figure 5.3, the bias of the proposed N_{cu} indicates a much more impartial model. Not only was the dependency on embedment eliminated, but the dependency on the observed N_{cu} values was reduced. Although the data indicate that there is still dependence of bias on magnitude of N_{cu} , this observation itself is biased by the fact that very shallow anchors are not common in full scale, real world applications, due to their limited capacity. For the range in likely H/D and associated N_{cu} , the new model is relatively unbiased, in contrast to the Mooney et al. (1985) uplift capacity factor model.

5.3 ACCOUNTING FOR UNCERTAINTY IN THE UPLIFT BEHAVIOR OF HELICAL ANCHORS

With the adoption of Load and Resistance Factor Design, LRFD, there has been increasing demand to assess the uncertainty and reliability in geotechnical engineering. LRFD is a form of limit state design, where geotechnical structures are generally designed for two states. The ultimate limit state refers to the critical load on the system, implying collapse upon exceedence. The second limit state is the serviceability limit state, under which a structure must remain functional for its intended use. The objective of LRFD is to ensure that for each of the limit states, and a certain probability of occurrence, the total load does not exceed the available resistance. This is accomplished by the load and resistance factors.

There are three levels of probabilistic design. Level I design methods express safety in terms of a safety factor, this method is the current standard of practice. Conversely, Level II accounts for safety in terms of target level of reliability or reliability index, β , which is implied based on current design standards. Level III is a fully probabilistic method, often in the form of monte carlo simulation (Allen, et al., 2005). Geotechnical practices typically incorporate Levels I and II due to the complex statistical requirements of Level III.

Figure 5.6 shows two probability density functions for a normally distributed load (Q) and resistance (R). The factor of safety is the ratio of the resistance to the

load, where the two functions overlap the resistance is less than the load generating a factor of safety less than one. The region where the load and resistance factors overlap represents an increased probability of failure. The combined probability distribution function for the margin of safety, shown in Figure 5.7, determines the reliability index, β . The reliability index is the number of standard deviations that separate the mean margin of safety, the difference between the resistance and load, from zero.

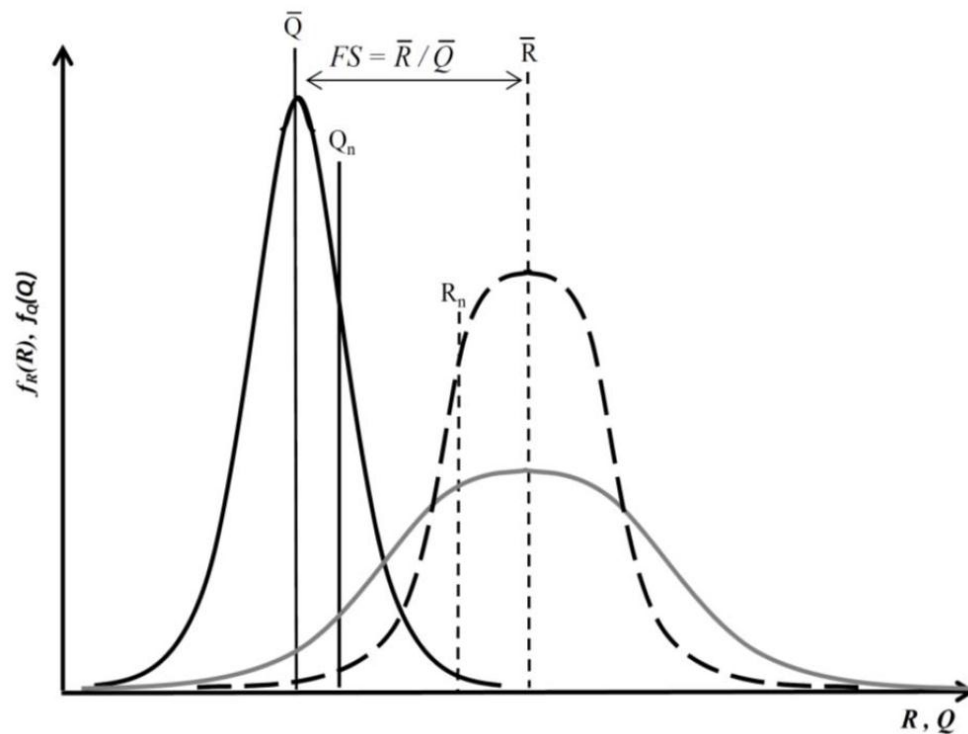


Figure 5.6 Conceptual illustration of potential probability distribution functions (PDF) for a normally distributed load and resistance, Q and R respectively; from (Stuedlein, 2008).

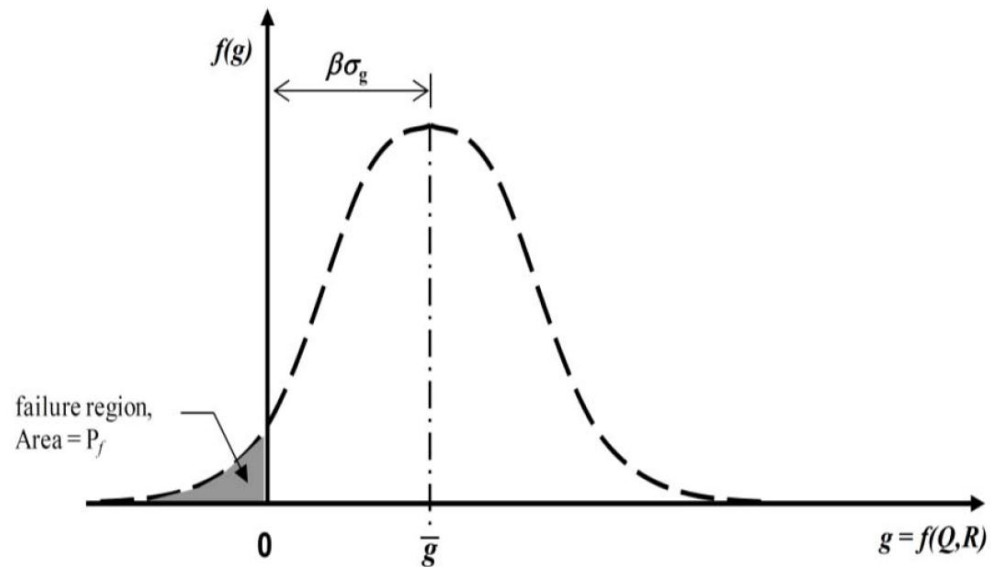


Figure 5.7 Conceptual illustration of the combined probability function representative of the margin of safety, β is the reliability index, adapted from (Stuedlein, 2008).

The goal of LRFD code development includes the generation of load and resistance factors that provide a margin of safety consistent with a target level of reliability (Allen, et al., 2005). There are four steps that must be completed to calibrate load and resistance factors for LRFD, outlined by Allen et al. (2005):

1. Develop the limit state equation to be evaluated,
2. Statistically characterize the data set to be calibrated,
3. Select the target reliability value, β , based the desired margin of safety,
and
4. Determine load and resistance factors, γ_Q and ϕ_R respectively.

The following equation is used to represent the limit state design:

$$\sum \gamma_i Q_{ni} \leq \phi R_n$$

5.5

where $\sum \gamma_i Q_{ni}$ is the total factored load associated with the limit state of interest, Q_{ni} is the nominal load and γ_i is the load factor for a specific load component, ϕ_R is the resistance factor, and R_n is the nominal resistance. These load and resistance factors are used in design to account for the uncertainty associated with natural variability and uncertainty in the magnitude of applied loads and resistances.

One objective of this research was to characterize the uncertainty associated with the uplift capacity factor and prediction of helical anchor capacity. To incorporate reliability-based design, the capacity model was not only characterized, but calibrated to account for safety in terms of a reliability index based on AASHTO load statistics. The following subsections describe the uncertainty analyses, and the generation of a helical anchor specific resistance factor for uplift capacity.

5.3.1 Uncertainty in the Uplift Capacity Factor

The uncertainty in the uplift capacity factor model was investigated for future LRFD calibration. The first step in characterizing the uncertainty in the uplift capacity factor was to calculate the point bias, λ , for every back-calculated N_{cu} value. The bias values were then associated with the corresponding H/D value and sorted and ranked

in ascending order from smallest to largest magnitude. The probability of occurrence, P_i , was determined for each point bias by:

$$P_i = \frac{i}{n + 1} \quad 5.6$$

which then allows a standard normal variate, Z , to be calculated:

$$Z_i = \Phi^{-1}(P_i) \quad 5.7$$

where n is the total number of bias values and i is the rank of each bias. The function Φ maps to the normal cumulative distribution function, CDF. The CDF is a function that represents the probability of not exceeding a given bias value, and is established by plotting the bias and its corresponding cumulative probability or standard normal variate.

For a theoretical normal distribution, the predicted bias is given by:

$$\lambda_n = \bar{\lambda} + \sigma * Z \quad 5.8$$

where all variables have been defined previously. However, most resistance data are lognormally distributed. To fit a lognormal distribution, the predicted bias is given by:

$$\lambda_{ln} = \exp(\bar{\lambda}_{ln} + \sigma_{ln} * Z) \quad 5.9$$

where the log mean is given by:

$$\bar{\lambda}_{ln} = \ln(\bar{\lambda}) - 0.5 * \sigma_{ln}^2$$

5.10

and the log standard deviation is given by:

$$\sigma_{ln} = \sqrt{\ln \left[\left(\frac{\sigma}{\bar{\lambda}} \right)^2 + 1 \right]}$$

5.11

When the predicted value is greater than the measured value, the bias values are less than 1.0 (unity), which indicates an unconservative prediction. Therefore, fitting the curve to bias values less than 1.0 is critical for preventing over-prediction of resistance. Figure 5.8 presents a CDF plot of the proposed uplift capacity factor bias with fitted approximations.

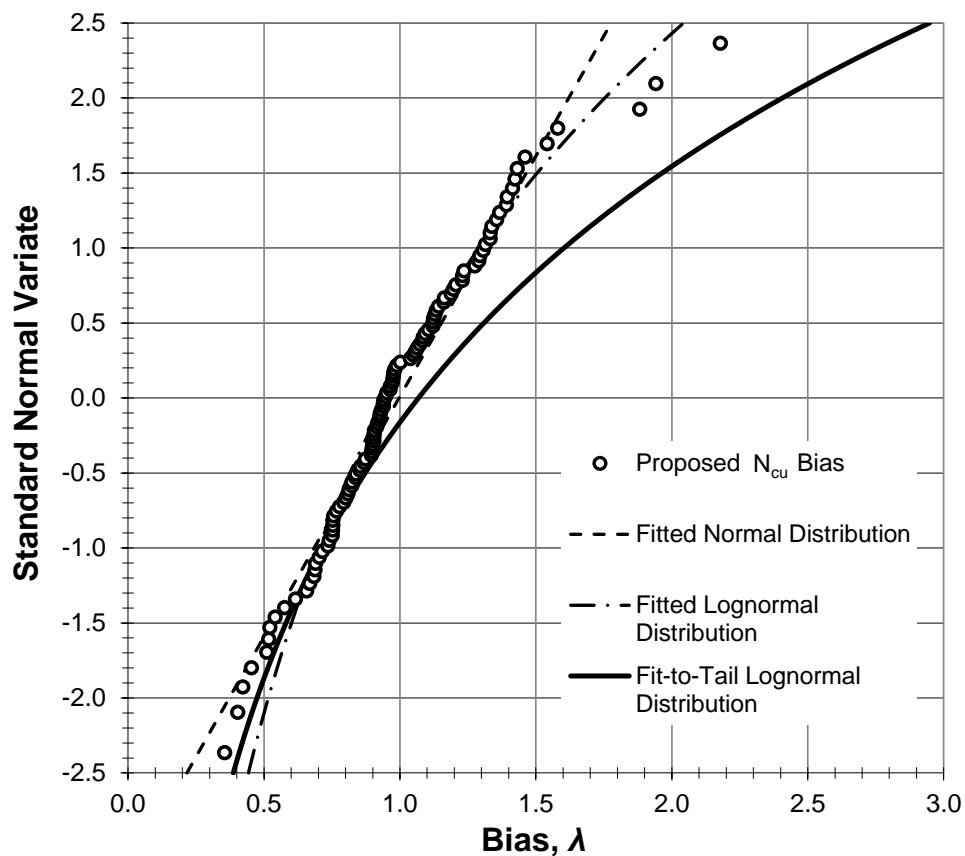


Figure 5.8 Cumulative distribution function (CDF) plot of the bias for the proposed uplift capacity factor model with fitted distributions.

The proposed uplift capacity factor has a lognormal distribution at the left tail where the bias values are unconservative, and the measured resistance is less than the predicted resistance. However, for bias values greater than unity, measured values are greater than predicted, and the model is conservative.

When the normal and lognormal curves do not adequately fit a data set it may be necessary to fit to a portion of the distribution that is more important for a specific

objective. For resistance values it is important to capture the left tail more accurately, focusing on the unconservative values that are more likely to result in failure.

In the proposed N_{cu} model, Figure 5.8, the left tail of the resistance bias followed a lognormal distribution. To characterize the model bias, a lognormal distribution was fit to the left tail of the data set by means of an ordinary least squares approach, concentrating on the data with a bias less than 1.0. This is presented in Figure 5.8 as the fit-to-tail distribution. As shown, the fit-to-tail distribution predicts the far left tail of the data, accurately characterizing the unconservative portion of the proposed model.

In comparison with the proposed N_{cu} model, the bias produced by the Mooney et al. (1985) N_{cu} model was also fit to a distribution and evaluated for uncertainty. Figure 5.9 presents a CDF plot for the Mooney et al. (1985) uplift capacity factor model.

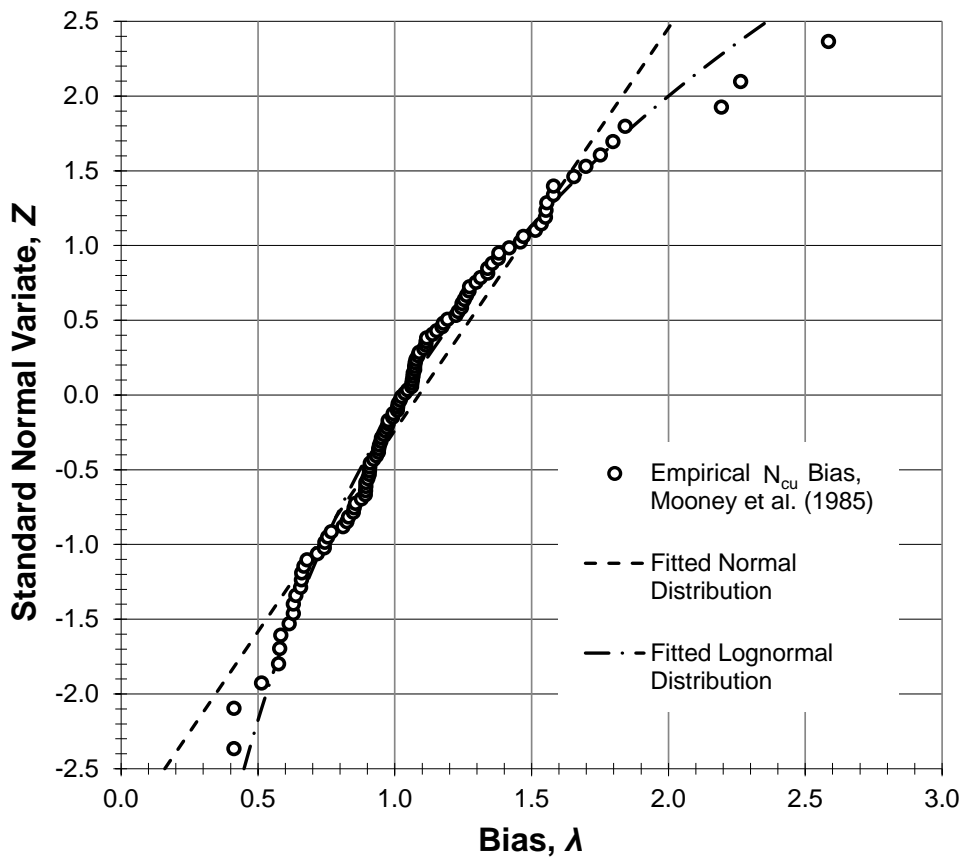


Figure 5.9 Cumulative distribution function (CDF) plot of the bias for the Mooney et al. (1985) uplift capacity factor model with fitted distributions.

The Mooney et al. (1985) N_{cu} seems to display some variability in distribution at the far left tail, if the dataset is normally distributed it may be considered unsuitable due to the possibility of returning a resistance of zero. The CDF also provides a visual representation of the variation within the model. In contrast to the proposed model, the Mooney et al. (1985) model demonstrates a wider range of bias values. A summary of the statistical comparison between the proposed model and the Mooney et al. (1985) uplift capacity model is presented in Table 5.1.

Table 5.1 Statistical summary of fitted distributions for the biases of both the Mooney et al. (1985) N_{cu} model and the proposed N_{cu} model.

N_{cu} Model	Normal Distribution			Lognormal Distribution			Fit-To-Tail Distribution		
	$\bar{\lambda}$	σ	COV	$\bar{\lambda}$	σ	COV	$\bar{\lambda}$	σ	COV
Mooney et al. (1985)	1.088	0.371	34%	1.084	0.353	33%	1.147	0.417	36%
Proposed	0.997	0.312	31%	0.993	0.298	30%	1.160	0.491	42%

Although both the distributions of the empirical Mooney et al. (1985) N_{cu} model and the proposed N_{cu} model are in reasonable agreement, the proposed model exhibits less variability, and a more unbiased distribution. The fit-to-tail displays slightly higher mean bias and standard deviation values; however this can be explained by the distribution of the right tail. The right tail of the proposed model cannot be described by the lognormal distribution fit to the portion of interest. Therefore, the inability to predict the bias of the right tail caused an increase in the model uncertainty; however, the consequence of error for this portion of the distribution is not critical.

Both models were developed empirically, and evaluated for dependency on the embedment depth, as well as dependency on the observed uplift capacity factors. The proposed N_{cu} model showed less dependence and exhibited a clearly defined lognormal distribution of bias values where critical.

5.3.2 Uncertainty in Capacity Models

In order to perform design of helical anchors in uplift accounting for uncertainty and an acceptable level of risk, the variability in the models used for capacity prediction needed to be fully characterized. The following sub-sections describe the characterization of uncertainty in uplift capacity predictions, and the development of resistance factors for LRFD.

5.3.2.1 Uncertainty in the Uplift Capacity

To characterize the uncertainty in the ultimate resistance, resistance predictions were calculated using four prediction models: existing cylindrical shear and individual plate bearing equations, and cylindrical shear and individual plate breakout models proposed herein.

In the individual plate breakout model each plate is expected to behave as a separate plate anchor, the capacity is therefore the sum of the capacities of each plate, calculated using Equation 2.3. In contrast, the top plate behavior is predicted using the breakout model and the cylindrical side shear is determined using the side shear model for the cylindrical shear models, calculated with Equation 2.4.

The difference between the existing and proposed capacity models is simply the uplift capacity factor, N_{cu} . In the existing capacity models the uplift capacity factor of 9.4, as presented by Mooney et al. (1985), is utilized, whereas the proposed

capacity models simply apply the proposed uplift capacity factor of 11.2. The data used to evaluate capacity included all of the load test data from Chapter 4.

Each of the models was individually characterized for uncertainty in capacity prediction by the same procedure used to evaluate the uncertainty in the uplift capacity factor, as discussed in Section 5.3.1. A point bias was calculated for each predicted capacity. These were then ranked and sorted in order of increasing magnitude. Finally Equations 5.6 and 5.7 were applied to calculate the probability, P_i , and the standard normal variate, Z_i .

Figure 5.10 presents the CDF with fitted distributions for capacities predicted using the proposed individual plate breakout model, based only on the available field data. The distribution is not well defined, but appears to be best fit by the normal distribution. To expand the dataset and determine the best fit distribution it was necessary to incorporate laboratory data. The Rao (1991) data was selected because Merifield (2011) found that the data compared well to values predicted for helical anchors in cohesive soil using FEA.

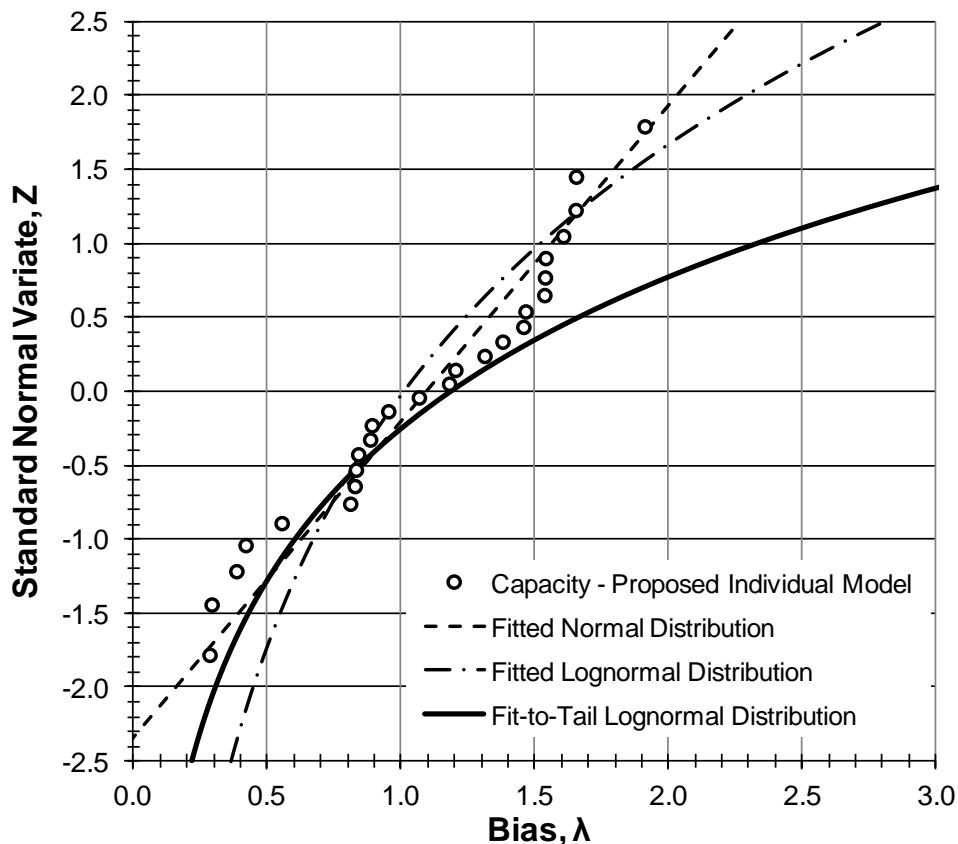


Figure 5.10 Fitted distribution for capacity, based solely on the available field data. The data seems to be normally distributed, however without more data, a clear distribution cannot be defined.

With the expanded dataset, including field and laboratory values, all of the distributions were clearly defined by lognormal distributions. The individual plate bearing equation and proposed individual plate breakout model were all well characterized by a fit-to-tail lognormal distribution, whereas the cylindrical shear equation and proposed cylindrical shear model were characterized by a fitted lognormal distribution. The fitted distributions for the bias of the two proposed models

are presented in Figures 5.11 and 5.12, followed by the distributions for the bias of the cylindrical shear and individual plate bearing equations in Figures 5.13 and 5.14.

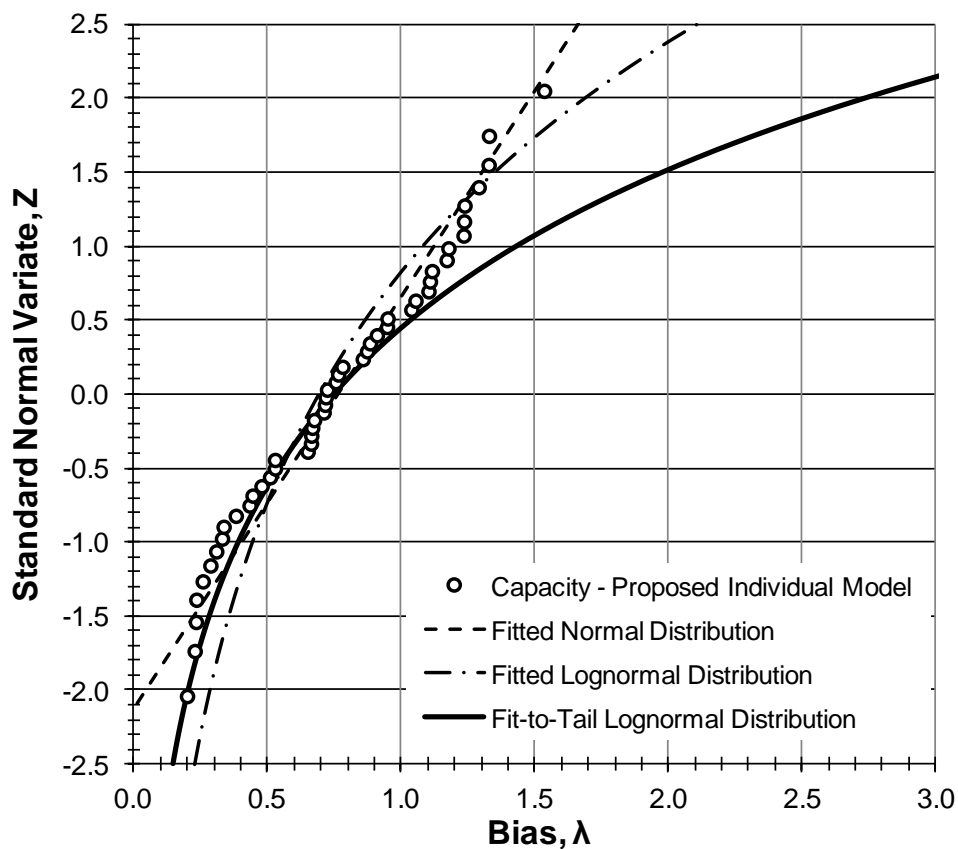


Figure 5.11 Fitted distribution for uplift capacity of helical anchors using the proposed individual plate breakout model.

Figure 5.11 presents the distribution fitting for the calculated capacity using the proposed individual plate breakout model. This distribution demonstrates a well-defined lognormal curve fit to the left tail, in contrast to Figure 5.10 where the distribution for the same model was unclear due a to lack of data.

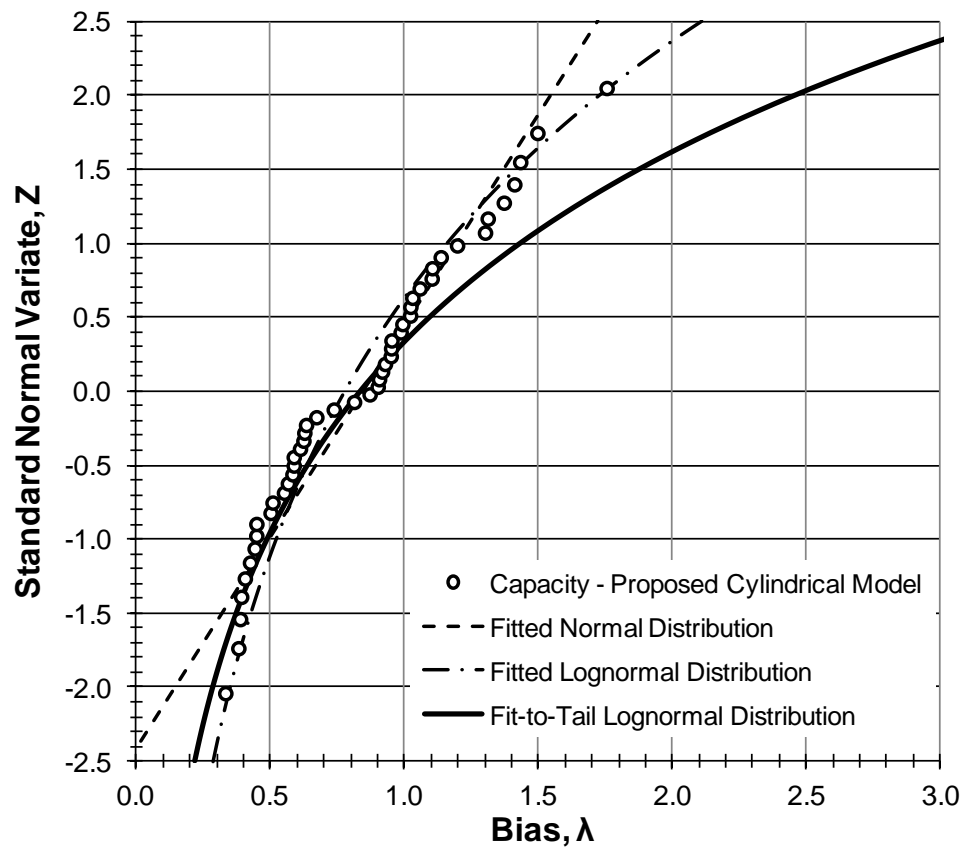


Figure 5.12 Fitted distribution for uplift capacity of helical anchors using the proposed cylindrical shear model.

The distribution of bias for the proposed cylindrical model, in Figure 5.12, produced the lowest *COV*, meaning that the distribution showed the least variability with respect to the mean bias. The entire dataset could be characterized by a lognormal function rather than just the left tail.

The two distributions based on bias values produced by the capacity equations, presented below in Figure 5.13 and Figure 5.14, have a similar distribution, generating similar mean bias and standard deviations to those of the proposed models. Both

equations have higher standard deviations than the proposed models, and slightly larger *COVs*.

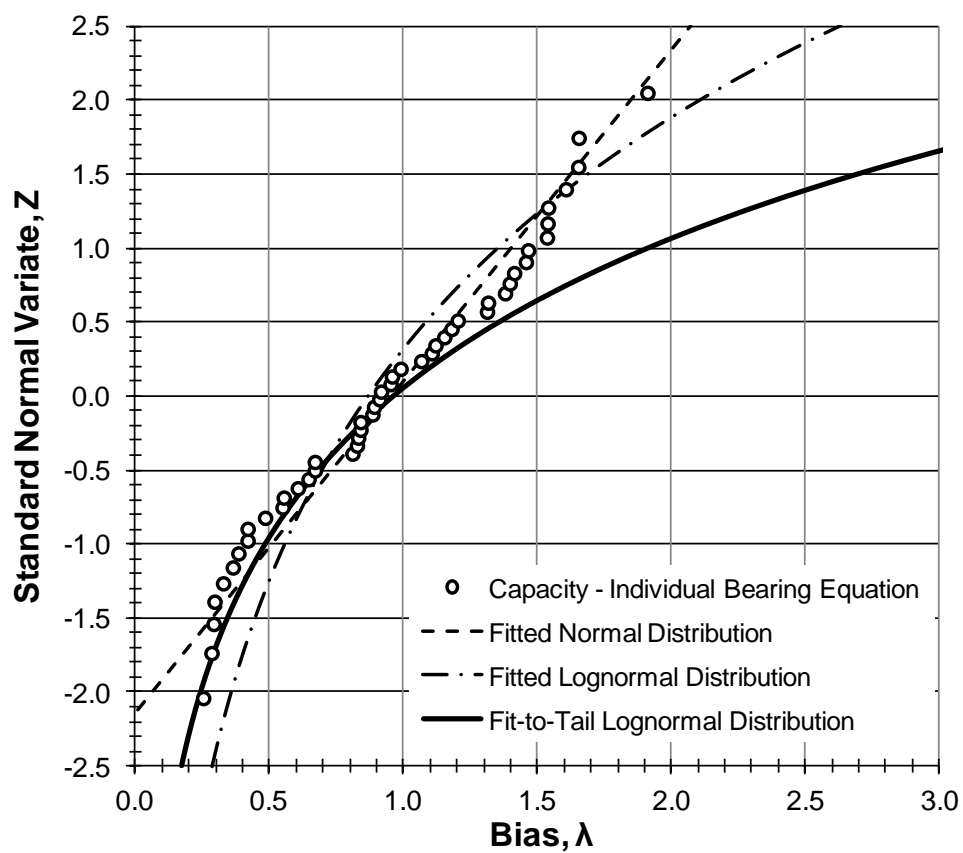


Figure 5.13 Fitted distribution for uplift capacity of helical anchors using the individual plate breakout equation.

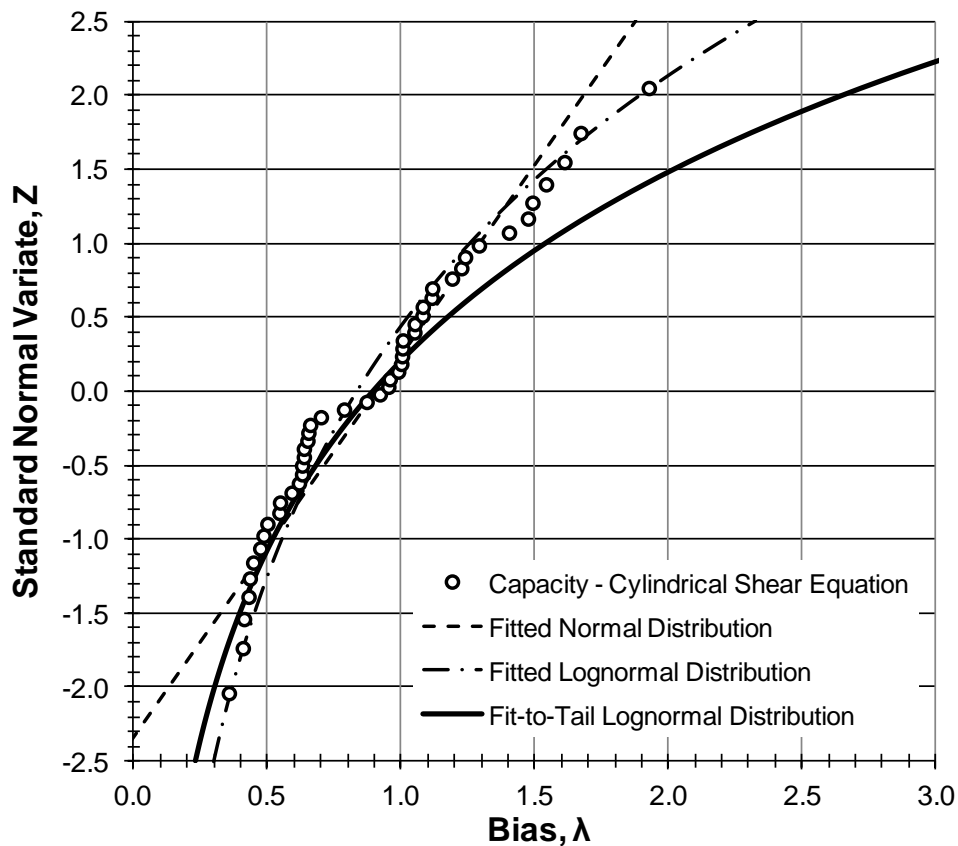


Figure 5.14 Fitted distribution for uplift capacity of helical anchors using the cylindrical shear equation.

Table 5.2 presents a summary of the best fit distribution for the four methods of predicting capacity of helical anchors in cohesive soils. The *COV* indicates reduced variability in the proposed models; however, all four of the methods have *COV* values greater than 40% signifying large variability in predicting the ultimate resistance.

Table 5.2 Statistical summary of the distribution approximations for the capacity bias calculations.

Capacity Model	Best Fit Distribution		
	$\bar{\lambda}$	σ	COV
Cylindrical Shear Equation	0.909	0.388	43%
Individual Plate Breakout Equation	1.217	0.941	77%
Proposed Cylindrical Model	0.843	0.351	42%
Proposed Individual Plate Breakout Model	0.924	0.664	72%

The difficulty in predicting ultimate resistance by all of the models suggested that with more research and a larger dataset it would be beneficial to separate out more of the parameters that affect uncertainty. For example, some anchors were anticipated to behave in a cylindrical shear manner, while others to develop capacity in individual plate breakout. The uncertainty analysis presented herein did not account for the difference in behavior; rather, the capacity of every anchor was predicted by each of the four methods.

5.3.2.2 Development of LRFD Load Resistance Factors

Once the uncertainty in the capacity was determined, the load resistance factors could be generated. The load resistance factors reported in this work were estimated using the closed-form solutions of the First Order Second Moment (FOSM) reliability procedures (Allen, et al., 2005). The resistance statistics from the two model bias distributions corresponding to the four models investigated were then analyzed for live load (LL) only and dead load (DL) only, and combined live and dead loading.

In the FOSM procedure, the reliability index, β , for a lognormal load distribution can be estimated by:

$$\beta = \frac{\ln \left[\frac{\gamma_Q * \lambda_R}{\varphi_R * \lambda_Q} * \sqrt{\frac{(1 + COV_Q^2)}{(1 + COV_R^2)}} \right]}{\sqrt{\ln[(1 + COV_Q^2) * (1 + COV_R^2)]}} \quad 5.12$$

where λ is the mean bias and COV_Q and COV_R is the coefficient of variation for the given load, Q , or resistance, R , respectively. As discussed previously, γ_Q is the load factor, and φ_R is the resistance factor. The goal of this calibration was to determine the resistance factor for helical anchors given assumed load statistics. To simplify the calculation process Equation 5.12 was solved algebraically for the resistance factor. Therefore closed form solution for the resistance factor for a lognormal load distribution is given by:

$$\varphi_R = \frac{\frac{\gamma_Q * \lambda_R}{\lambda_Q} \sqrt{\frac{1 + COV_Q^2}{1 + COV_R^2}}}{e^{\beta * \sqrt{\ln[(1 + COV_Q^2) * (1 + COV_R^2)]}}} \quad 5.13$$

where all values were previously defined.

The selected input parameters included a reliability index of 1% and 0.1% which corresponds to β equal to 2.33 and 3.09, respectively. The load statistics were selected based on the American Association of State Highways and Transportation

Officials, or AASHTO, design specification. The values of the *COV*, bias and load factor used in the analysis are presented in Table 5.3 for dead and live load only.

Table 5.3 The AASHTO load statistics used in resistance factor calibration

Dead Load Only		Live Load Only	
$COV_{Q_{DL}}$	0.10	$COV_{Q_{LL}}$	0.20
$\lambda_{Q_{DL}}$	1.05	$\lambda_{Q_{LL}}$	1.15
$\gamma_{Q_{DL}}$	1.25	$\gamma_{Q_{LL}}$	1.25

To account for resistance effects with applied combined loading, Stuedlein et al. (2012) presented a weighted average for the load factor, given by:

$$\gamma_{AVG} = \frac{\lambda_{DL} + \gamma_{DL} * \xi + \lambda_{LL} + \gamma_{LL}}{\lambda_{DL} * \xi + \lambda_{LL}}$$

5.14

where ξ is the ratio of dead load to live load, DL/LL. Similarly, the combined load bias was estimated by:

$$\lambda_{AVG} = \frac{\lambda_{DL} * \xi + \lambda_{LL}}{\xi + 1}$$

5.15

The average coefficient of variation (COV_{AVG}) was determined using the same weighted average equation as the bias, given by:

$$COV_{AVG} = \frac{COV_{DL} * \xi + COV_{LL}}{\xi + 1}$$

5.16

In this study, ξ was varied from one to ten in the calculations, and produced the load statistics presented in Table 5.4.

Table 5.4 Combined statistics for dead load and live load based on the AASHTO load statistics.

$\xi_{(DL/LL)}$	1	2	3	4	5	6	7	8	9	10
$COV_{Q_{DL+LL}}$	0.150	0.133	0.125	0.120	0.117	0.114	0.113	0.111	0.110	0.109
$\lambda_{Q_{DL+LL}}$	1.100	1.083	1.075	1.070	1.067	1.064	1.063	1.061	1.060	1.059
$\gamma_{Q_{DL+LL}}$	2.045	1.708	1.535	1.430	1.359	1.309	1.271	1.241	1.217	1.197

The resistance factors for helical anchors in cohesive soils were generated using both live loading and dead loading. The resulting resistance factors are presented in Tables 5.5 and 5.6.

Table 5.5 Calculated load resistance factors for $\beta = 1.0\%$ and 0.1% accounting only for dead load.

Dead Load Only				
Calculation Method	Cylindrical Shear	Individual Plate Breakout	Combined Displacement	Individual Plate Breakout Displacement
$\Phi_{R,1.0\%} =$	0.374	0.230	0.357	0.196
$\Phi_{R,0.1\%} =$	0.272	0.136	0.261	0.119

Table 5.6 Calculated load resistance factors for $\beta = 1.0\%$ and 0.1% accounting only for live load.

Live Load Only				
Calculation Method	Cylindrical Shear	Individual Plate Breakout	Combined Displacement	Individual Plate Breakout Displacement
$\varphi_{R,1.0\%} =$	0.321	0.203	0.305	0.172
$\varphi_{R,0.1\%} =$	0.227	0.118	0.218	0.103

The combined loading results are presented in Figure 5.15 and Figure 5.16. Figure 5.15 presents the resistance factors produced for the proposed cylindrical shear model, and Figure 5.16 presents the resistance factors generated for the proposed individual plate breakout model.

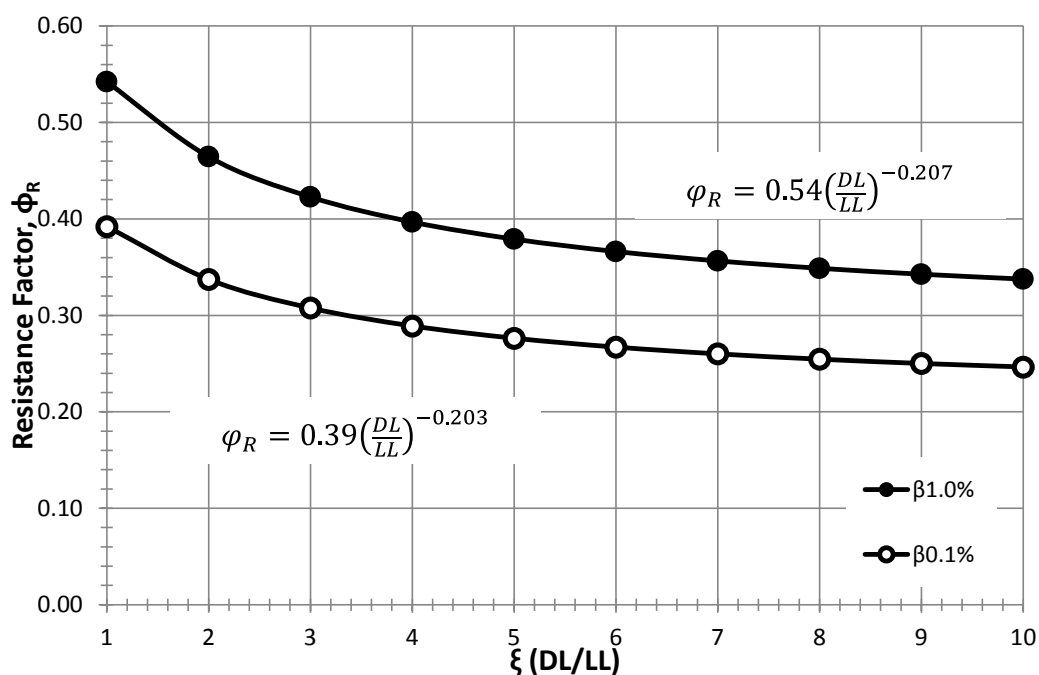


Figure 5.15 Resistance factors for calculating helical anchor capacity with the proposed cylindrical shear model.

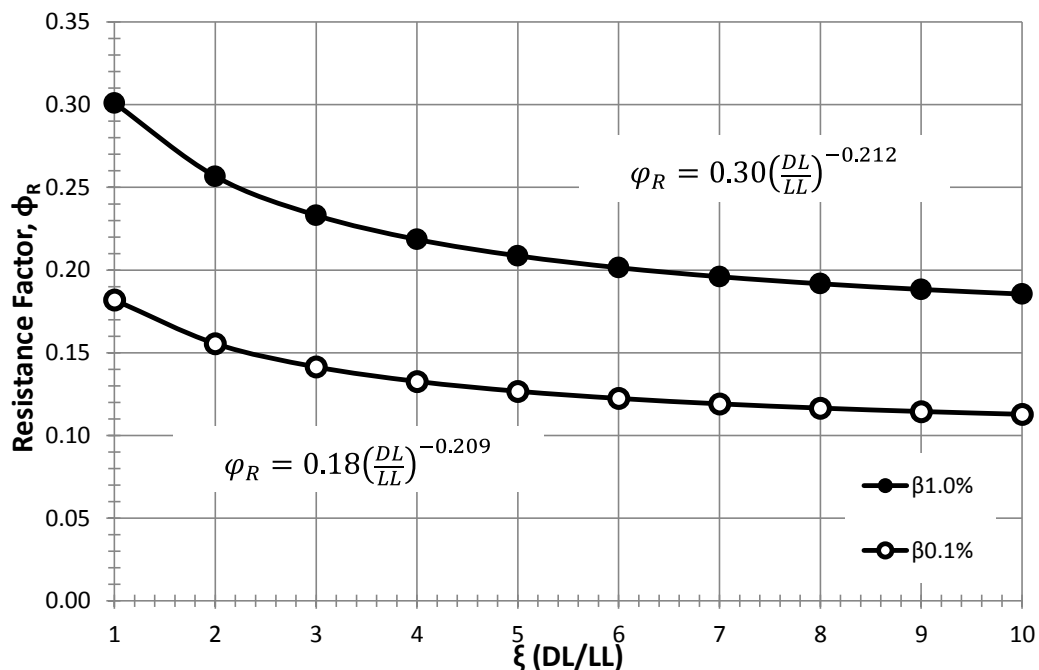


Figure 5.16 Resistance factors for calculating helical anchor capacity with the proposed individual plate breakout model.

The resistance factors follow power curves, defined by the equations presented in the figures, and in Table 5.7. The sensitivity due to the ratio of dead and live load is minimal; this can be explained by the large variability in the capacity mode and small variability in the load statistics. The *COV* for the proposed cylindrical shear model was 42%, and the *COV* for the proposed individual plate breakout model was 72%. These are much greater than the load *COV* of 10% for dead load and 20% for live load.

Table 5.7 Generated resistance factor equations for varying ratios of dead and live load.

Probability of Failure	Proposed Cylindrical Shear Model	Proposed Individual Plate Breakout Model
1.0%	$\varphi_R = 0.54\left(\frac{DL}{LL}\right)^{-0.207}$	$\varphi_R = 0.30\left(\frac{DL}{LL}\right)^{-0.212}$
0.1%	$\varphi_R = 0.39\left(\frac{DL}{LL}\right)^{-0.203}$	$\varphi_R = 0.18\left(\frac{DL}{LL}\right)^{-0.209}$

5.4 SUMMARY

The preceding chapter presents an analysis of the accuracy and uncertainty of four capacity models: the existing cylindrical shear and individual bearing equations, and the proposed cylindrical shear and individual plate breakout models. The models were evaluated in accordance with the calibration techniques for LRFD outlined by Allen et al. (2005) to facilitate reliability-based design. Contributions and conclusions from this work include:

- The uplift capacity factor, N_{cu} , proposed by Mooney et al. (1985) was found to be dependent on the embedment depth of the anchor and the magnitude of the back-calculated N_{cu} values used in uplift capacity factor model development.
- A proposed uplift capacity factor model was developed to eliminate the dependence of the anchor capacity on its embedment, and to have significantly reduced dependence on the magnitude of the back-calculated N_{cu} values.

- All of the methods for predicting the helical anchor uplift capacity exhibited large variability in capacity prediction (*COV* ranging from 42% to 77%). Specifically,
 - The existing cylindrical shear model (Mooney, et al., 1985) produced a mean bias of 0.91 and a *COV* of 43%
 - The existing individual plate bearing model (Mooney, et al., 1985) produced a mean bias of 1.22 and a *COV* of 77%
 - The proposed cylindrical shear model produced a mean bias of 0.84 and a *COV* of 42%
 - The proposed individual plate breakout model produced a mean bias of 0.92 and a *COV* of 72%
- Resistance factors for anchor capacity calculated using the two proposed capacity models were developed through LRFD calibration for probabilities of failure of 1 and 0.1 percent, and are presented in Tables 5.5 and 5.6, and in Figures 5.13 and 5.14.

6 DEVELOPMENT OF A LOAD-DISPLACEMENT MODEL

Previous engineering estimates of capacity for helical anchors have been based on the calculation of the ultimate resistance. However, current engineering requirements call for more detailed estimates of performance than in the past. Often displacement, rather than capacity, governs the geotechnical and structural design. Therefore, displacement performance predictions are becoming more common. To date, no displacement prediction model for helical anchors has been reported in the literature. To develop a displacement model, this research evaluated the displacement behavior of a number of single and multi-helix anchors.

6.1 DEVELOPMENT OF NORMALIZED LOAD TEST CURVES

The load test database presented in Chapter 4 was developed utilizing published load-displacement curves to characterize the displacement behavior of helical anchors. For model development, the load-displacement curves were normalized with respect to the anchor geometries. The displacement at each load increment was normalized with respect to the average plate diameter. The loads were converted to uplift pressure by dividing each reported load by the average anchor area. This pressure was then normalized with respect to the maximum uplift pressure. The testing conditions, load test data, and procedures for each anchor were discussed in Chapter 4.

The effort to normalize the load-test data generated a set of curves for which a displacement model could be based. Figure 6.1 presents an example of a load test and the corresponding normalized load curve. The normalization does not affect the behavior of the load curve; however, it allows the data to be readily compared with other load tests.

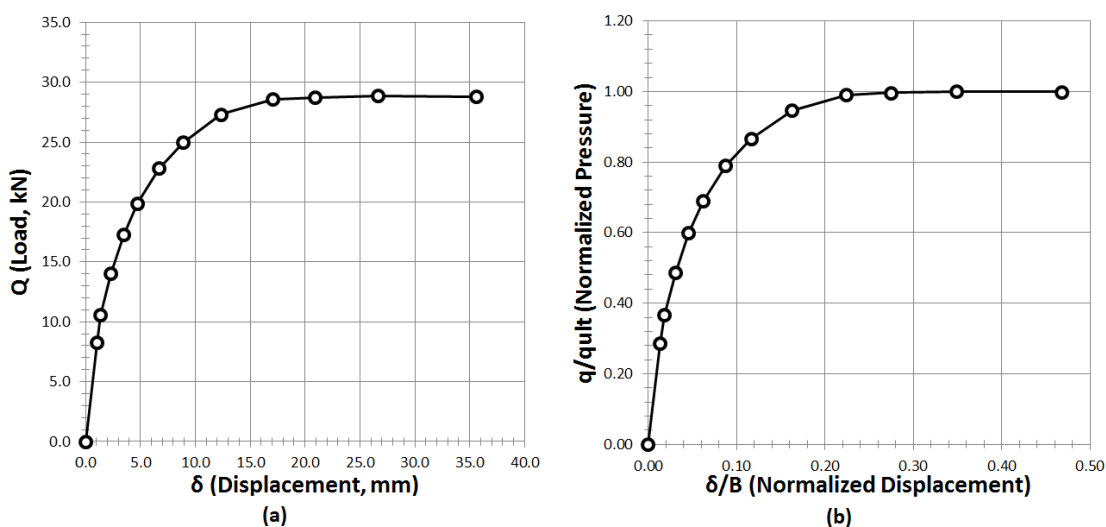


Figure 6.1 Observed load test data and normalized load test data for plate anchor A4, (a) observed load-displacement curve (b) normalized load-displacement curve.

6.2 BREAKOUT LOAD-DISPLACEMENT MODEL FOR SINGLE PLATE ANCHORS

Anchor breakout is one of the two contributing factors in uplift capacity of helical anchors, and is therefore critical to developing a model for displacement predictions. The breakout behavior of a plate anchor governs the top helical plate

when cylindrical shear controls anchor performance, and every plate when an anchor performs consistent with individual plate breakout behavior.

For this research load tests from Ali (1969) were utilized for the development of the individual plate breakout curve. In order to evaluate the plate breakout performance, each load test was normalized and plotted as discussed in the previous section. The data was then fitted by a piecewise hyperbolic curve using ordinary least squares.

Figure 6.2 shows the piecewise hyperbolic curve fit to the normalized load-displacement curves from the Ali (1969) plate anchor load tests. This curve was used as the starting point for the determination of the side shear component as well as a basis the individual plate anchor behavior in cohesive soils.

As shown in Figure 6.2, it appears that the H/D does not affect the plate anchor behavior under tensile loading. All of the normalized load-displacement curves for the plate anchors showed a clear plateau and similar behavior throughout the loading. Therefore only one design curve was necessary to capture the breakout behavior of the plate anchors.

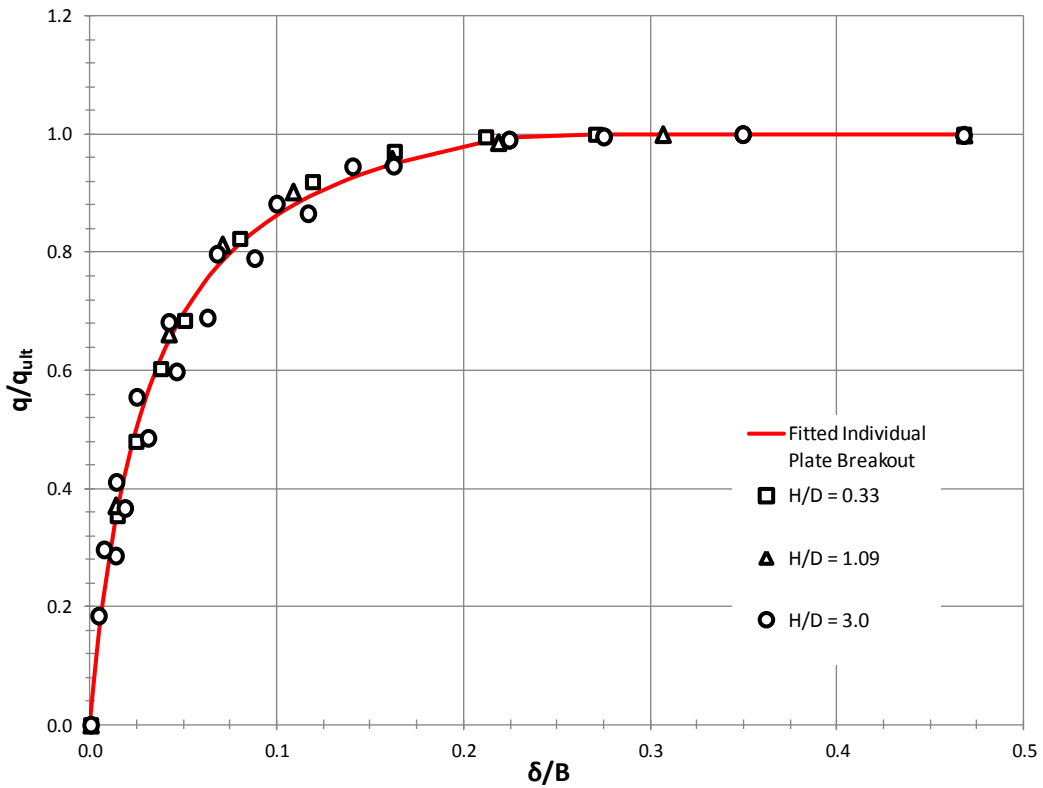


Figure 6.2 Proposed normalized breakout curve for plate anchors in cohesive soil compared to the normalized load-displacement curves, original data after Ali (1969).

The best fit curve for the data, a piecewise hyperbolic function, was given by:

$$\frac{q}{q_{ult}} = \frac{\frac{\delta}{B}}{a + (b * \frac{\delta}{B})} \quad \text{for } \frac{\delta}{B} < 0.24$$

$$\frac{q}{q_{ult}} = 1 \quad \text{for } \frac{\delta}{B} \geq 0.24$$

where δ is the displacement, B is the average plate diameter, and the coefficients a and b were found to be 0.028 and 0.881 respectively. Using Equation 6.1, the normalized breakout displacement can be calculated for any anchor component where individual plate breakout behavior governs for any uplift pressure.

6.3 SIDE SHEAR LOAD-DISPLACEMENT MODEL FOR MULTI-HELIX ANCHORS

After the breakout behavior was characterized, as discussed in section 6.2, the next step was to estimate displacements for multi-helix anchors when cylindrical shear governed, by incorporating a side shear component. As described in Section 2.2, helical anchors with minimal spacing between helical plates are considered to act similarly to a shaft. Side shearing forces are mobilized along a soil shaft flanked by the helical plates, eventually leading to breakout of the top helix, shown in Figure 2.13.

Mutli-plate load tests provided by Clemence (1983) were normalized, as described in Section 6.1. The uplift resistances for each of the discrete load increments were calculated using Equation 6.1, and were then utilized to define the side shear capacity for each load test. The side shear was determined by subtracting the breakout load for each discrete load-displacement data pair, from the measured load at the corresponding displacement. Figure 6.3 presents the original load-displacement curve

for anchor C1, plotted with the back-calculated side shear estimate for each displacement.

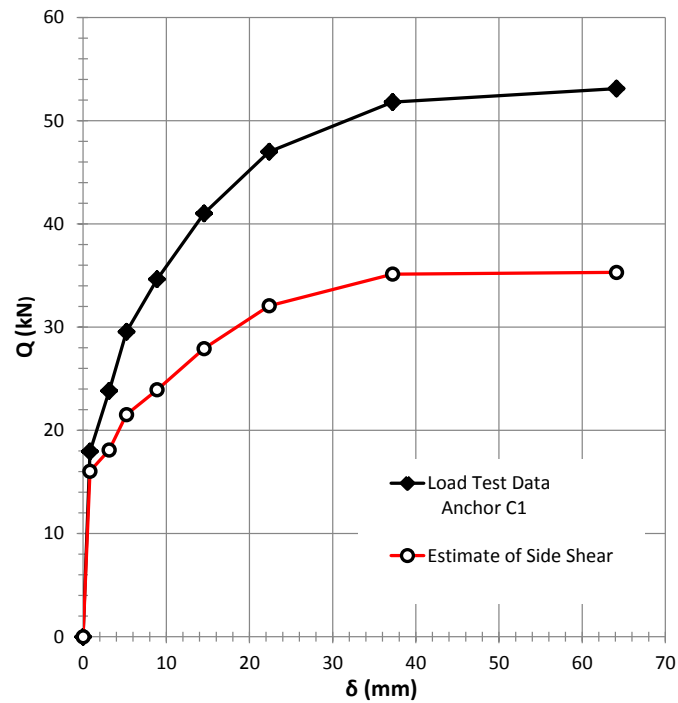


Figure 6.3 Graphical representation of a side shear calculation.

To develop the cylindrical shear load-displacement model, each back-calculated side shear estimate curve from the Clemence (1983) tests was normalized as previously discussed. These normalized side shear curves were plotted as a function of normalized displacement and a generalized curve was fit to the aggregated data. Unlike the plate breakout behavior, the side shear was affected by the ratio of depth to diameter (H/D). The anchors with H/D greater than eight exhibited the same normalized behavior, but differed from the behavior of the anchors with an H/D of

four. To capture this difference in the side shear model, two piecewise power functions were fit using ordinary least squares. Figure 6.4 presents the final side shear model incorporating all of the marine clay field tests. The proposed side shear model is given by:

$$\frac{q}{q_{ult}} = a \left(\frac{\delta}{B} \right)^b \quad \text{for } \frac{\delta}{B} < \frac{\delta^*}{B}$$

$$\frac{q}{q_{ult}} = 1 \quad \text{for } \frac{\delta}{B} \geq \frac{\delta^*}{B}$$

6.2

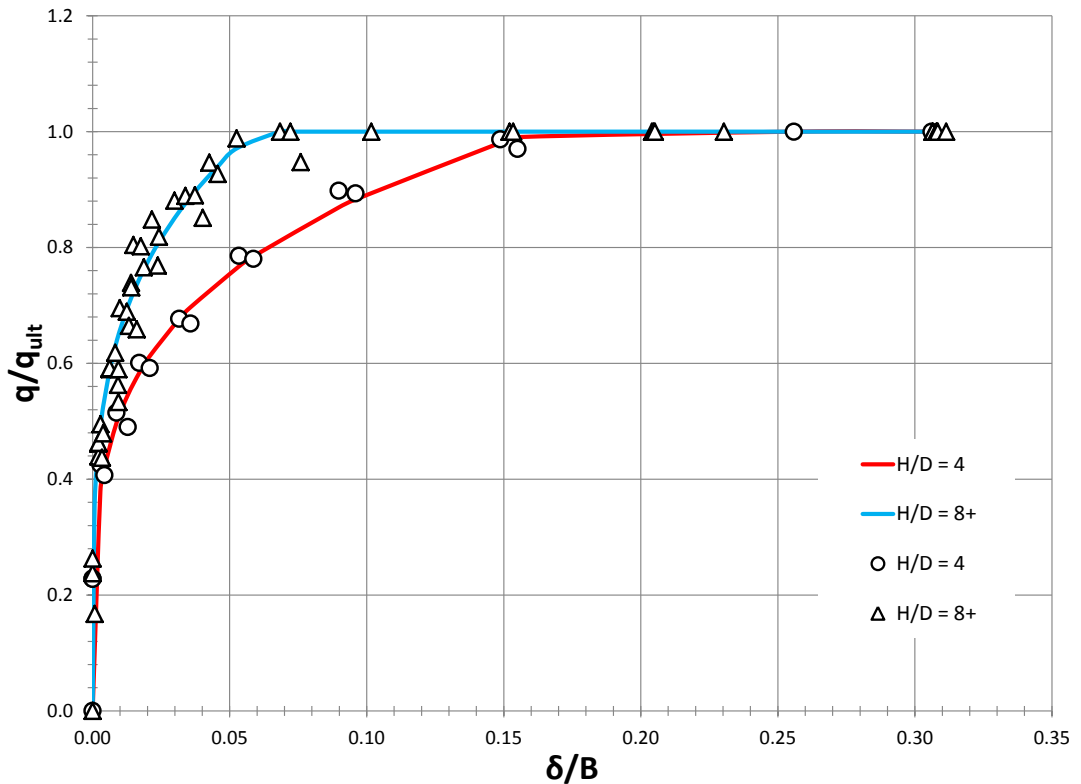


Figure 6.4 Final normalized side shear displacement model for multi-plate helical anchors in cohesive soil.

For an anchor with an H/D value equal to four, the limiting value of $\frac{\delta}{B}$ for the displacement curve, is 0.20. For this case, the coefficients a and b are equal to 1.55 and 0.24 respectively. For an H/D value greater than or equal to eight the limiting value of normalized displacement, $\frac{\delta}{B}$ equals 0.06, and the coefficients a and b are equal to 0.94 and 0.234 respectively. All other variables have been defined previously.

6.4 DISPLACEMENT PREDICTION MODELS

To predict the load-displacement behavior of single and multi-plate anchors for both the cylindrical shear and the individual plate behavior, the two displacement prediction models were developed as described in Sections 6.2 and 6.4. The combined displacement prediction model was developed to evaluate anchors that behaved in a cylindrical shear fashion. This model utilized both the breakout load-displacement curve and the cylindrical shear displacement curves to predict anchor behavior. The individual plate breakout displacement prediction model employed only the breakout load-displacement curve, assuming that each plate behaved individually.

6.4.1 Individual Displacement Prediction Model

The individual plate breakout curve, defined in Section 6.2, was utilized to develop an individual plate breakout displacement model used in the combined displacement model. This model was similar to the individual plate breakout equation currently used in practice; however, the individual plate breakout displacement

prediction model can be used to predict the expected capacity of a given anchor at a specified displacement increment.

To determine the overall displacement behavior of a helical anchor with individual plate behavior, the individual plate breakout of each anchor plate must be evaluated for the displacement values of interest, using the generalized individual plate breakout curve. The summation of the individual plate breakout values for any one displacement value provides the total capacity, given by:

$$Q = \sum_{i=1}^n \left[\left(\frac{q}{q_{ult}} \right)_i * N_{cu} * s_{ui} * A_i \right] \quad 6.3$$

where $\left(\frac{q}{q_{ult}} \right)_i$ equals the normalized plate breakout capacity and is calculated by Equation 6.1, and A_i is the area of each individual plate. All other variables have been previously defined.

6.4.2 Combined Displacement Prediction Model

After characterizing both the plate breakout behavior and the side shear behavior a combined displacement prediction model could be generated. By utilizing the anchor geometry and a series of displacement values, the breakout of the top plate and side shear behavior can be predicted by Equations 6.1 and 6.2. The summations of the individual plate breakout and side shear are the combined displacement prediction model, with the capacity equation given by:

$$Q = \left[\left(\frac{q}{q_{ult}} \right)_B * N_{cu} * s_u * A_T \right] + \left[\left(\frac{q}{q_{ult}} \right)_{SS} * s_u * A_S \right] \quad 6.4$$

where $\left(\frac{q}{q_{ult}} \right)_B$ equals the normalized plate breakout pressure at a given displacement, and is calculated using Equation 6.1, and $\left(\frac{q}{q_{ult}} \right)_{SS}$ equals the normalized side shear pressure at the same displacement and is calculated using Equation 6.2, A_S is the surface area of the cylinder producing side shear, and A_T is the area of the top helical plate.

6.5 EVALUATION OF DISPLACEMENT MODEL ACCURACY

The breakout behavior of individual plate breakout and cylindrical side shear of multi-plate anchors was evaluated to find generalized behavior curves, after which the combined displacement and individual plate breakout displacement prediction models were defined. The load-displacement behavior of a helical anchor in cohesive soil, based on these models, can be predicted using Equations 6.1 through 6.4.

To evaluate the two models for accuracy, each load test from the multi-helix anchor database, discussed in Chapter 4, was evaluated. Figure 6.5 presents the comparison of Anchor C1; for this example, the individual plate breakout and cylindrical shear displacement models were calculated using the uplift capacity factor of 11.2, based on the proposed N_{cu} model (Chapter 5).

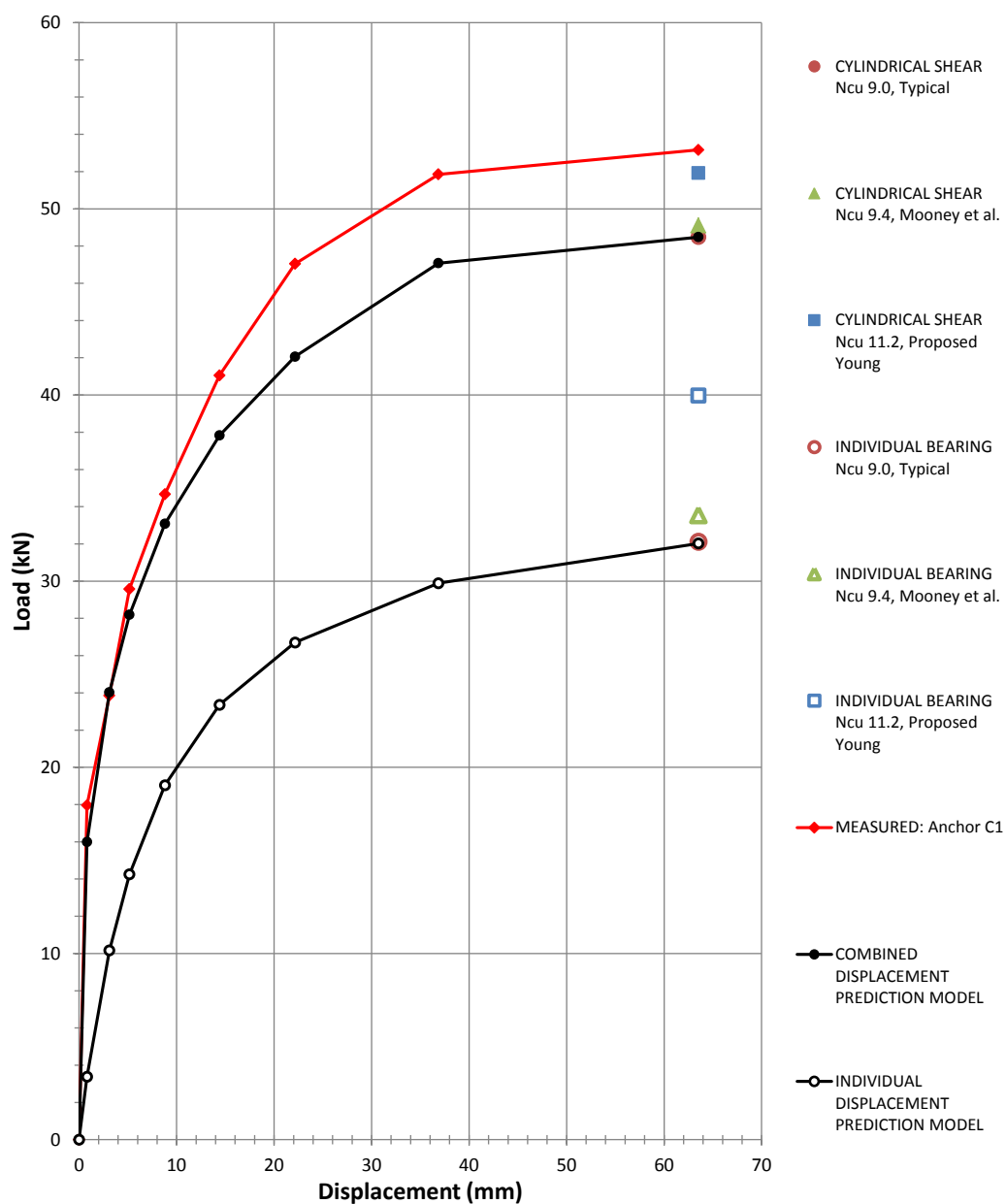


Figure 6.5 Calculated versus measured load-displacement curve for Anchor C1, the displacement models are calculated with an N_{cu} of 11.2.

The displacement model including side shear better predicts the anchor behavior as compared to the individual plate breakout model for Anchor C1. Previous

researchers have indicated, as discussed in Chapter 2, that a transition from cylindrical shear to individual plate breakout is affected by plate spacing. Therefore, some of the anchors in the load test database will be more accurately predicted by the combined displacement and others by a multi-plate individual plate breakout model.

All of the comparisons for the cylindrical shear displacement and individual plate breakout displacement prediction models for the load-displacement tests discussed in Chapter 4 are documented in Figures A.1 through A.18 in Appendix A. For the 18 load tests, nine were well characterized by the individual plate breakout model and nine were well characterized by the cylindrical shear model. For each model, the overall accuracy in characterizing the nine load-displacement curves is summarized in Table 6.1.

Table 6.1 Statistical summary of the performance of the two proposed displacement prediction models

Displacement Prediction Models	Proposed Cylindrical Shear Model			Proposed Individual Plate Model		
	$\bar{\lambda}$	σ	COV	$\bar{\lambda}$	σ	COV
N_{cu} Model						
Mooney et al. (1985)	0.987	0.137	14%	1.173	0.565	48%
Proposed	0.934	0.129	14%	0.906	0.368	41%

Using the proposed N_{cu} , both of the models appear to slightly over predict the load displacement curves as apparent in the mean bias. However, the variation in the model predictions for individual plate breakout is reduced, providing more consistent

results. In reliability-based design the slight reduction in the mean bias can be offset by properly calibrated resistance factors, therefore the reduction in variability is the more desirable. Although it is important to understand the overall behavior, the displacements of interest generally range from zero to 50 mm (zero to two inches).

The cylindrical shear displacement model provided good estimates of the Clemence (1983) load tests; this was as expected as the load tests were used to develop the side shear design model. The other anchor that behaved in a cylindrical manner was L1. Figure 6.6 shows the measured and predicted load-displacement curves for L1.

The load-displacement behavior of anchor L1 seems to be slightly over predicted for the first 20 mm (0.8 inches), however the predicted load curves model the general behavior well and provide a good estimate of the helical anchor resistance. A second anchor, tested by Lutenecker (2009), anchor L2, was also analyzed. The spacing ratio for L2 was 3.0, this anchor geometry is indicative of either transitional or individual plate breakout behavior. As presented in Figure 6.7 the anchor behaved in an individual manner. Once more the displacement model captured the general anchor behavior well, slightly over predicting for the first 25 mm (1 inch).

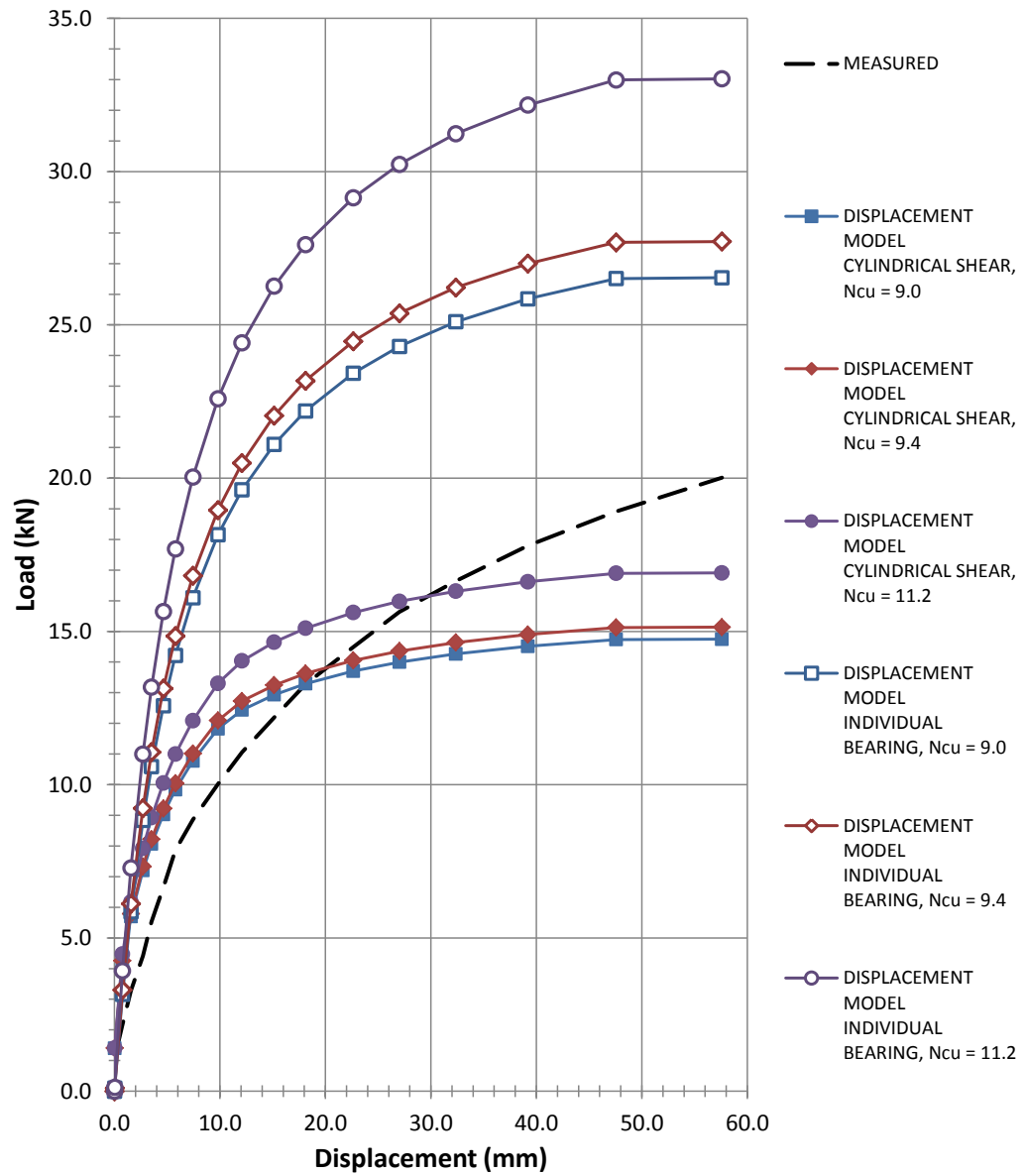


Figure 6.6 Predicted and measured load displacement curves for Anchor L1, $S/D = 0.75$.

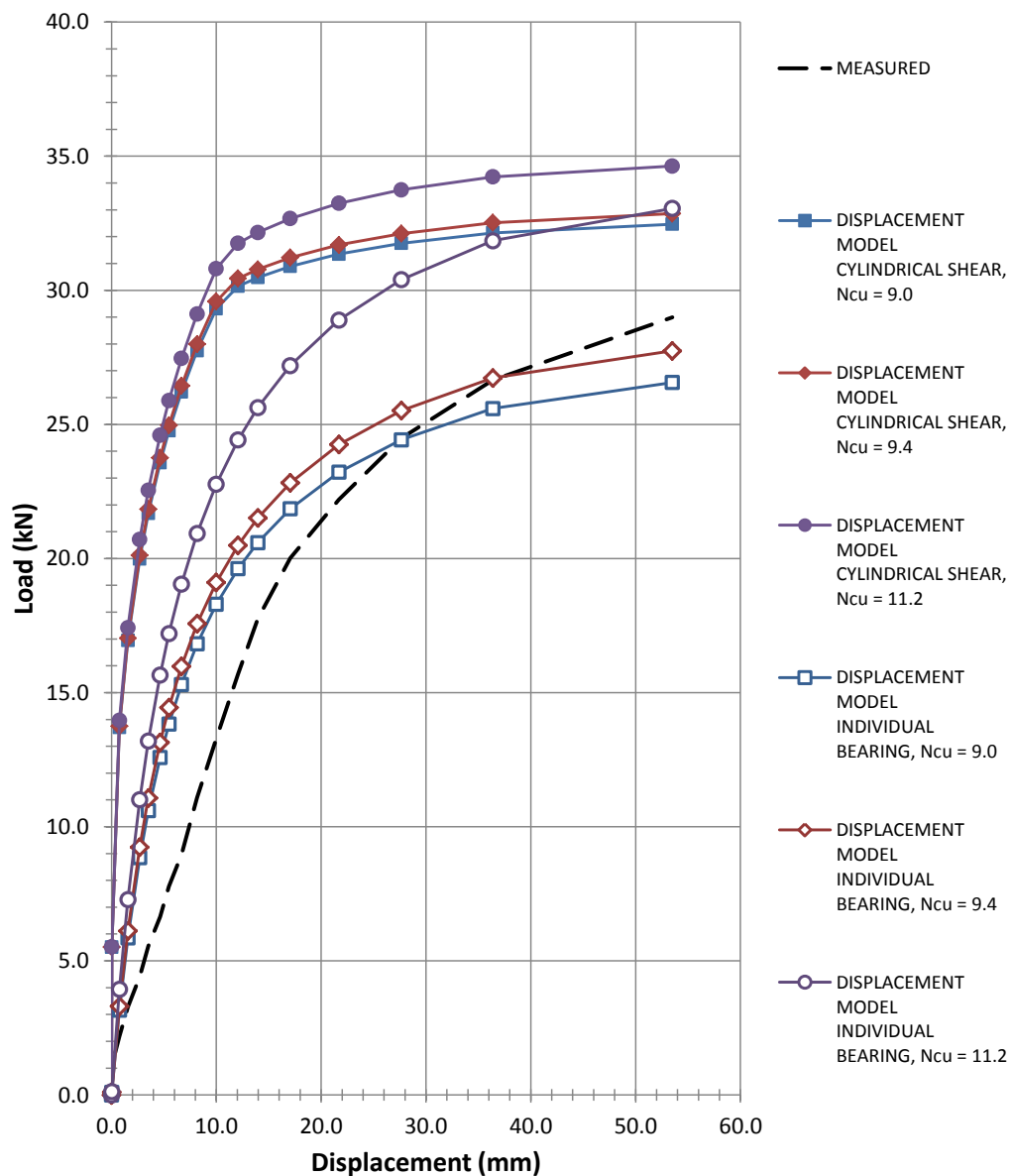


Figure 6.7 Predicted and measured load displacement curves for Anchor L2, $S/D = 3.0$.

The other anchors shown to behave in an individual plate manner were those tested by Stuedlein (2005). The displacement prediction models were able to characterize the anchors with well-defined load-displacement curves with reasonable

accuracy for the roughly the first 25 mm (1 inch); however, not all of the anchors presented well defined curves. An example of this is anchor S4, presented in Figure 6.8.

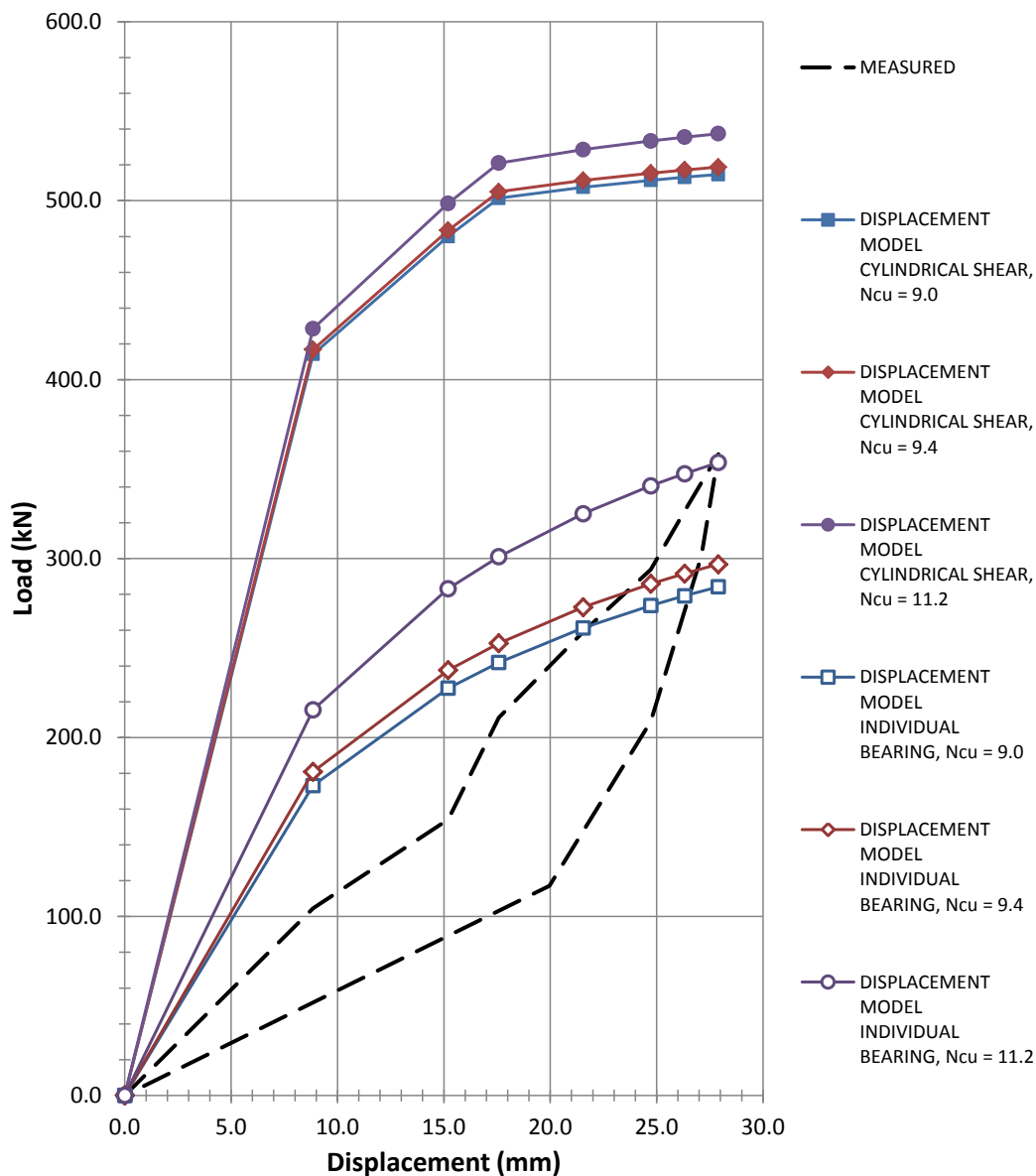


Figure 6.8 Predicted and measured load displacement curves for Anchor S4, S/D = 3.0.

The soil at the test site was a dessicated and highly fissured clay (Stuedlein, 2008). This secondary soil structure is likely the cause for such varied test results as presented in Figures 4.14 and 4.15. In such a soil, discontinuous planes of weakness (i.e., joints, slickensides) could prevent a cylindrical type failure if present in the soil adjacent to the anchor. However, the individual plate breakout displacement model accurately predicted the maximum observed resistance for all of the anchors not loaded to failure.

To further evaluate the displacement models, the CDF of the bias values for both the cylindrical shear and the individual plate breakout displacement model with an N_{cu} of 11.2 was developed, using methods described in Chapter 6. The cylindrical shear model, as presented in Figure 6.9, slightly over predicts as evident by the mean bias value of 0.93 however the left tail is lognormally distributed and relatively well defined by a fit-to-tail approximation.

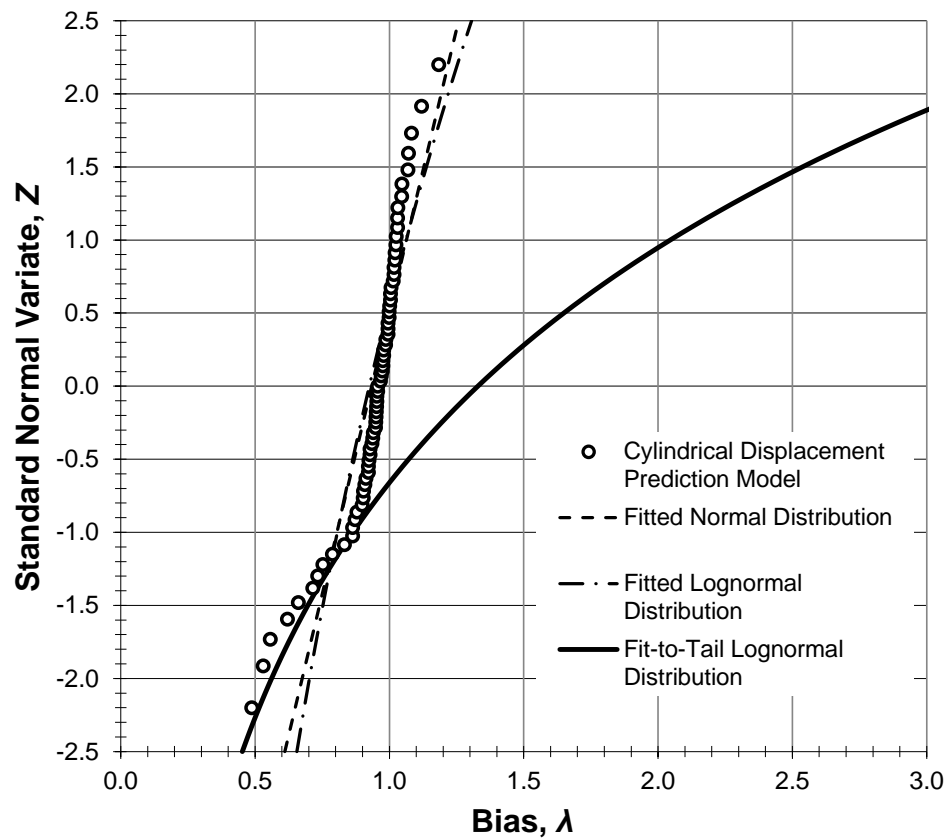


Figure 6.9 Bias CDF for the cylindrical shear displacement prediction model. The model shows a narrow range of variability, and a lognormally distributed tail.

The overall *COV* of 0.14, indicates a consistent model. This uniformity is also evident in the CDF. The individual plate breakout displacement model showed much more variability. As presented in Figure 6.10 the individual model bias was clearly lognormally distributed, with a similar tendency to over predict the resistance. The mean bias and *COV* developed using the fit-to-tail distribution was 0.91 and 0.41 respectively.

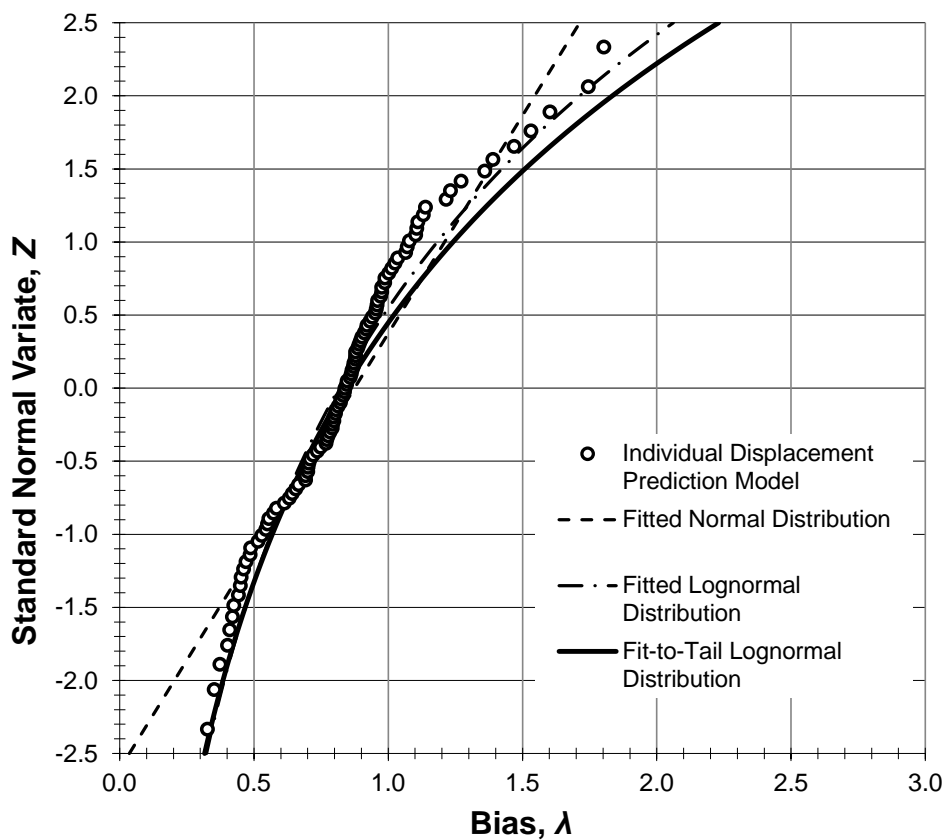


Figure 6.10 Bias CDF for the individual plate breakout displacement prediction model. The model shows a lognormal distribution well characterized by the fit-to-tail.

When the expected failure mechanism, either cylindrical shear or individual plate breakout, is unknown both prediction models should be evaluated, and the smaller resistance used as an estimate. To evaluate the case where the failure mechanism is unknown, both methods of prediction were used to estimate the resistance of each anchor in the database. For an unknown failure mechanism the means bias was 0.95 and the *COV* was 56%. This indicated an increase in variability

which as expected, and assumed to be due to the failure mechanism being unidentified.

6.6 SUMMARY

This Chapter has discussed the development and evaluation of displacement prediction models for helical anchor behavior. The models were developed using the work discussed in Chapter 5, and evaluated through comparisons with load-displacement curves presented in Chapter 4. The following conclusions and contributions were made:

- Displacement models assuming individual plate breakout and cylindrical shear failure mechanisms were developed to predict the load-displacement behavior of helical anchors loaded in uplift in clay soils.
- The mean bias and *COV* for the cylindrical shear displacement prediction model was 0.93 and 14%, respectively.
- The mean bias and *COV* for the individual plate breakout displacement model was 0.91 and 41%, respectively.
- When the governing failure mechanism is unclear the mean bias and *COV* including both individual plate breakout and cylindrical shear analyses was 0.95 and 56%, respectively.
- In general, both the individual plate breakout and cylindrical shear models appear to capture the shape of the helical anchor load displacement curves.

7 SUMMARY AND CONCLUSIONS

7.1 SUMMARY OF FINDINGS

Engineering knowledge of helical anchor behavior in cohesive soils has been uncertain, with improvements to helical anchor design almost non-existent over the last two decades. Although some research has been completed, the majority of helical anchors are still designed using the methods outlined in 1985. In this research, the load-displacement behavior of helical anchors in cohesive soils was assessed, and the existing design methods were evaluated.

A database of load tests including load-displacement curves was established through an extensive search of literature. This database was then utilized to evaluate the performance of the existing model for cylindrical shear and individual plate breakout capacity in uplift loading, as well as the existing uplift capacity factor model.

The uplift capacity factor is critical for the determination of the uplift capacity of a helical anchor; this research determined that the existing uplift capacity factor model was inaccurate. Therefore, a new uplift capacity factor was developed with the addition of new back-calculated N_{cu} data. The proposed uplift capacity factor showed an increase in the maximum of roughly 20%, from 9.4 to 11.2. The improved model also showed a significant decrease in the variability.

The uncertainty inherent in each capacity model was evaluated through the use of reliability-based design methods, to facilitate an LRFD calibration. Through the LRFD calibration, resistance factors were generated for the proposed helical anchor capacity models with assumed AASHTO loading.

Finally, two new displacement based models were developed to predict helical anchor displacement behavior, the proposed cylindrical shear and individual plate breakout displacement model. These new models were utilized to predict the capacity and displacement of each anchor in the load test database.

7.2 CONCLUSIONS

The completed research and findings are summarized for the behavior of helical anchors in cohesive soils, including the evaluations of the uplift capacity factor and the proposed and existing capacity prediction methods, in the following sections.

7.2.1 Development of an Uplift Capacity Model

A load test database was used to evaluate existing and proposed models of uplift capacity of helical anchors in clay to determine the accuracy and variability associated with each capacity model. The findings of the research on the capacity of helical anchors include:

- The uplift capacity factor, N_{cu} , proposed by Mooney et al. (1985) was found to be dependent on the embedment depth of the anchor and the magnitude of the back-calculated N_{cu} values used in uplift capacity factor model development.
- A proposed uplift capacity factor model was developed to eliminate the dependence of the anchor capacity on its embedment, and to have significantly reduced dependence on the magnitude of the back-calculated N_{cu} values.
- All of the methods for predicting the helical anchor uplift capacity exhibited large variability in capacity prediction (Coefficient of variation, COV , ranging from 42% to 77%). Specifically,
 - The existing cylindrical shear model (Mooney, et al., 1985) produced a mean bias of 0.91 and a COV of 43%
 - The existing individual plate breakout model (Mooney, et al., 1985) produced a mean bias of 1.22 and a COV of 77%
 - The proposed cylindrical shear model produced a mean bias of 0.84 and a COV of 42%
 - The proposed individual plate breakout model produced a mean bias of 0.92 and a COV of 72%
- Resistance factors for anchor capacity calculated using the two proposed capacity models were developed through LRFD calibration for probabilities of failure of 1 and 0.1 percent, and are presented in Tables 5.5 and 5.6, and in Figures 5.13 and 5.14.

The evaluation of the uplift capacity model led to the improvement of the uplift capacity factor, N_{cu} , reducing model dependence and increasing the available capacity. Additionally, the outcome of the uncertainty analysis reaffirmed previous research, presenting a large variability in predicting the ultimate resistance of a helical anchor. This further affirmed the need for a new model to predict helical anchor capacity.

7.2.2 Development of a Load-Displacement Model

Two displacement prediction models to estimate the behavior of helical anchors in uplift capacity were developed, utilizing load-displacement curves from load tests performed on helical anchors in cohesive soils. The load-displacement data was normalized and used to develop models for the prediction of anchor breakout and side shear.

The breakout model was developed using single plate load-displacement curves, through normalization it became apparent that the breakout behavior of the plates could be characterized by a single curve regardless of the embedment depth of the plate. Similarly, the side shear model was developed using multi-plate load-displacement curves; however, the side shear was characterized by two distinct curves, one for anchors with an embedment depth of four and one for anchors with an embedment depth of eight or greater. By combining these models the displacement of helical anchors in cohesive soils could be predicted.

The two proposed displacement prediction models were evaluated using a load test database to determine the accuracy and variability associated with each model. The findings of the research on the displacement prediction models for helical anchor behavior include:

- Displacement models assuming individual plate breakout and cylindrical shear failure mechanisms were developed to predict the load-displacement behavior of helical anchors loaded in uplift in clay soils.
- The mean bias and *COV* for the cylindrical shear displacement prediction model was 0.93 and 14%, respectively.
- The mean bias and *COV* for the individual plate breakout displacement model was 0.91 and 41%, respectively.
- When the governing failure mechanism is unclear the mean bias and *COV* including both individual plate breakout and cylindrical shear analyses was 0.95 and 56%, respectively.
- In general, the two models appear to capture the shape of the helical anchor load displacement curves.

The existing design methods produce a discrete resistance value, the ultimate resistance. The proposed displacement models predict the load-displacement behavior providing an estimate of anchor resistance for any value of displacement, and allowing engineers to generate a predicted load-displacement curve. These proposed

displacement models present a new technique which will alter the way engineers design for helical anchors.

7.3 STATEMENT OF LIMITATIONS

The models created in this research were based on data from helical anchor load tests in cohesive soils, with a maximum plate diameter of roughly 406 mm (16 inches). The use of these models in other soils or with significantly larger plate diameters is not recommended without further testing and verification.

7.4 SUGGESTIONS FOR FUTURE RESEARCH

The research discussed herein has identified improvements in predicting helical anchor capacity and displacement in cohesive soils. Nonetheless, there are areas of further study into helical anchor displacement behavior that may be performed to increase understanding and improve the models described in this thesis. Areas recognized as future opportunities can include:

- Full scale helical anchor tests should be conducted in well characterized cohesive soils to refine the models proposed in this thesis.
- Following the collection of more data, a new study into the uplift capacity factor should be undertaken, to remove model dependency and uncertainty, improving overall helical anchor predictions.

- Research should be conducted to develop displacement models for helical anchors in granular soils.

REFERENCES

- AASHTO. (2007). *LRFD Bridge Design Specifications* (4th ed.). Washington, D.C.: AASHTO.
- Ali, M. S. (1969). *Pullout Resistance of Anchor Plates and Anchor Piles in Soft Bentonite Clay*. Durham, North Carolina: Duke University.
- Allen, T. M., Nowak, A. S., & Bathurst, R. J. (2005). *Calibration to Determine Load and Resistance Factors for geotechnical and Structural Design*. Washington, D.c.: Transportation Research Board.
- Bathurst, R. J., Allen, T. M., & Nowak, A. S. (2008). Calibration concepts for load and resistance factor design (LRFD) of reinforced soil walls. *Canadian Geotechnical Journal*(45), 1377-1392.
- Clemence, S. P. (1983). *The Uplift and Bearign capacity of Helix Anchors in Soil*. Department of Civil Engineering. Syracuse, New York: Syracuse University.
- Clemence, S. P., & Hoyt, R. M. (1989). *Uplift Capacity of Helical Anchors in Soil*. AB Chance Company.
- Das, B. M. (2007 (Reprint c1987)). *Theoretical Foundation Engineering*. Fort Lauderdale, Florida: J. Ross Publishing.

- Das, B. M. (2007 (Reprint c1990)). *Earth Anchors*. Fort Lauderdale, Florida: J. Ross Publishing.
- Davis, R. K. (1982). The Behavior of Anchor Plates in Clay. *Geotechnique*, 32, 9-23.
- Francis & Lewis International, L. (2012, February 27). *FLI Structures Site Services*. Retrieved from FLI Structures Screw Pile Foundations: <http://www.fliscrew piles.co.uk/site-services.php>
- Handojo, H. (1997). *Uplift Capacity of Helical Anchors*. Corvallis, Oregon: Oregon State University.
- Hoyt, R. M., & Clemence, S. P. (1989). *Uplift Capacity of Helical Anchors in Soil*. Centralia, MO.: A.B. Chance Company.
- Hubbel, I. (2012, February 27). *Helical Pile Walkway Report*. Retrieved from ABCHance Civil Construction: <http://www.abchance.com/resources/case-histories/04-0701.pdf>
- Kondner, R. (1963, February). Hyperbolic Stress Strain Response: Cohesive Soils. *Journal of the Soil Mechanics and Foundations Division*, 89(SMI), 115-144.
- Lutenegger, A. J. (2003). Helical Screw Piles and Screw Anchors - An Historical Prospective and Introduction. *Proceedings of the Helical Foundations and Tie-Backs Seminar*. Unpublished.

- Lutenegger, A. J. (2009). Cylindrical Shear or Plate Bearing? - Uplift Behavior of Multi-Helix Screw Anchors in Clay. *International Foundation Congress and Equipment Expo*, 456-463.
- Magnum Piering, I. (2012, February 27). *Magnum Helical Pile System*. Retrieved from Magnum Piering, Rock Solid: http://www.magnumpiering.com/commercial/helical_pier_system.aspx
- Merifield, R. S. (2011). Ultimate Uplift Capacity of Multiplate Helical Type Anchors in Clay. *Journal of Geotechnical and Geoenvironmental Engineering*, 704-716.
- Mooney, J. S. (1985). Uplift Capacity of Helical Anchors in Clay and Silt. *Uplift Behavior of Anchor Foundations in Soil* (pp. 48-72). Detroit, Michigan: American Society of Civil Engineers.
- Mooney, J. S., Adamczak, Jr., S., & Clemence, S. P. (1985). Uplift Capacity of Helical Anchors in Clay and Silt. *Uplift Behavior of Anchor Foundations in Soil* (pp. 48-72). Detroit, Michigan: American Society of Civil Engineers.
- Pack, J. S. (2000). Design of Helical Piles for Heavily Loaded Structures. *New Technological and Design Developments in Deep Foundations (GSP 100)* (pp. 353-367). Denver, Colorado: American Society of Civil Engineers.

- Pack, J. S. (2006). Performance of Square Shaft Helical Pier Foundations in Swelling Soils. *Geo-volution*, 76-85.
- Perko, H. A. (2000). Energy Method for Predicting Installation Torque of Helical Foundations and Anchors. *New Technological and Design Developments in Deep Foundations (GSP 100)* (pp. 342-352). Denver, Colorado: American Society of Civil Engineers.
- Perko, H. A. (2009). *Helical Piles, A practical Guide to Design and Installation*. Hoboken, New Jersey: John Wiley & Sons, Inc.
- Prasad, Y., & Rao, S. (1996). Lateral Capacity of Helical Piles in Clays. *Journal of Geotechnical Engineering*, 938-941.
- Rao, S., & Prasad, Y. (1993). Estimation of Uplift Capacity of Helical Anchors in Clays. *Journal of Geotechnical Engineering*, 352-357.
- Rao, S., Prasad, Y., & Shetty, M. (1991). The Behavior of Model Screw Piles in Cohesive Soils. *Soils and Foundations*, 31, 35-50.
- Rao, S., Prasad, Y., & Veeresh, C. (1993). Behavior of Embedded Model Screw Anchors in Soft Clays. *Geotechnique*, 43, 605-614.
- Sakr, M. (2009). Performance of Helical Piles in Oil Sand. *Canadian Geotechnical Journal*, 46, 1046-1061.

- Shipton, B. A. (1997). *The Effect of Uplift, Compressive, and Repeated Loads on Helical Anchors*. Corvallis, Oregon: Oregon State University.
- Strahler, A. W. (2012). *Bearing Capacity and Immediate Settlement of Shallow Foundations on Clay*. Corvallis, Oregon: Oregon State University.
- Structures, F. (2012, February 27). *Screw Pile Foundations - Site Services*. Retrieved from FLI Structures Screw Pile Foundations: <http://www.fliscrew piles.co.uk/site-services.php>
- Stuedlein, A. W. (2008). *Bearing Capacity and Displacements of Spread Footings on Aggregate Pier Reinforced Clay*. University of Washington, Civil and Environmental Engineering. Seattle, Washington: University of Washington.
- Stuedlein, A. W., Neely, W., & Gurtowski, T. (2012). Reliability Based Design of Augered Cast-In-Place Piles in Granular Soils. *Journal of geotechnical and Geoenvironmental Engineering*, 138(6), 23.

APPENDICES

APPENDIX A: DISPLACEMENT PREDICTIONS

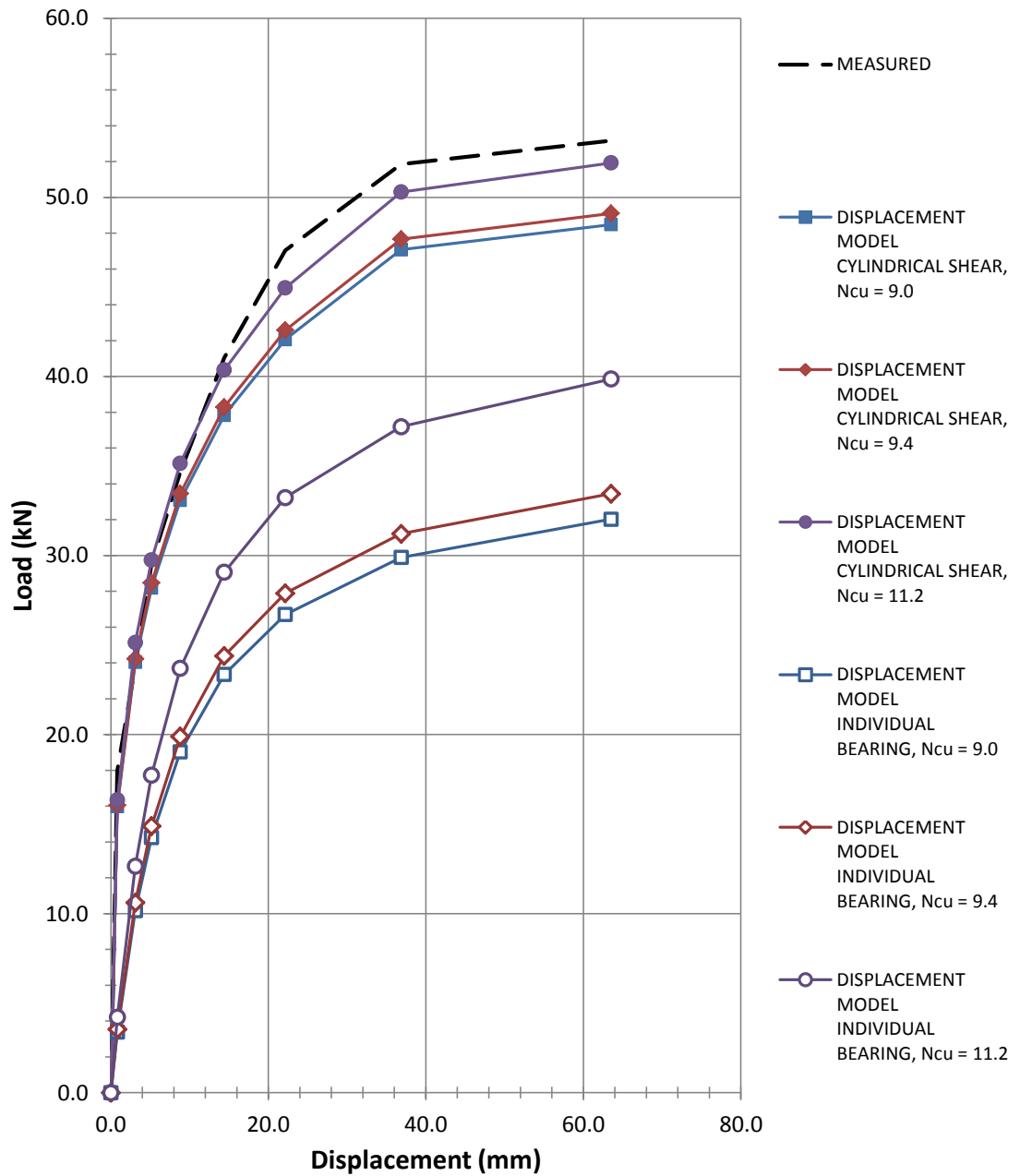


Figure A.1 Load-displacement curve for anchor C1, compared to the predicted curves using the proposed cylindrical shear and individual plate breakout models, calculated with the typical, theoretical, and proposed N_{cu} values of 9.0, 9.4, and 11.2 respectively.

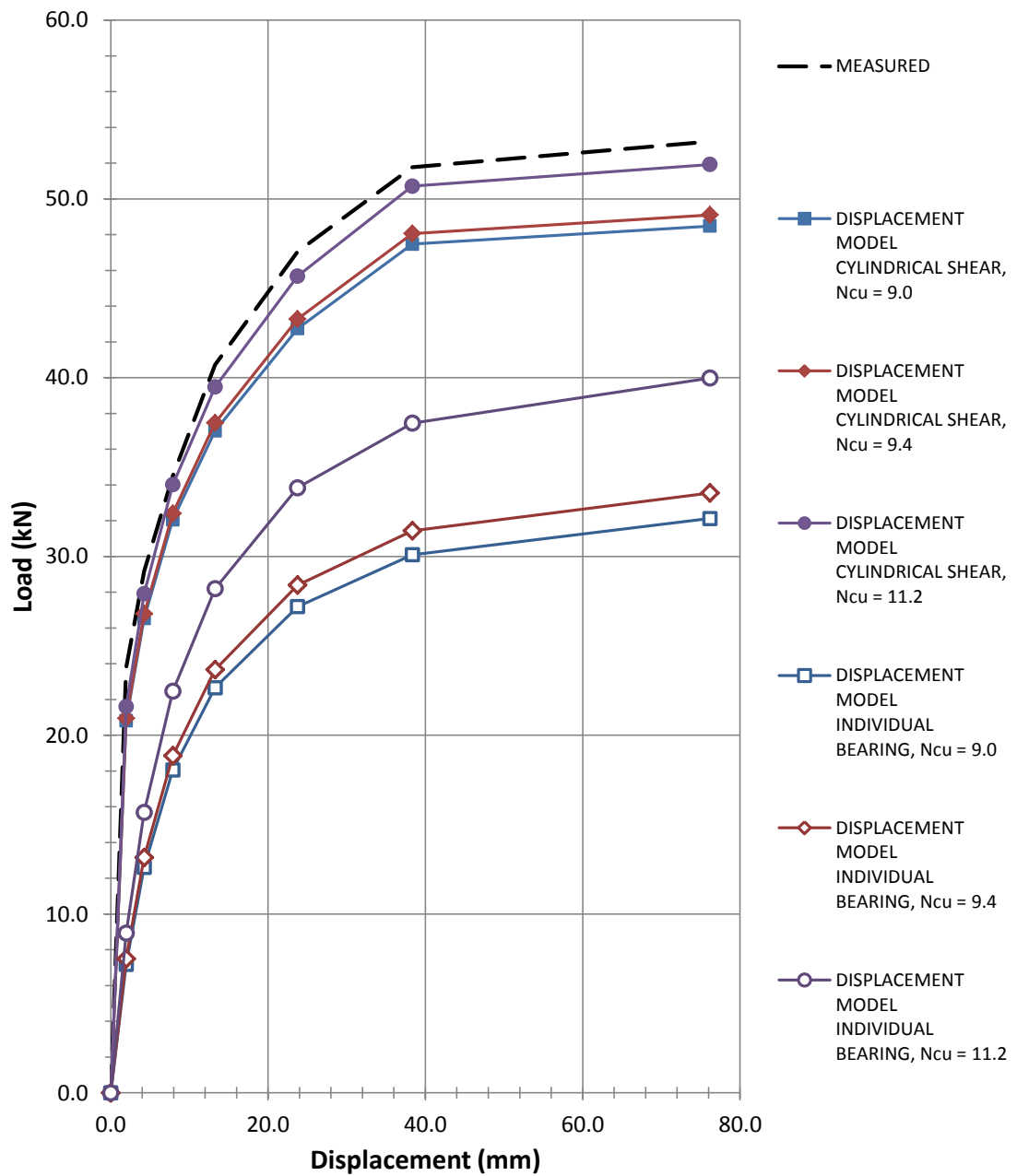


Figure A.2 Load-displacement curve for anchor C2, compared to the predicted curves using the proposed cylindrical shear and individual plate breakout models, calculated with the typical, theoretical, and proposed N_{cu} values of 9.0, 9.4, and 11.2 respectively.

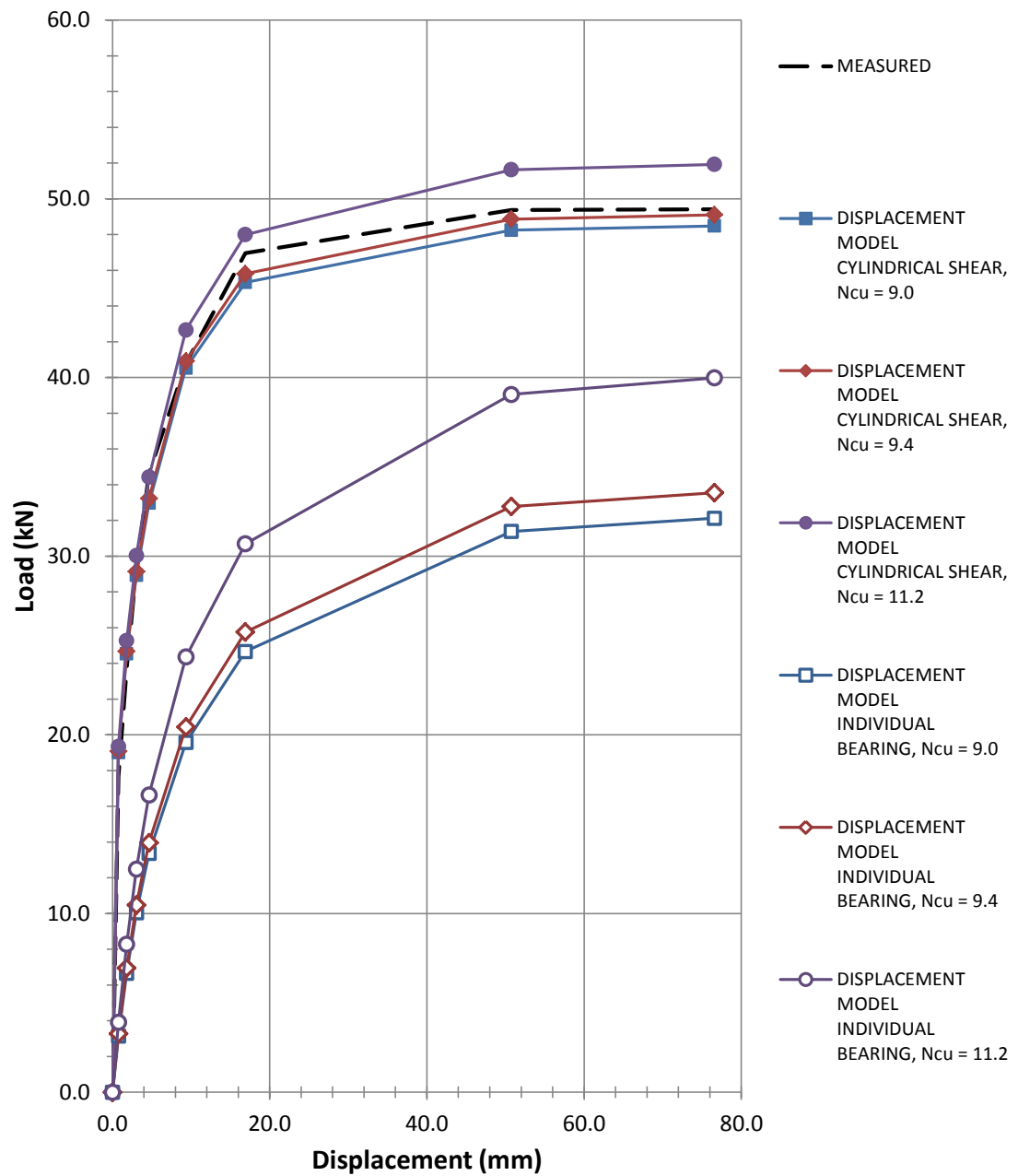


Figure A.3 Load-displacement curve for anchor C3, compared to the predicted curves using the proposed cylindrical shear and individual plate breakout models, calculated with the typical, theoretical, and proposed N_{cu} values of 9.0, 9.4, and 11.2 respectively.

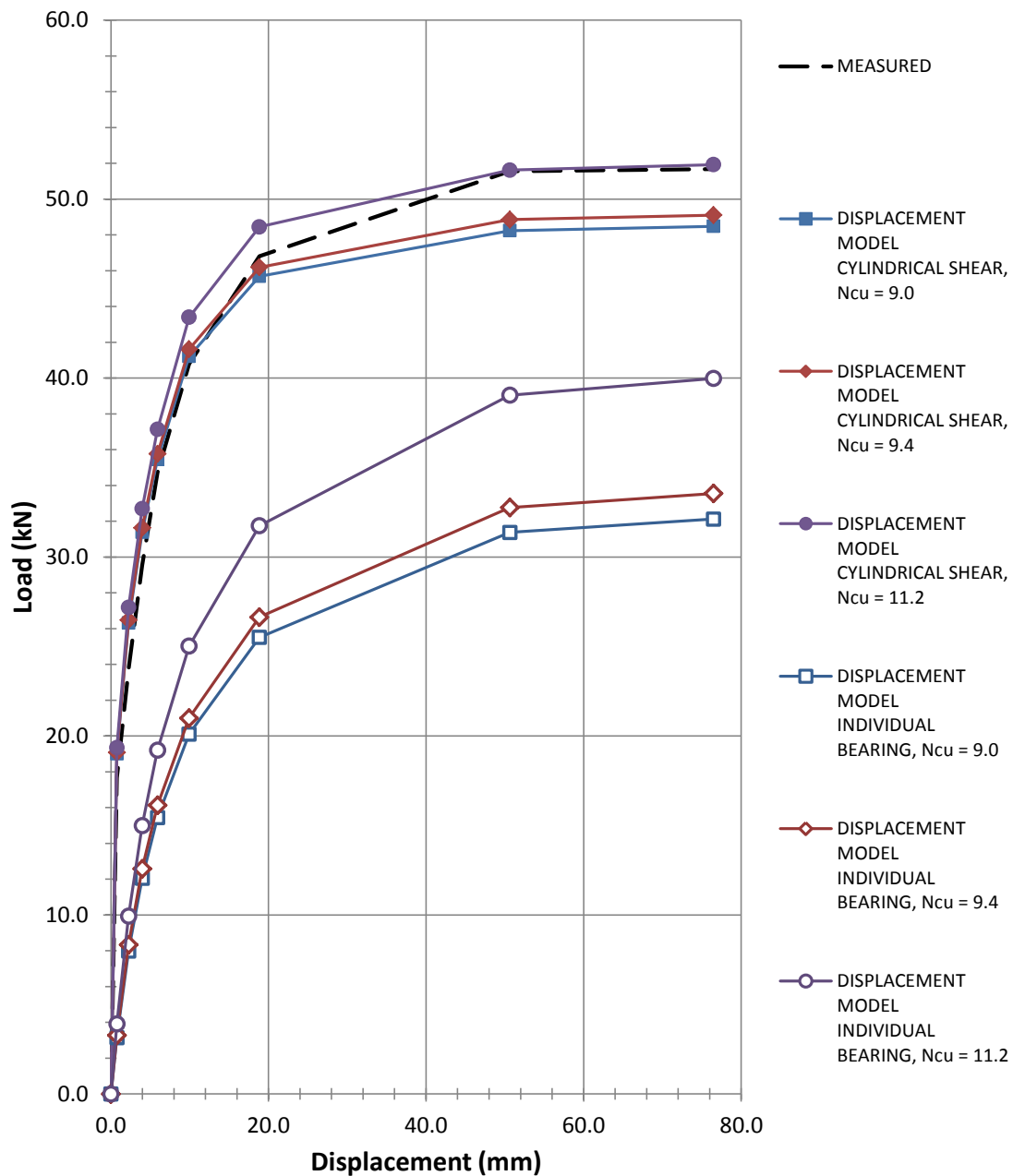


Figure A.4 Load-displacement curve for anchor C4, compared to the predicted curves using the proposed cylindrical shear and individual plate breakout models, calculated with the typical, theoretical, and proposed N_{cu} values of 9.0, 9.4, and 11.2 respectively.

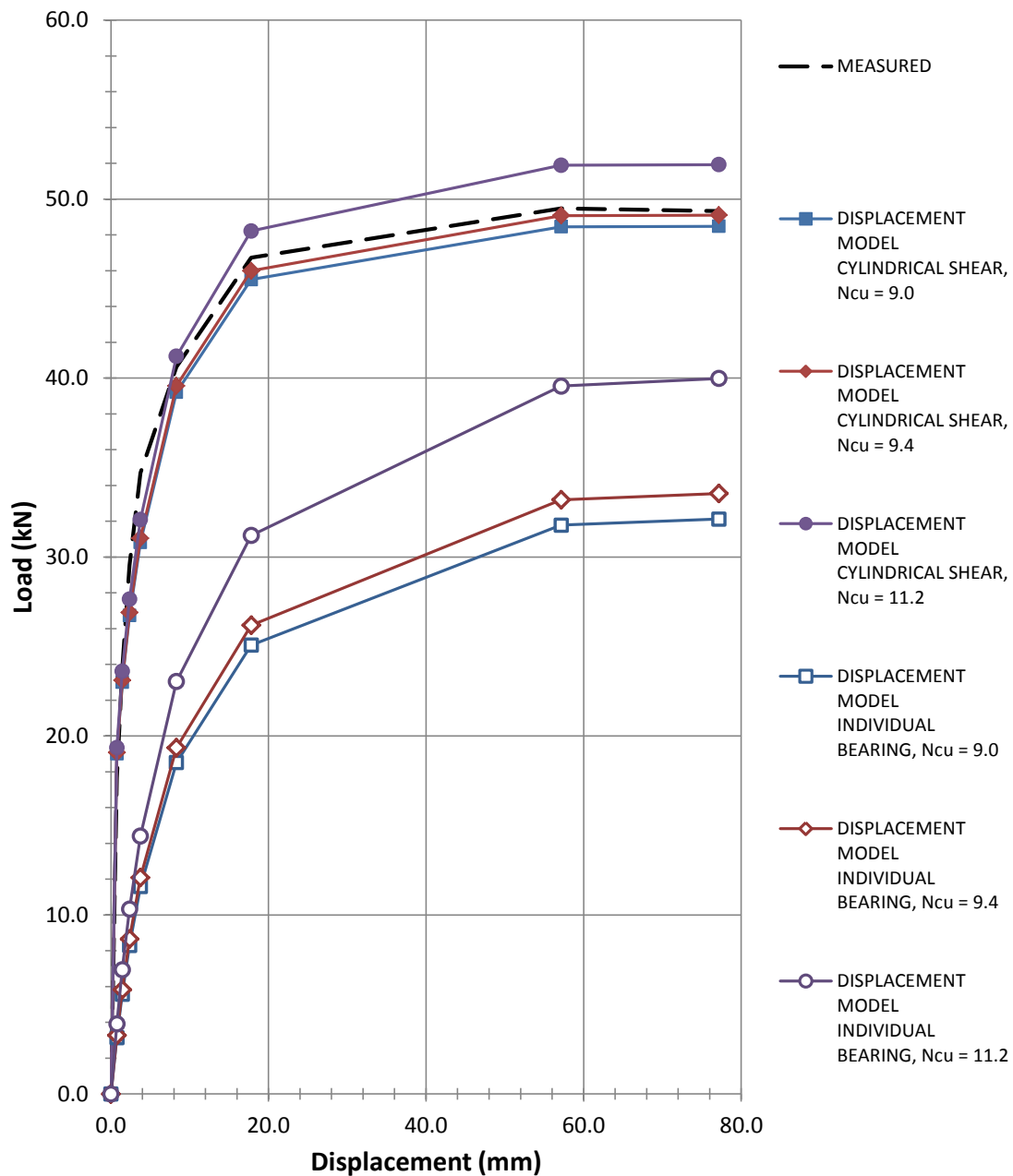


Figure A.5 Load-displacement curve for anchor C5, compared to the predicted curves using the proposed cylindrical shear and individual plate breakout models, calculated with the typical, theoretical, and proposed N_{cu} values of 9.0, 9.4, and 11.2 respectively.

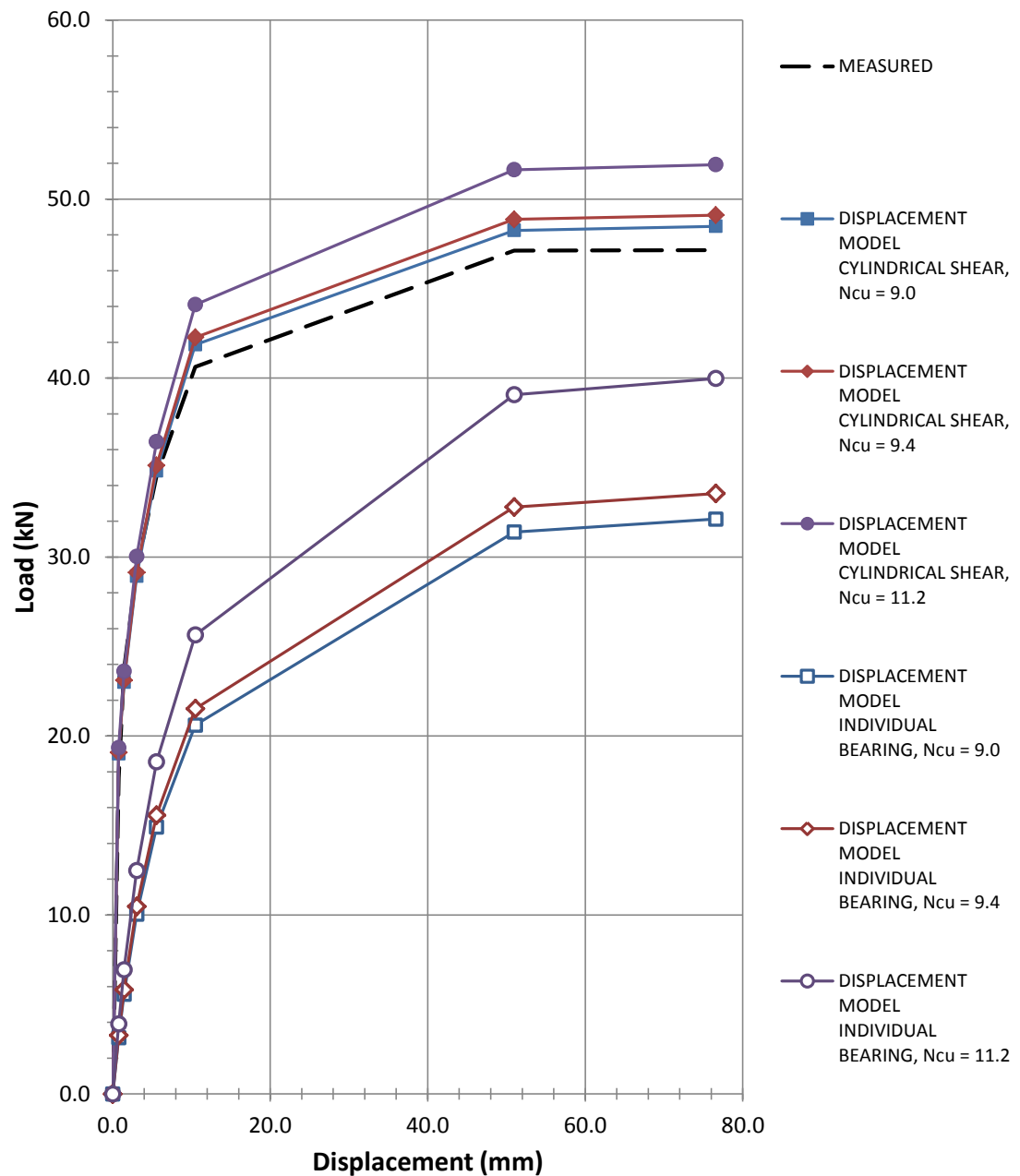


Figure A.6 Load-displacement curve for anchor C6, compared to the predicted curves using the proposed cylindrical shear and individual plate breakout models, calculated with the typical, theoretical, and proposed N_{cu} values of 9.0, 9.4, and 11.2 respectively.

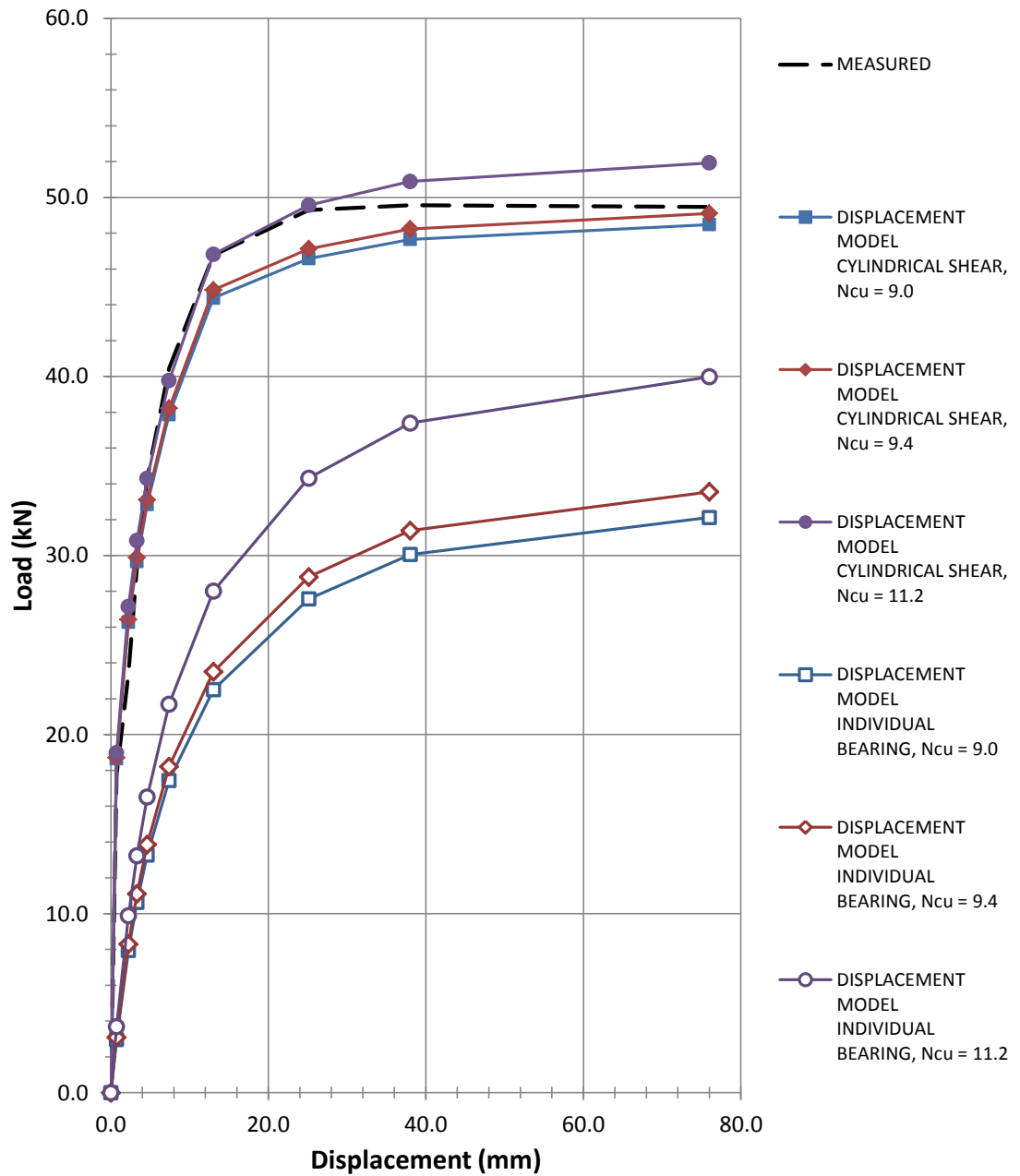


Figure A.7 Load-displacement curve for anchor C7, compared to the predicted curves using the proposed cylindrical shear and individual plate breakout models, calculated with the typical, theoretical, and proposed N_{cu} values of 9.0, 9.4, and 11.2 respectively.

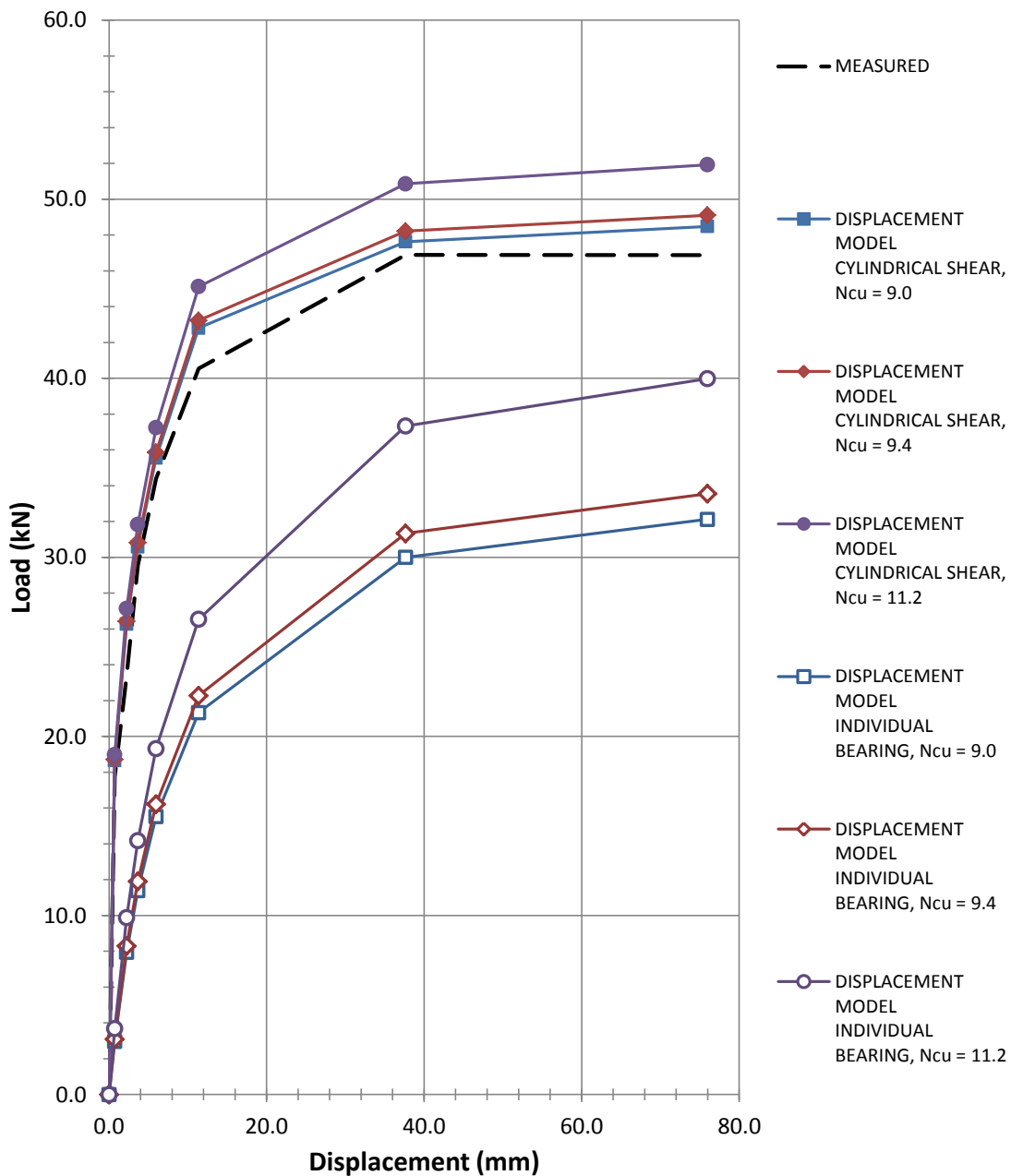


Figure A.8 Load-displacement curve for anchor C8, compared to the predicted curves using the proposed cylindrical shear and individual plate breakout models, calculated with the typical, theoretical, and proposed N_{cu} values of 9.0, 9.4, and 11.2 respectively.

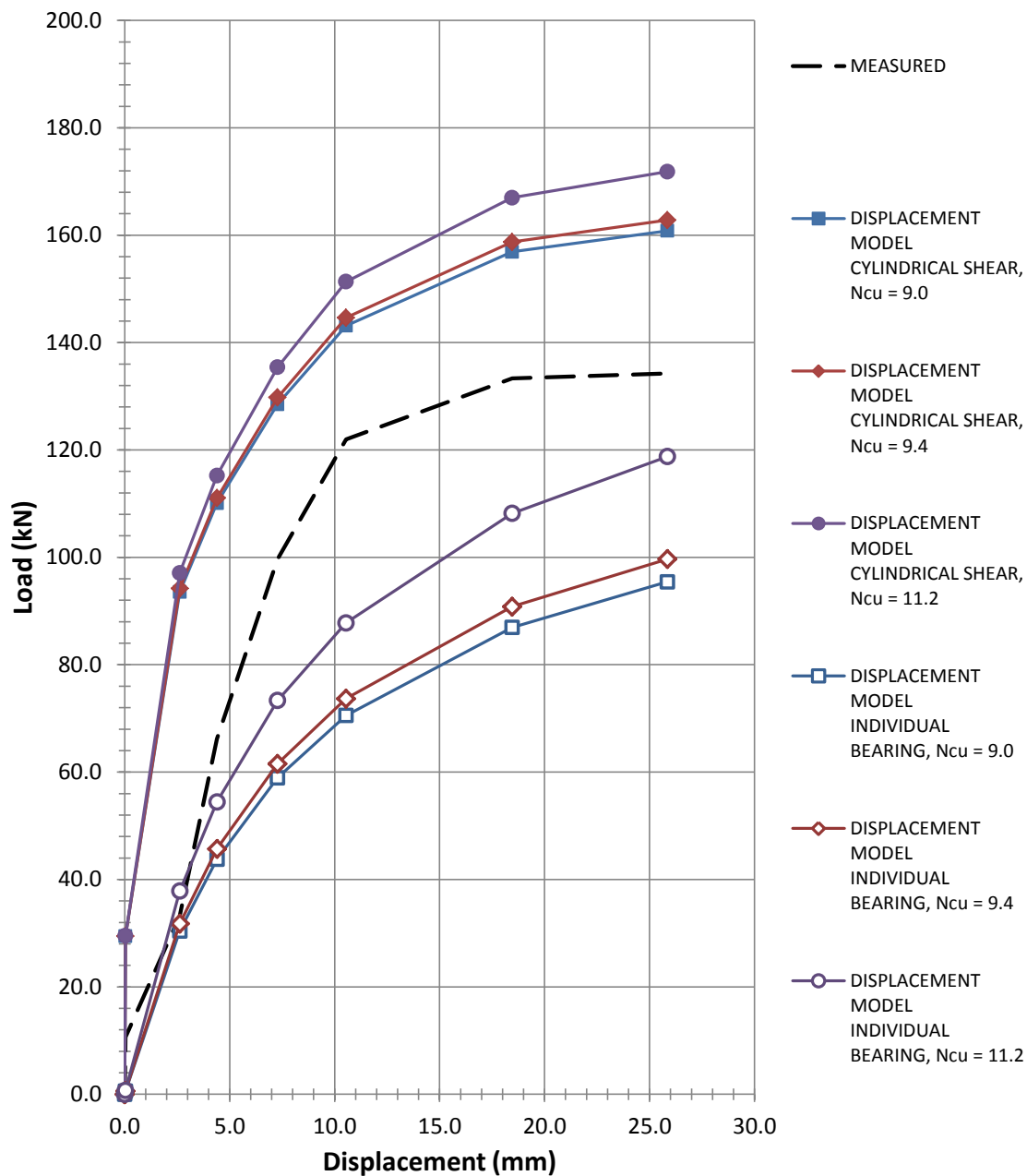


Figure A.9 Load-displacement curve for anchor H1, compared to the predicted curves using the proposed cylindrical shear and individual plate breakout models, calculated with the typical, theoretical, and proposed N_{cu} values of 9.0, 9.4, and 11.2 respectively.

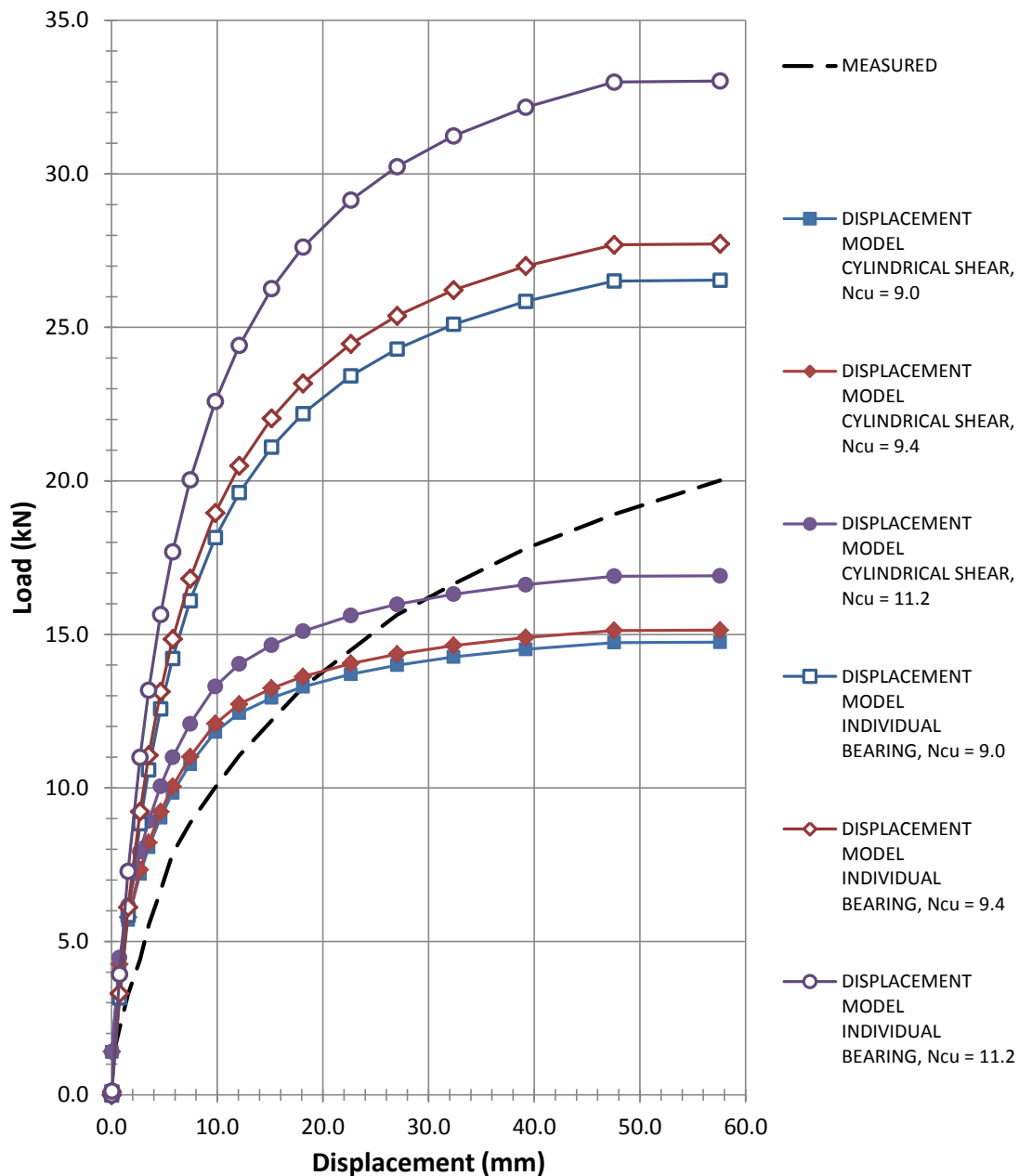


Figure A.10 Load-displacement curve for anchor L1, compared to the predicted curves using the proposed cylindrical shear and individual plate breakout models, calculated with the typical, theoretical, and proposed N_{cu} values of 9.0, 9.4, and 11.2 respectively.

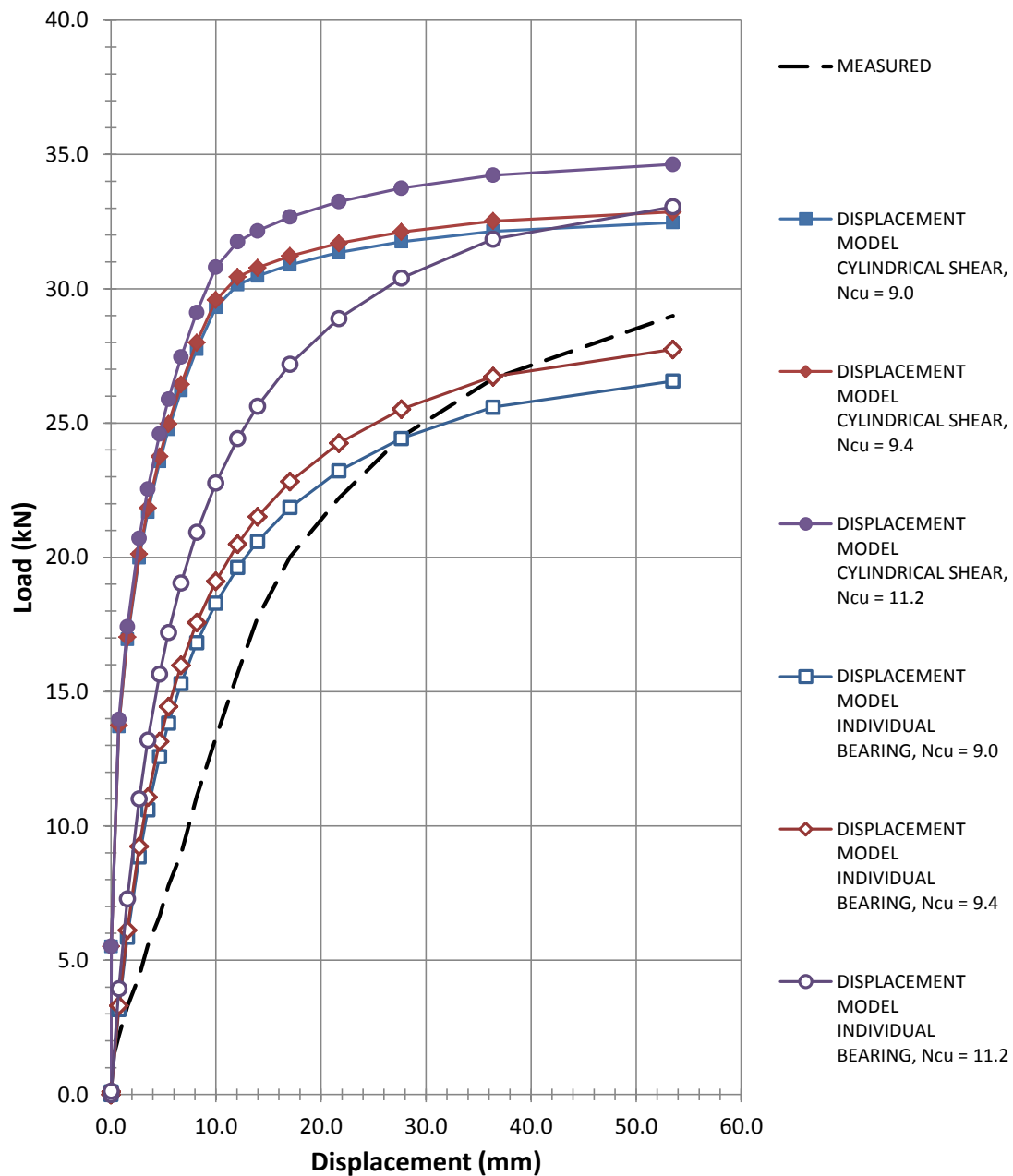


Figure A.11 Load-displacement curve for anchor L2, compared to the predicted curves using the proposed cylindrical shear and individual plate breakout models, calculated with the typical, theoretical, and proposed N_{cu} values of 9.0, 9.4, and 11.2 respectively.

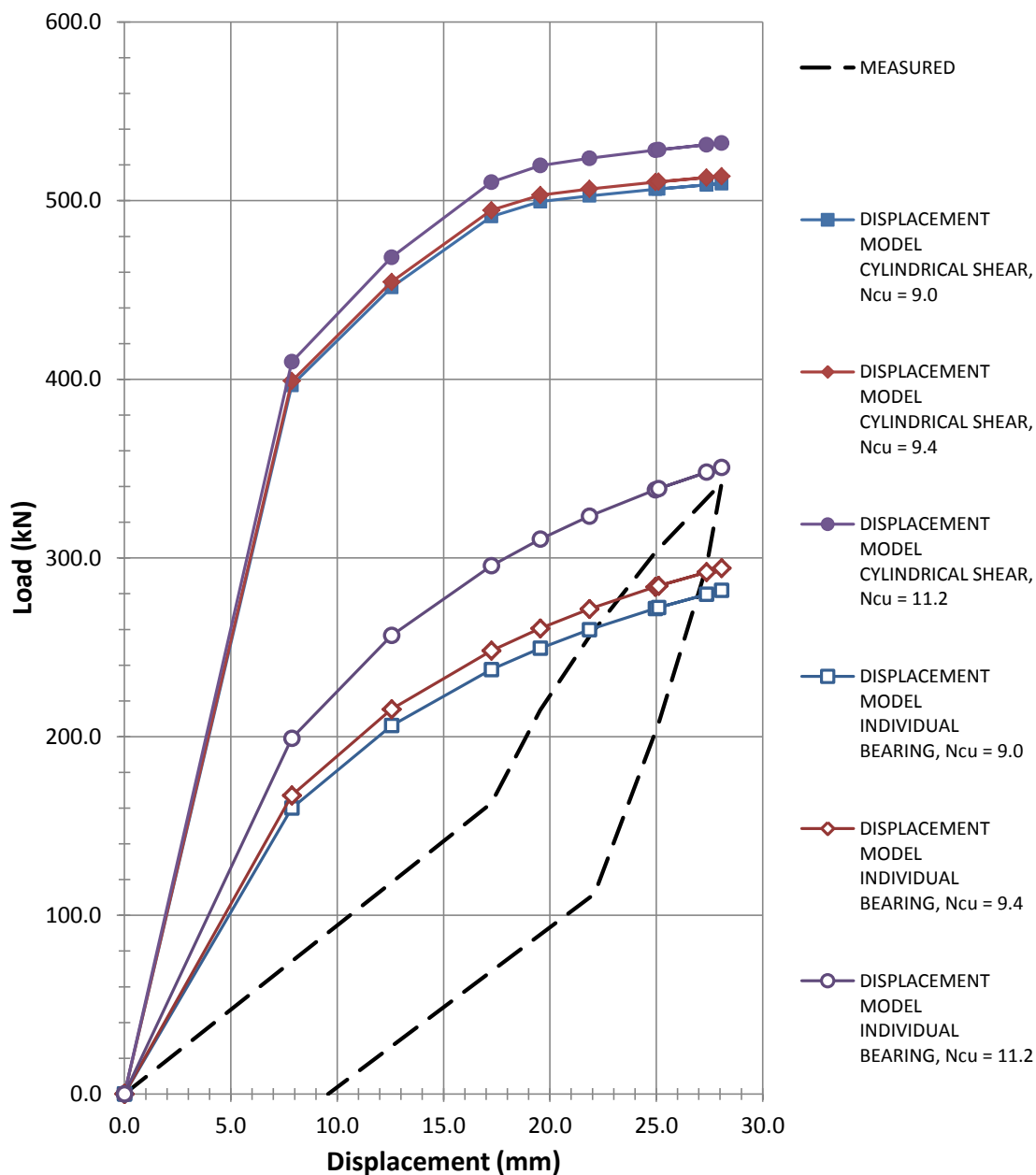


Figure A.12 Load-displacement curve for anchor S1, compared to the predicted curves using the proposed cylindrical shear and individual plate breakout models, calculated with the typical, theoretical, and proposed N_{cu} values of 9.0, 9.4, and 11.2 respectively.

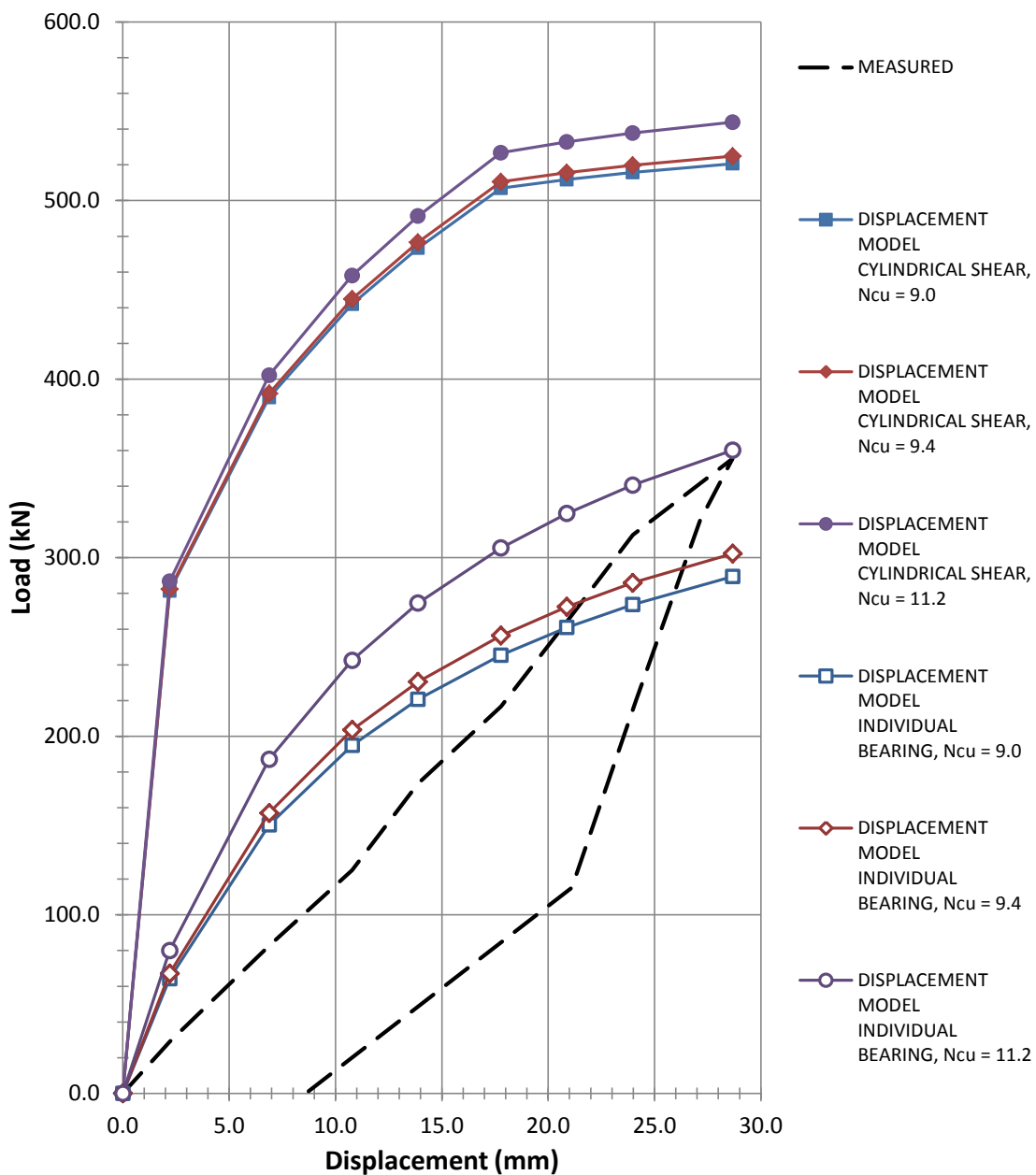


Figure A.13 Load-displacement curve for anchor S2, compared to the predicted curves using the proposed cylindrical shear and individual plate breakout models, calculated with the typical, theoretical, and proposed N_{cu} values of 9.0, 9.4, and 11.2 respectively.

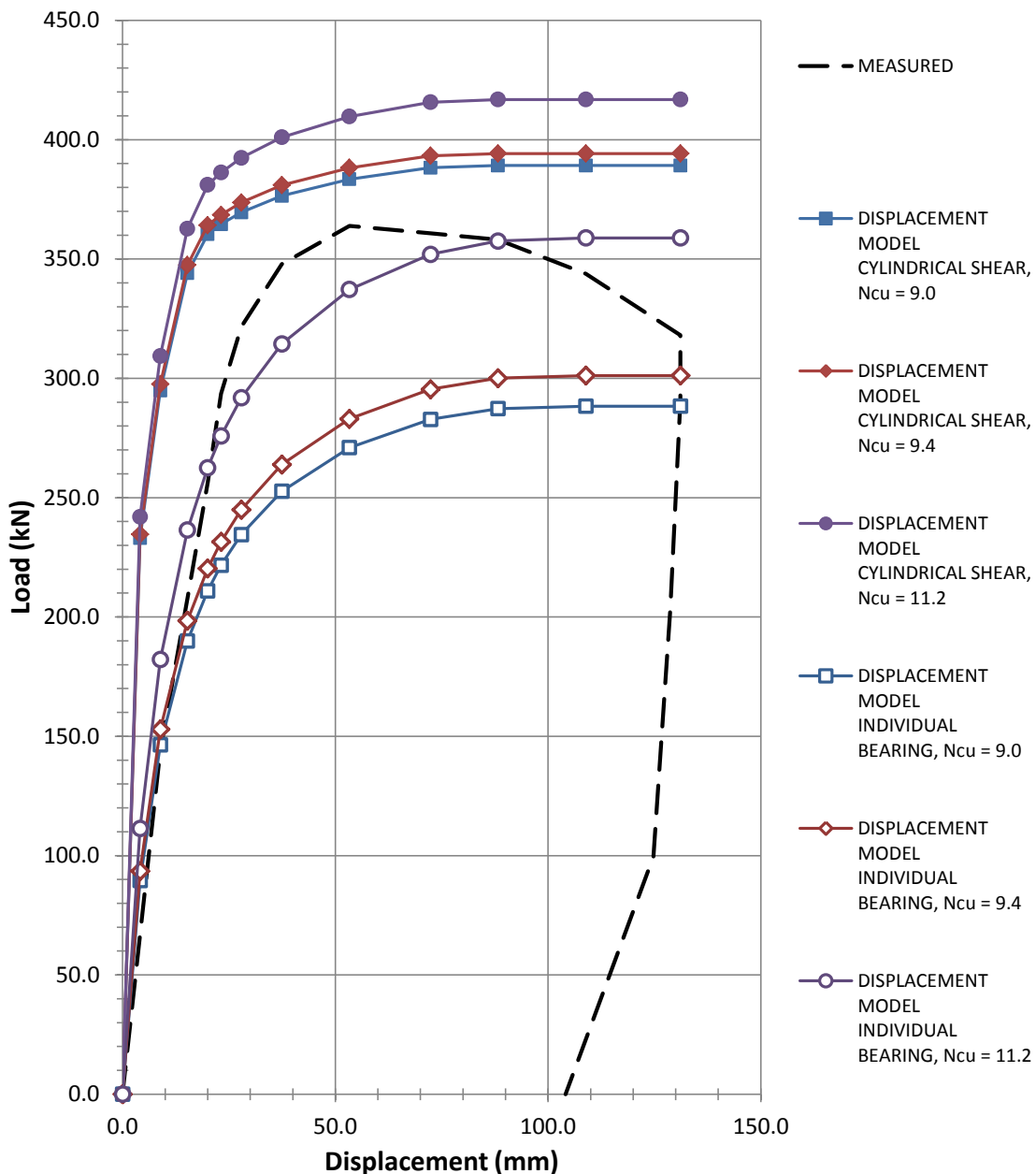


Figure A.14 Load-displacement curve for anchor S3, compared to the predicted curves using the proposed cylindrical shear and individual plate breakout models, calculated with the typical, theoretical, and proposed N_{cu} values of 9.0, 9.4, and 11.2 respectively.

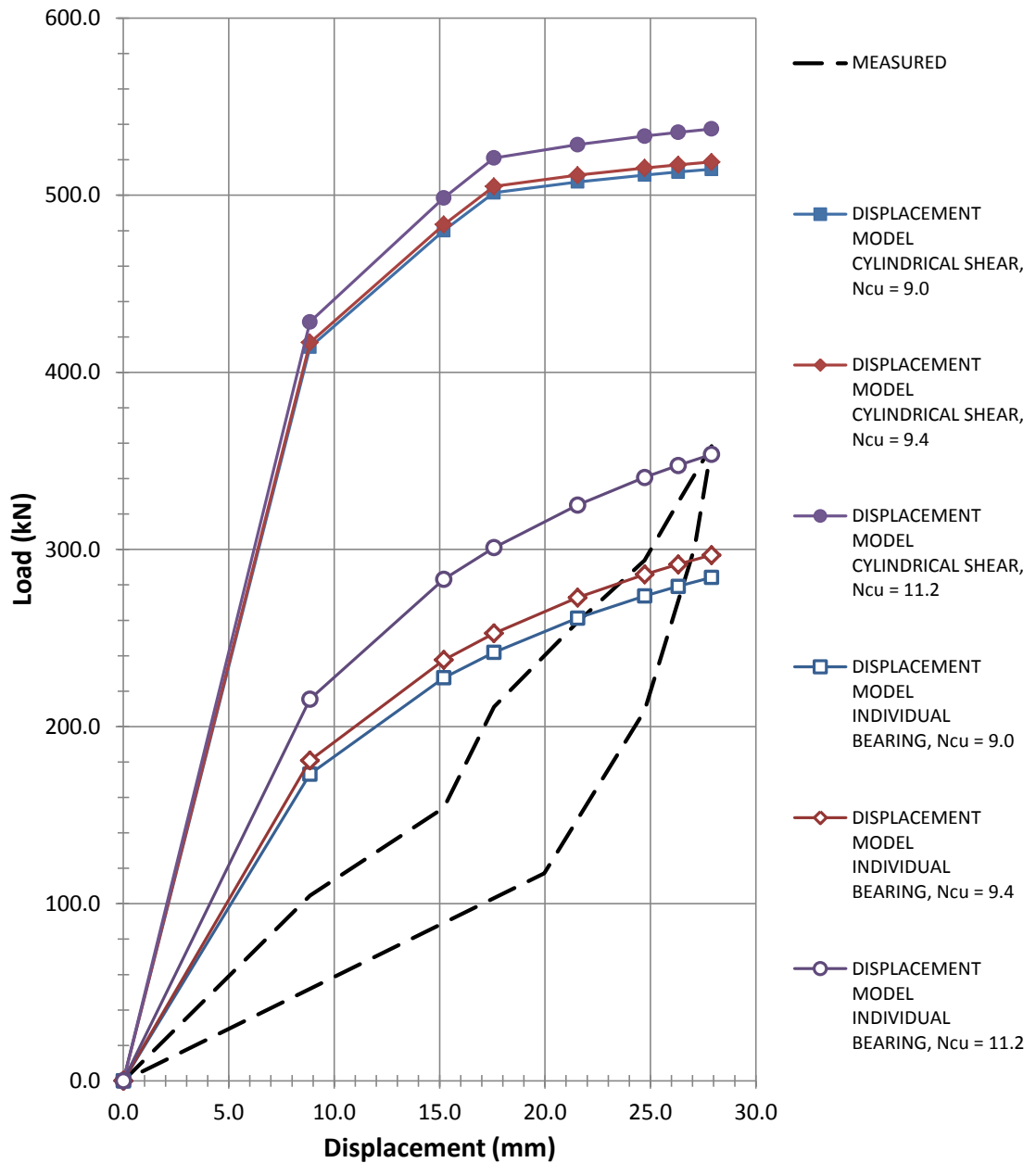


Figure A.15 Load-displacement curve for anchor S4, compared to the predicted curves using the proposed cylindrical shear and individual plate breakout models, calculated with the typical, theoretical, and proposed N_{cu} values of 9.0, 9.4, and 11.2 respectively.

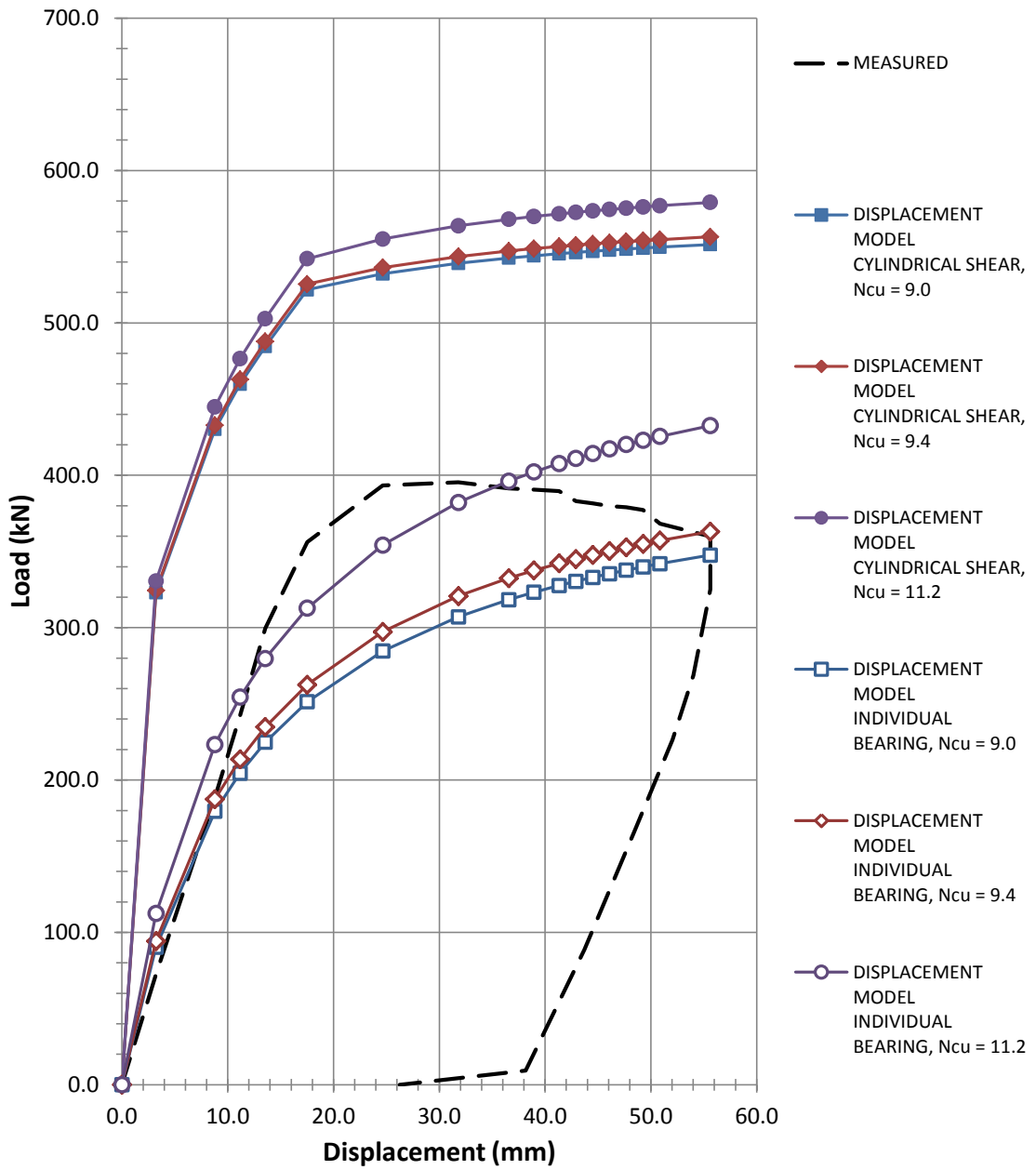


Figure A.16 Load-displacement curve for anchor S5, compared to the predicted curves using the proposed cylindrical shear and individual plate breakout models, calculated with the typical, theoretical, and proposed N_{cu} values of 9.0, 9.4, and 11.2 respectively.

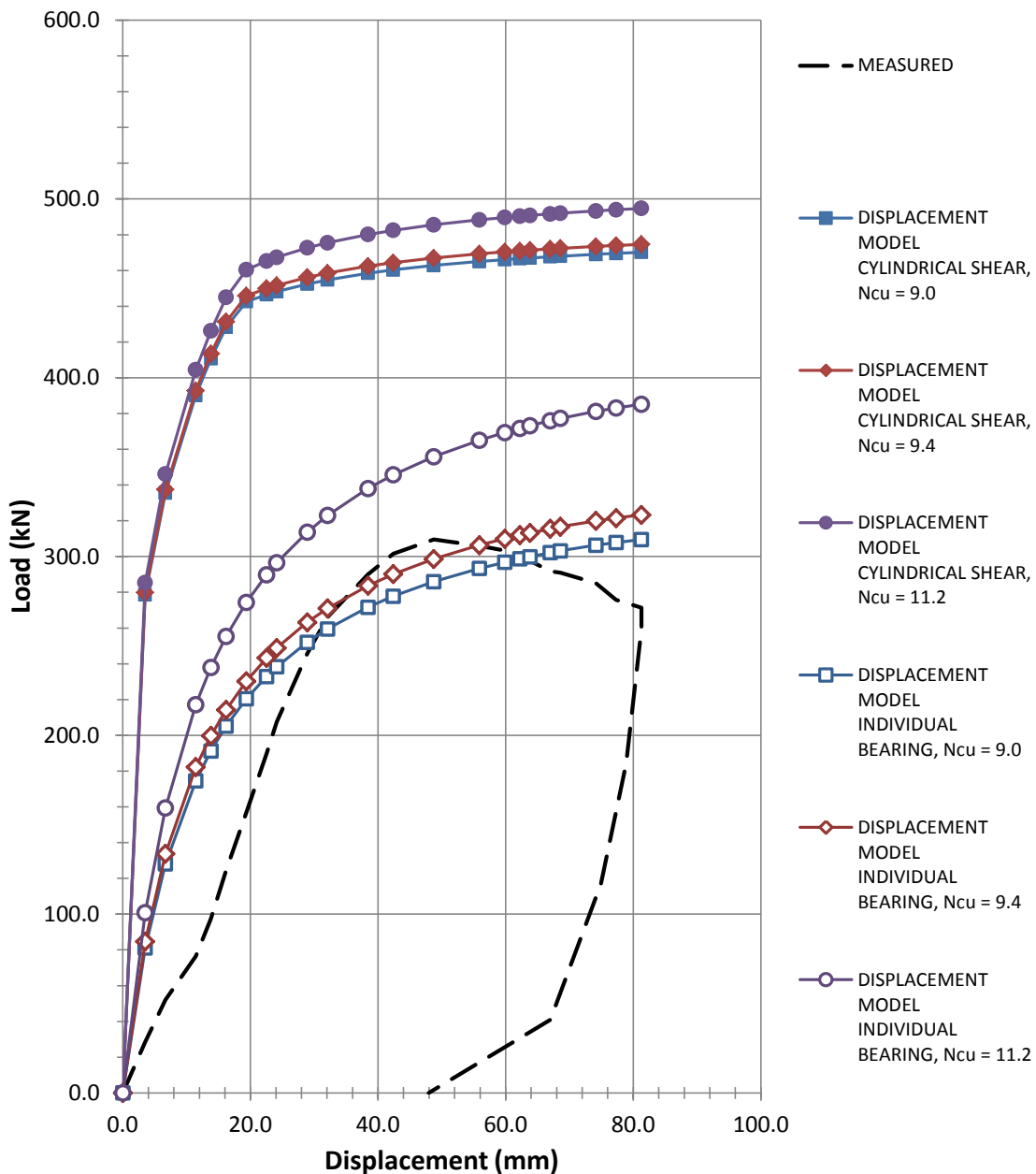


Figure A.17 Load-displacement curve for anchor S6, compared to the predicted curves using the proposed cylindrical shear and individual plate breakout models, calculated with the typical, theoretical, and proposed N_{cu} values of 9.0, 9.4, and 11.2 respectively.

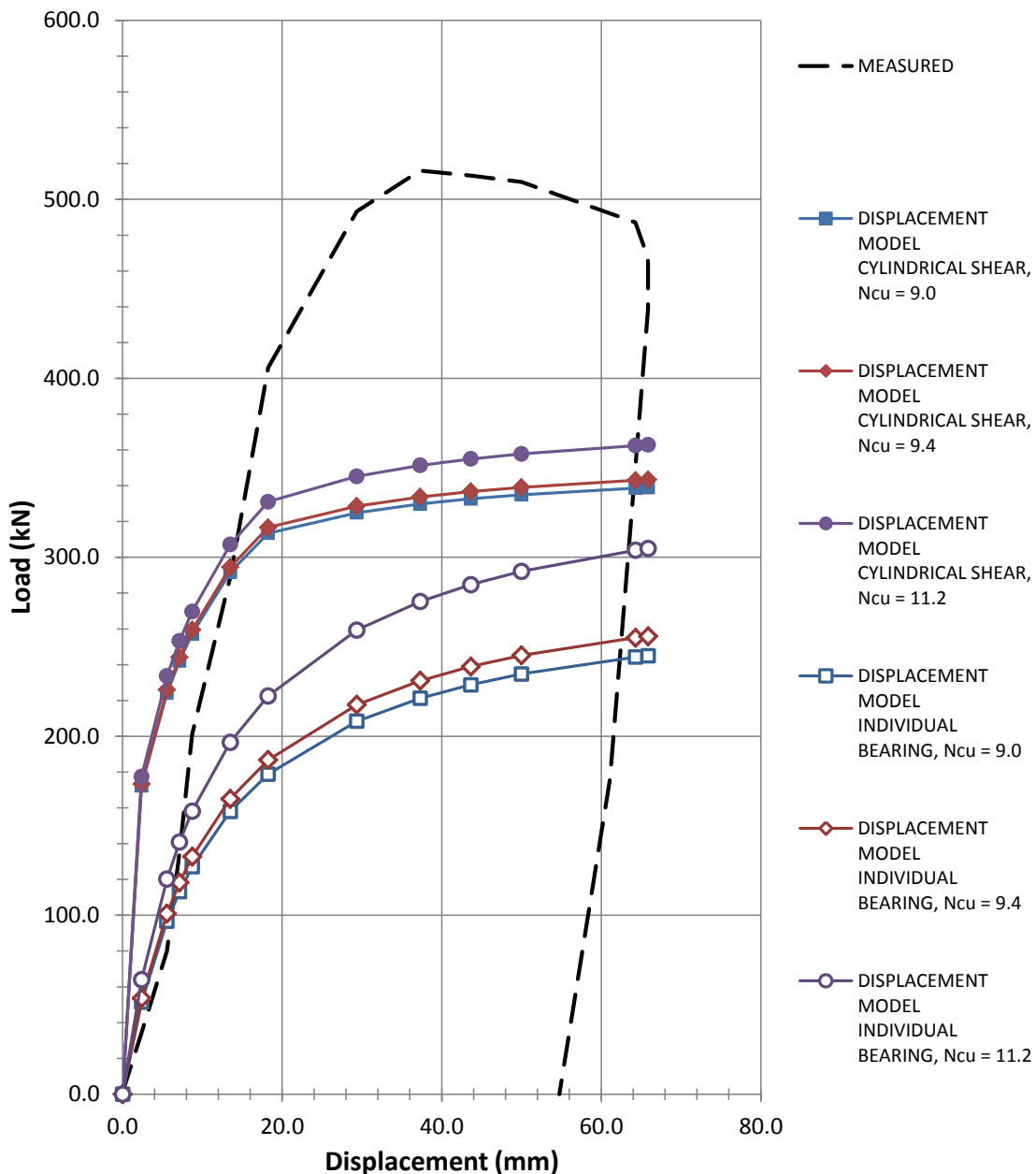


Figure A.18 Load-displacement curve for anchor S7, compared to the predicted curves using the proposed cylindrical shear and individual plate breakout models, calculated with the typical, theoretical, and proposed N_{cu} values of 9.0, 9.4, and 11.2 respectively.